PTB bericht
Wissenschaftliche Veröffentlichungen
Diss-22
September 2025

Dissertation

Windi Kurnia Perangin-Angin

Development of a Dielectric Waveguide Microcalorimeter as the Primary Standard for Millimeter-Wave Power Measurements

ISSN 2941-1297
ISBN 978-3-944659-54-1

DOI 10.7795/110.20250905

Development of a Dielectric Waveguide Microcalorimeter as the Primary Standard for Millimeter-Wave Power Measurements

Von der Fakultät für Elektrotechnik, Informationstechnik, Physik
der Technischen Universität Carolo-Wilhelmina zu Braunschweig

zur Erlangung des Grades eines Doktors

der Ingenieurwissenschaften (Dr.-Ing.)

genehmigte Dissertation

von Windi Kurnia Perangin-Angin

aus Bangun Setia, Indonesien

1. Referent: Prof. Dr.-Ing. Thomas Kleine-Ostmann
2. Referent: Prof. Dr.-Ing. Jörg Schöbel

eingereicht am: 23.05.2025

mündliche Prüfung am: 25.08.2025

Druckjahr: 2025

Dissertation an der Technischen Universität Braunschweig,
Fakultät für Elektrotechnik, Informationstechnik, Physik

Acknowledgment

This dissertation has been completed with the support of many individuals. Firstly, I would like to express my deepest gratitude to my supervisor, Prof. Dr.-Ing. Thomas Kleine-Ostmann, Head of the Department of High Frequency and Electromagnetic Fields at the Physikalisch-Technische Bundesanstalt (PTB), for his patience and insightful feedback, which have been invaluable throughout this doctoral program. I am extremely grateful to Prof. Dr.-Ing. Jörg Schöbel, the second member of the Doctoral Committee, for his support and supervision of this dissertation. I would like to express my deepest appreciation to my mentor at PTB, Dr. Karsten Kuhlmann, for his expertise and guidance throughout the research process.

I am deeply thankful to the Chair of the Doctoral Board, Prof. Dr.-Ing. Thomas Kürner for carrying out the examination process.

I would like to extend my sincere thanks to Dr.-Ing. Rolf Judaschke, Head of the Department of Direct Current and Low Frequency at PTB, for his guidance and valuable feedback on this dissertation. I am sincerely thankful to Jürgen Rühaak for his technical support in completing this research. I am also grateful to Thomas Baron, Dr. Frauke Gellersen, Florian Rausche, Alexander Fernandez Scarioni, Steffen Weiß, and the members of Working Group 2.22 – High-Frequency Base Quantities at PTB for their invaluable assistance.

I would like to acknowledge the Deutscher Akademischer Austauschdienst (DAAD) for funding this research.

I acknowledge the use of ChatGPT to assist with proofreading this dissertation.

Finally, special thanks go to my parents and my wife, Hayuningtiyas Purbashinta, for their continuous support and motivation throughout this journey.

 DOI: 10.7795/110.20250905

Abstract

The rapid growth of telecommunication applications requires support from reliable millimeter-wave power measurement standards and systems. A highly accurate and precise measurement system is essential not only for validating the performance of telecommunication devices but also for ensuring safety, meeting regulatory requirements, and improving system efficiency. Currently, microcalorimeters, which serve as the primary measurement standard for radio frequency (RF) power at National Metrology Institutes (NMIs), are limited at frequencies up to 170 GHz. However, there is a growing demand for measurement standards at higher frequencies, such as those required for the sixth-generation (6G) technology for wireless communications. This dissertation focuses on developing a millimeter-wave power measurement standard and system for the frequency range of 140 GHz to 220 GHz to support telecommunications infrastructure.

Millimeter-wave technology applications, whose frequency range is not covered by existing standards, have encouraged research to find solutions. The development of microcalorimeters for the millimeter-wave range is challenging, primarily due to significant losses in the transmission lines. Since a microcalorimeter is a heat-measuring instrument, fluctuations in ambient temperature further complicate its implementation. In this work, a microcalorimeter was designed with a twin-line structure, featuring a symmetrically arranged transfer standard and a dummy load. The dummy load serves as the temperature reference, while the transfer standard is connected to a feeding line, and the dummy load to a dummy line. Both lines were constructed from dielectric waveguides, rather than metal waveguides as used in many conventional microcalorimeters. The feeding line utilizes metal waveguides as a transition section to connect the dielectric waveguide with rectangular waveguide (WR) devices, particularly WR-5 standardized devices.

A dielectric waveguide microcalorimeter was fabricated as the primary measurement standard for millimeter-wave power, demonstrating good performance. Effective transmission line matching has been achieved by tapering the ends of the dielectric rod waveguide and shaping the hollow metal waveguide into a trumpet structure. Enclosing the microcalorimeter in thermal jackets maintains a stable temperature. The twin-line structure minimizes the effects of temperature variations. The dielectric waveguide microcalorimeter is utilized to calibrate power sensors, establishing measurement traceability for millimeter-wave devices. This microcalorimeter represents a novel application of dielectric waveguides in the WR-5 band, contributing to quality assurance in the development of telecommunications systems.

DOI: 10.7795/110.20250905

Zusammenfassung

Das rasche Wachstum von Telekommunikationsanwendungen erfordert die Unterstützung durch zuverlässige Messnormale und -systeme für Millimeterwellenleistung. Ein hochgenaues und präzises Messsystem ist nicht nur wesentlich, um die Leistung von Telekommunikationsgeräten zu validieren, sondern auch, um Sicherheit zu gewährleisten, regulatorische Anforderungen zu erfüllen und die Effizienz von Systemen zu steigern. Derzeit sind Mikrokalorimeter, die als primäre Messnormale für Hochfrequenzleistung (HF-Leistung) in Nationalen Metrologieinstituten (NMIs) dienen, bei Frequenzen bis zu 170 GHz verfügbar. Es gibt jedoch eine wachsende Nachfrage nach Messnormalen für höhere Frequenzen, wie sie für Technologien der sechsten Generation (6G) des Mobilfunks erforderlich sind. Diese Dissertation konzentriert sich auf die Entwicklung eines Messnormals für Millimeterwellenleistung im Frequenzbereich von 140 GHz bis 220 GHz, um die Telekommunikationsinfrastruktur zu unterstützen.

Anwendungen der Millimeterwellentechnologie, dessen Frequenzbereich nicht durch bestehende Normale abgedeckt wird, haben die Forschung angeregt, nach Lösungen zu suchen. Die Entwicklung von Mikrokalorimetern für Frequenzen oberhalb von 100 GHz ist herausfordernd, da in den Übertragungsleitungen erhebliche Verluste auftreten. Da ein Mikrokalorimeter ein Wärmemessgerät ist, erschweren Schwankungen der Umgebungstemperatur die Implementierung zusätzlich. Das hier zum Einsatz kommende Mikrokalorimeter entspricht dem sogenannten Zwillingsaufbau (twin-type): parallel zur Messleitung und dem Sensor wird eine identische Kombination aus Leitung und Sensor implementiert, welche als thermische Referenz dient. Beide Leitungen bestehen aus dielektrischen Wellenleitern, anstelle von Metallwellenleitern, die in herkömmlichen Aufbauten verwendet werden. Die Einspeiseleitung besteht aus Metall, um den dielektrischen Wellenleiter mit rechteckigen Wellenleitern (WR), insbesondere WR-5-Geräten, zu verbinden.

Ein Mikrokalorimeter mit dielektrischen Wellenleitern wurde erfolgreich als primäres Messnormal für Millimeterwellenleistung hergestellt. Eine effektive Anpassung der Übertragungsleitung wird durch die Verjüngung der Enden des dielektrischen Stab-Wellenleiters und die Formung des hohlen Metallwellenleiters zu einer Trompetenstruktur erreicht. Das Umschließen des Mikrokalorimeters mit thermische Isolierhüllen gewährleistet eine stabile Temperatur. Die symmetrische Zweileiterstruktur minimiert die Auswirkungen von Temperaturschwankungen. Das dielektrische Wellenleiter-Mikrokalorimeter ermöglicht die Kalibrierung von Leistungssensoren und stellt die Rückführbarkeit von Messungen für Millimeterwellen-Geräte sicher. Dieses Mikrokalorimeter stellt eine neuartige Anwendung von dielektrischen Wellenleitern im WR-5-

Band dar und trägt zur Qualitätssicherung bei der Entwicklung von Telekommunikationssystemen bei.

 DOI: 10.7795/110.20250905

Contents

 DOI: 10.7795/110.20250905

DOI: 10.7795/110.20250905

DOI: 10.7795/110.20250905

1 Introduction

In daily life, measurements are involved in many human activities. Measurement science supports industries in producing high-quality products and complying with relevant regulations. Metrology facilities, as one of the key components of quality infrastructure, play a significant role in enhancing the competitiveness of companies [1]. Some industries, such as telecommunications, aviation, and military sectors, require the measurement of millimeter-wave power as part of their technical equipment. This dissertation describes the development of a measurement standard and system for millimeter-wave power.

1.1 Background

The applications of telecommunication systems have grown rapidly over the last few decades. This development has been supported by reliable radio frequency (RF) power measurement, as RF power is one of the most fundamental quantities in telecommunication devices. National Metrology Institutes (NMIs) including the Physikalisch-Technische Bundesanstalt (PTB), the NMI of Germany, strive to develop measurement standards and systems for millimeter-wave power to support industries, particularly RF test equipment manufacturers [2], [3].

A measurement system for millimeter-wave power is required not only to verify the quality of telecommunications devices but also to ensure safety, to meet regulatory standards, and to increase the efficiency of telecommunication systems. Precise power measurements help maintain the integrity of signal transmission. By performing highly accurate power measurements, manufacturers can optimize the design and enhance the performance of RF devices. High power in millimeter-wave signals can cause nonlinear effects, distortion, and even device failure. Conversely, a millimeter-wave signal can be obscured by noise if its power is below the specified level for a device [4]. Therefore, the millimeter-wave power of telecommunication instruments must be measured accurately and precisely.

Usually a calorimetric set up, often a microcalorimeter, serves as the highest (primary) measurement standard for RF power. A primary standard represents the highest level of measurement accuracy for calibrating secondary or working standards used in calibration and testing of RF devices [5]. Several NMIs have developed microcalorimeters for many frequency bands. For instance, the National Institute of Standards and Technology (NIST) in the United States has developed a range of RF and microwave power standards up to 110 GHz and is currently developing microcalorimeters for higher frequency bands [6]. Similarly, the

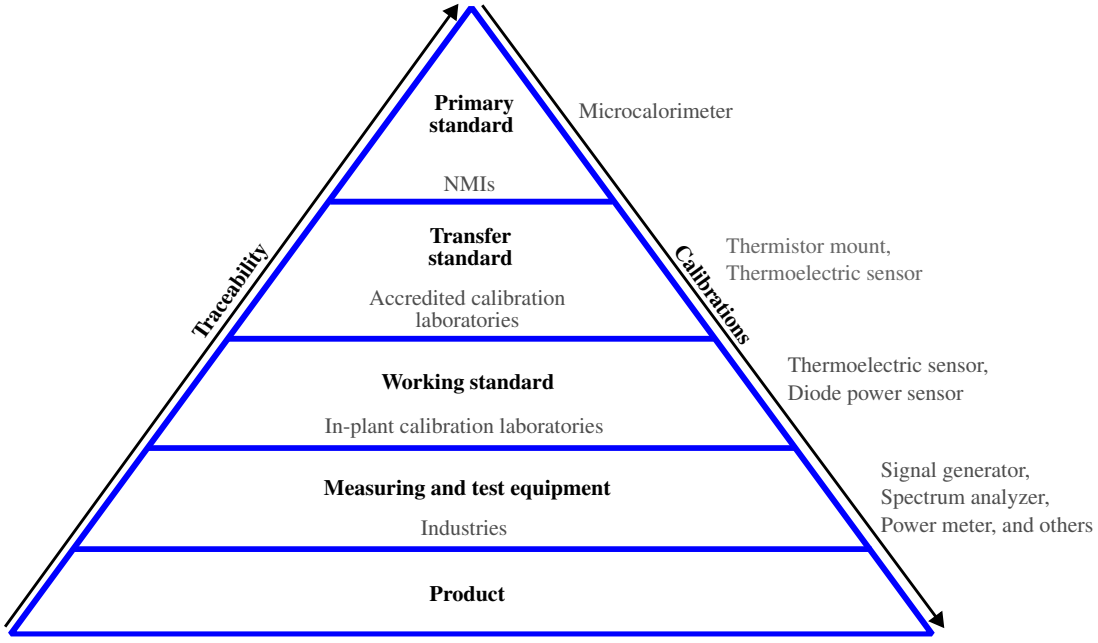

Figure 1.1: Measurement traceability of RF power.

National Physical Laboratory (NPL) in the United Kingdom offers RF power measurement systems using microcalorimeters for frequencies up to 170 GHz [7]. Other institutes, such as the Laboratoire national de métrologie et d'essais (LNE) in France, the National Metrology Institute of Japan (NMIJ) in Japan, and the Korea Research Institute of Standards and Science (KRISS) have also been developing microcalorimeters for the millimeter-wave band [2], [3], [8], [9].

In most cases, these microcalorimeters are not commercially available but custom-made devices. NMIs perform calibration services for calibration laboratories or industries. The measurement results of a transfer (reference) standard, calibrated using the primary standard, are disseminated to a working standard. These values are then subsequently transferred to commercial instruments through further calibration steps. Figure 1.1 illustrates the measurement traceability of RF power, showing how measurements assure the quality of RF products [10]. These products are linked to a national standard, which is typically a primary standard of RF power maintained by NMIs.

PTB offers calibration services for millimeter-wave power up to 170 GHz. This is currently the highest measurement frequency range for millimeter-wave power among all NMIs [11]. However, there is a growing need for measurement standards at even higher frequencies,

DOI: 10.7795/110.20250905

particularly for millimeter-wave applications such as satellite systems, radar technologies, medical devices, autonomous vehicles, and advanced sensing systems [12]. PTB and other leading NMIs conduct research to develop millimeter-wave power standards for frequencies beyond those currently available. Recently, the development and implementation of sixth-generation (6G) technology have also been progressing. The frequency band of 140 GHz to 220 GHz is one of the potential bands for 6G technology, among other frequency bands [13]. Therefore, it is essential to develop a measurement standard and system for millimeter-wave power at higher frequencies to support quality assurance in telecommunications technology development. This dissertation explores the design, development, and validation of such a microcalorimeter.

1.2 Problem Statement

The rapid advancement of millimeter-wave technology has led to a wide range of applications. These applications operate at increasingly higher frequencies, necessitating precise power measurements. However, a discrepancy exists between the capabilities of current primary measurement standards for millimeter-wave power and the growing demands of these applications, which require higher frequency ranges and higher accuracy. NMIs support the rapid technological advancements in millimeter-wave systems by continuously developing reference standards.

Developing microcalorimeters for the millimeter-wave range is challenging due to significant losses in transmission lines. High propagation loss is a common issue in millimeter-wave measurements and applications, affecting the efficiency and accuracy of power standards. As the frequency increases, signal losses become more obvious, reducing transmitted power and limiting the reliability of measurement systems. These losses mainly occur within transmission lines, making their design and fabrication crucial to the successful operation of millimeter-wave microcalorimeters [14].

One of the main difficulties lies in constructing the feeding line that delivers signals to and from the microcalorimeter. At millimeter-wave frequencies, the cross-sectional dimensions of the feeding line are significantly reduced, often reaching sub-millimeter scales. These small sizes introduce manufacturing difficulties and additional challenges, such as maintaining precise alignment and minimizing unwanted signal reflections [15].

Both coaxial and waveguide microcalorimeters are used as primary measurement standards for RF power, with the latter being preferred by NMIs for frequencies above 40 GHz [16]. One reason for this preference is that waveguides transmit signals with lower losses than coaxial lines [17]. Generally, available waveguide microcalorimeters use metal waveguides as trans-

mission lines, which experience increasing losses, especially at very high frequencies, due to conduction losses and surface roughness in the metal elements. These losses become more significant in metal waveguides operating above 100 GHz [18], [19].

Fundamentally, a microcalorimeter is a heat-measuring instrument designed to detect temperature changes caused by the absorption of RF power. However, in real application, unwanted heat, such as that from ambient temperature variations, poses a significant challenge. Even slight fluctuations in the surrounding environment can introduce errors in the measurement process, reducing the accuracy and reliability of the microcalorimeter. This sensitivity to ambient conditions necessitates solutions to mitigate the effects of external heat disturbances [4]. A thermal isolation section (TIS) is integrated into rectangular metal waveguide microcalorimeters to minimize the fraction of heat contributing to the temperature difference between the measuring (feeding) line and the reference (dummy) line. Manufacturing this thermal isolation section is an essential step in establishing a microcalorimeter.

Maintaining a stable laboratory room temperature is one of the most effective strategies for minimizing the impact of ambient temperature variations. Additionally, thermal insulation techniques are essential to shield the microcalorimeter from temperature fluctuations and external heat sources. Thermal jackets are an effective method for isolating the microcalorimeter from unwanted heat intrusion by acting as a barrier that prevents heat exchange between the microcalorimeter and its surroundings. By reducing the influence of ambient thermal fluctuations, thermal jackets help ensure that the microcalorimeter measures only the heat generated by the millimeter-wave source. These solutions improve the precision and reliability of the instrument, enabling it to serve as a robust tool for establishing primary measurement standards in millimeter-wave power applications [20].

A thermopile is utilized to measure the temperature difference between the transfer standard and a temperature reference during the measurement process. The response of the thermopile should be as linear as possible with respect to the temperature difference [21]. Therefore, fabricating a high-quality thermopile is another critical process in the development of a microcalorimeter.

Figure 1.2 shows a schematic of the microcalorimeter line, illustrating the unwanted heat and unmeasured power in the measurement system. When a microcalorimeter measures millimeter-wave power, not all the power is absorbed by the sensing element of the transfer standard used as a load in the microcalorimeter. Some power is reflected back to the waveguide source, while other portions are dissipated in the walls of the microcalorimeter feeding line and the transfer standard [22]. The reflected signal is caused by impedance mismatches, which origi-

 DOI: 10.7795/110.20250905

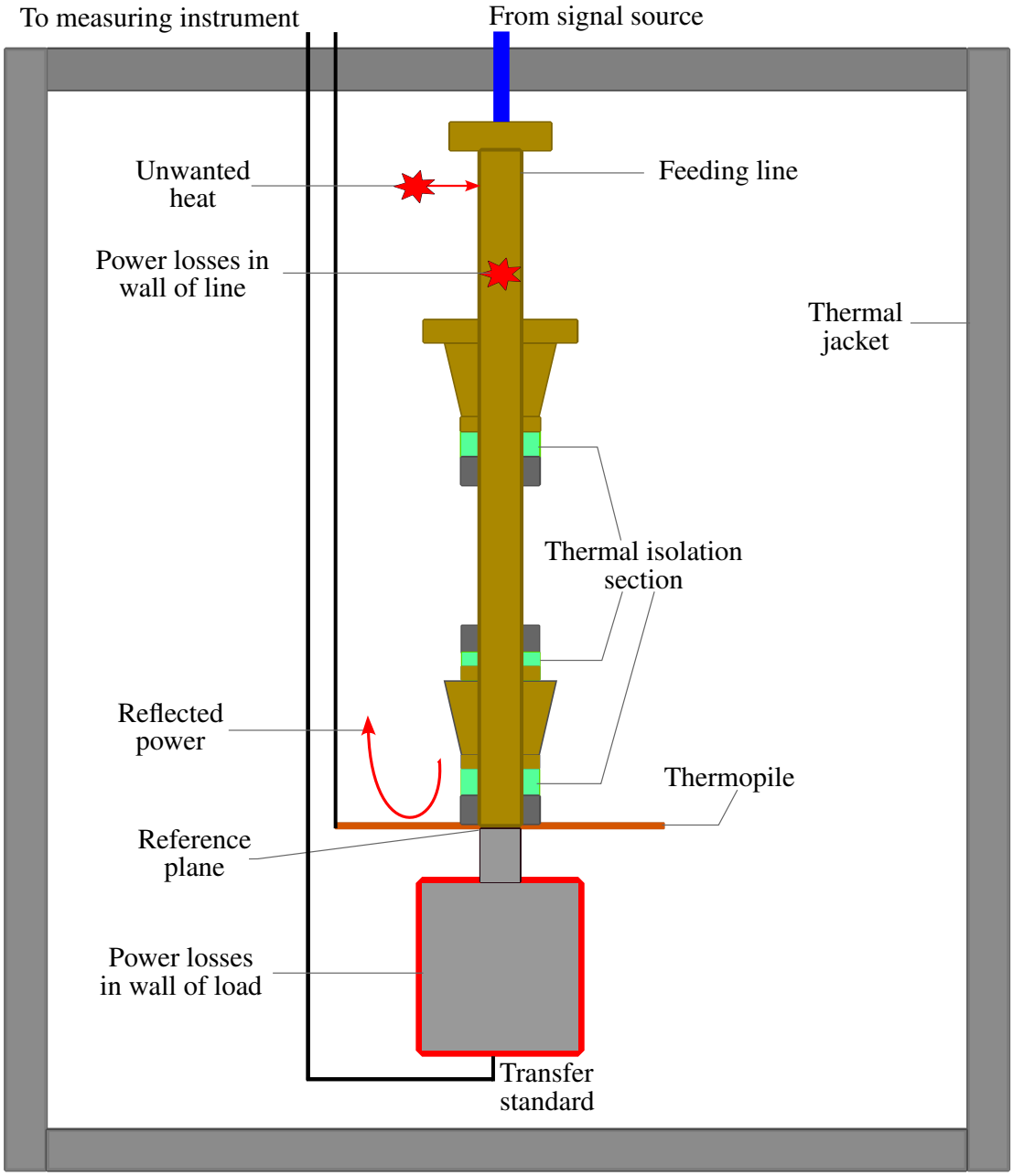

Figure 1.2: Unmeasured power and unwanted heat in microcalorimeter measurement. The black lines represent DC voltage signals, whereas the blue line represents RF power.

DOI: 10.7795/110.20250905

nate at the interfaces between the source and the transmission line, and between the transmission line and the load.

Measurement uncertainty is a key concept in metrology, providing a quantitative estimate of the quality and reliability of measurement results. According to the Guide to the Expression of Uncertainty in Measurement (GUM), uncertainty is defined as a parameter associated with the result of a measurement that characterizes the dispersion of values that could reasonably be attributed to the measurand. The GUM establishes a comprehensive framework for evaluating and expressing uncertainty by identifying and combining individual uncertainty components. These are typically classified as Type A, based on statistical analysis of measured data, and Type B, derived from other sources such as previous measurement data, calibration certificates, or established theoretical models and professional experience. This structured approach ensures that measurements are both traceable and comparable across laboratories and institutions, forming the basis for reliable calibration and standardization [23].

The calibration of a standard aims to achieve the lowest possible measurement uncertainty. Unlike direct current (DC) power primary standards, which have uncertainties as low as tens of parts per million, the available primary standards for RF power exhibit uncertainties in the range of 0.01 % to 3 %. The measurement uncertainty of millimeter-wave power above 170 GHz can be higher, presenting an additional challenge in the development of a microcalorimeter. Significant sources of measurement uncertainty in millimeter-wave power include millimeter-wave signal loss, thermopile nonlinearity, and uncertainties in the DC measurement components. These sources of uncertainty must be determined experimentally to compensate for unmeasured power [4].

Transfer standards, which are essential components in the traceability chain of RF power measurements, are not yet commercially available. They enable calibration laboratories, research institutions, and industries to maintain measurement accuracy and consistency when direct access to primary standards is not feasible. These standards serve as reliable reference artifacts, ensuring the comparability of power measurements across different facilities and supporting the calibration of commercial RF test equipment. Transfer standards are particularly important in applications such as telecommunications, aerospace, semiconductor manufacturing, and next-generation wireless technologies.

1.3 Research Objectives

The objective of this research is to develop a reliable millimeter-wave power measurement standard and system for frequencies ranging from 140 GHz to 220 GHz. This frequency

 DOI: 10.7795/110.20250905

range is crucial for supporting the growth of telecommunication infrastructures and addressing the expanding demands of high frequency applications. A key focus of this work is to reach high measurement accuracy, minimize uncertainties, and maintain compatibility with emerging millimeter-wave power measurement systems. To meet the measurement requirements of millimeter-wave technology at frequencies higher than those covered by existing millimeter-wave power measurement standards, a waveguide microcalorimeter is constructed. The microcalorimeter is designed to serve as a primary measurement standard for millimeter-wave power at PTB. By providing highly accurate and traceable power measurements, it ensures that RF industrial products meet the required performance and reliability standards. Measurement and testing standards for telecommunication devices and other RF applications above 170 GHz can be calibrated with this microcalorimeter.

In this work, a dielectric waveguide is used as the transmission line in the microcalorimeter, instead of the conventional metal waveguides. The application of dielectric waveguides in microcalorimeter measurements is a relatively new concept, as most NMIs continue to rely on metallic waveguide-based microcalorimeters as primary standards for RF power measurements [6], [16], [19], [24], [25]. This dissertation discusses the design of a dielectric waveguide microcalorimeter, focusing on optimizing the transmission line. The design incorporates tapering sections and trumpet structures to achieve smooth transitions between the dielectric waveguide and the standard rectangular WR-5 metallic waveguide.

It should be noted that dielectric waveguide microcalorimeters do not require additional thermal isolation sections, which are essential for all microcalorimeters. When using metallic waveguides in a microcalorimeter, thermal isolation sections mitigate heat conduction along the metallic walls, a factor that can introduce significant uncertainties in power measurement. However, in this dielectric waveguide microcalorimeter, the dielectric itself acts as the thermal isolation section [26].

DOI: 10.7795/110.20250905

DOI: 10.7795/110.20250905

2 Fundamental Theory

This chapter outlines the fundamental theory of RF power measurement using a microcalorimeter, including millimeter-wave power standards. Detailed explanations are provided for the microcalorimeter and the dielectric waveguide. The fundamental theory provides the foundation for understanding the development of a dielectric waveguide microcalorimeter as a primary standard for millimeter-wave power measurements.

2.1 RF Power Measurement Basics

RF covers the frequency range of the electromagnetic (EM) spectrum from 30 kHz to 300 GHz, while millimeter waves lie between 30 GHz and 300 GHz [27]. Power is one of the fundamental quantities in RF measurements. It is typically measured using a power sensor and meter, with the sensor converting the RF or millimeter-wave signal into a readable output [28]. Figure 2.1 shows the basic principle for measuring RF power using a power sensor and a power meter.

2.1.1 Power Source

A signal generator is often combined with other devices, such as a directional coupler, power splitter, attenuator, or isolator, to generate a well matched and stable power source. The power splitter or directional coupler is used for power leveling, improving the output match of the signal source. The stabilization is typically improved by a monitoring power sensor and a power meter [29]. The signal source requires isolation from the load to prevent detuning caused by a mismatched load. Generally, an attenuator or isolator is utilized to achieve this isolation. These components also help reduce the reflection coefficient of the signal source [28], [30].

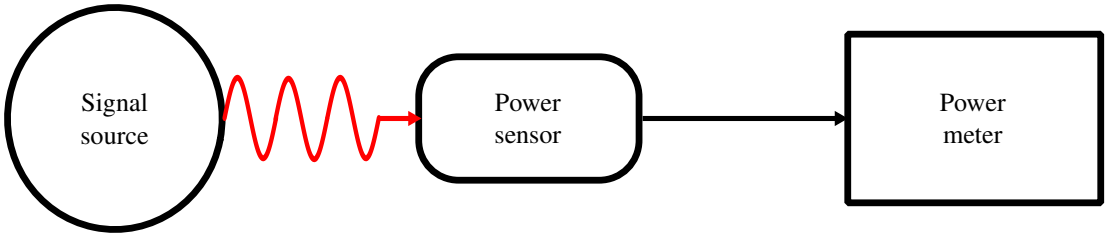

Figure 2.1: Basic technique for measuring RF power.

Commercially available signal sources are inherently limited in their ability to directly generate signals at extremely high frequencies, such as those required for millimeter-wave applications. This limitation arises from the physical constraints of signal generation at high frequencies, necessitating the use of auxiliary components to achieve the desired frequency range. Frequency multipliers are employed to increase the frequency of their input signal by producing harmonics that are multiples of the original frequency. By utilizing these harmonics, frequency multipliers enable the generation of signals up to THz range [31].

The operation of frequency multipliers can sometimes generate additional harmonics and produce unwanted signals and noise that interfere with the desired signal. To address this issue, filters are integrated into the system to selectively eliminate these unwanted signals and minimize noise levels. These filters are carefully designed so that only the desired harmonic frequency passes through while suppressing the undesired harmonics and other interference. This process preserves signal integrity and guarantees that the output signal is suitable for high precision applications.

2.1.2 Power Sensor and Power Meter

Power sensors are used in conjunction with power meters to measure RF power. A power sensor detects RF power and converts it into a measurable signal for a power meter. The power meter measures and displays the detected signal as DC substituted power or indicated power from the power sensor [32].

There are three fundamental types of power sensors commonly available for RF metrology objectives: bolometer sensors, thermoelectric sensors, and diode sensors. Power sensors have evolved from the first generation of bolometer elements to the innovation of thermoelectric sensors, and more recently, to the advancements in diode sensors. Each type of power sensor operates based on a different principle and has its own strengths and weaknesses for RF power measurement which are given in Table 2.1 [33].

Bolometer sensors operate based on RF-DC power substitution. The sensor resistance changes due to temperature variations caused by RF power dissipation in the bolometric element. There are two main types of bolometers: barretters and thermistors. Thermistor mounts are often utilized as transfer standards by NMIs due to their long-term stability and excellent linearity. Nevertheless, bolometer sensors have limitations, including restricted power capability, very slow response times, and low dynamic range [24]. Additionally, coaxial thermistor mounts are no longer commercially available for frequencies above 50 GHz, and waveguide thermistor mounts have not been produced in recent decades [16]. Industry and end-users pre-

 DOI: 10.7795/110.20250905

Table 2.1: Key information on RF power sensors [4], [33], [34].

Aspect	Bolometer sensor	Thermoelectric sensor	Diode sensor
Operating principle	RF-DC power substitution	Thermocouple principle	Rectification properties
Linearity	Best	Good	Poor
Dynamic range	Narrow	Wide	Widest
Response times	Slow	Fast	Fastest
Applications	Transfer standard	Transfer standard Working standard	Working standard

fer fast response sensors with a large dynamic range. Only research institutes and universities still use or even develop bolometer sensors, usually for fundamental research or metrology purposes.

Thermoelectric sensors work on the thermocouple principle. They generate a DC voltage proportional to the temperature difference between two dissimilar metals at two junctions, which in turn is a measure of RF power. Recently, NMIs have applied thermoelectric sensors as transfer standards in the millimeter-wave range, particularly since thermistor mounts are no longer commercially available. Thermoelectric sensors offer a wider dynamic range and faster response times (up to a few milliseconds). On the other hand, these sensors are sensitive to environmental temperature fluctuations [28], [35].

Diode sensors use a rectification process to convert RF power into DC voltage. Unlike the other two types, diode sensors are not thermal power sensors. These sensors have the widest dynamic range and the fastest response times among the types discussed in this dissertation. However, they have the worst linearity specification. Due to these drawbacks, diode sensors are not applied as transfer standards by NMIs in microcalorimeter measurements. Instead, they serve as working standards for calibrating measurement and test equipment in RF and millimeter-wave applications [34].

2.2 Microcalorimeter

A microcalorimeter is an instrument used as the primary standard for measuring RF and millimeter-wave power. Due to the high costs of building and maintaining, microcalorimeters are usually only operated at NMIs (e.g., PTB) and are not commercially available. NMIs without

microcalorimeters rely on traceable transfer standards as their main measurement standard. These transfer standards, which can be either thermistor mounts or thermoelectric sensors, are employed to disseminate the measurement results of microcalorimeters within their country. The core components of a microcalorimeter include the feeding line, thermal isolation sections, thermopile, and thermal jacket. In twin-type microcalorimeters, the primary standard includes an associated transfer standard and a dummy load [21].

2.2.1 Working Principle of Microcalorimeter

The working principle of a microcalorimeter is based on the RF-DC substitution technique, which measures RF power in terms of DC power. The DC power is assumed to be proportional to the applied RF power. RF-DC substitution refers to the process of determining RF power by measuring the amount of DC power that must replace the RF power in the transfer standard to produce an equivalent thermal effect. Basically, the DC substituted power P_{DC} is calculated using Equation 2.1

$$P_{DC} = \frac{V_1^2 - V_2^2}{R_0} \tag{2.1}$$

where V_1 is the DC voltage across the bolometer element without RF power, V_2 the DC voltage across the bolometer element with applied RF power, and R_0 is the operating resistance of the transfer standard.

In RF power measurements, the incident RF power refers to the total electromagnetic power delivered to the input port of a power sensor. On the other hand, absorbed RF power is the portion of the incident RF power that is effectively absorbed by the load of the power sensor. Only a fraction of the absorbed power is converted into heat in the absorbing element of the power sensor, while some power is lost in other parts. The relationship between incident RF power and absorbed RF power is determined by the principle of power conservation. The absorbed power $P_{RF_{abs}}$ is calculated by subtracting the reflected RF power P_r from the incident RF power $P_{RF_{in}}$, as expressed in Equation 2.2.

$$P_{RF_{abs}} = P_{RF_{in}} - P_r \tag{2.2}$$

Microcalorimeters measure RF power by assessing the heat generated in the transfer standard, ensuring traceability through the equivalence of thermal effects. When RF power is applied to the transfer standard, it is absorbed and converted into heat energy, causing a change

 DOI: 10.7795/110.20250905

in the temperature of the load resistor [4]. Ideally, the temperature change caused by RF power is equivalent to that caused by DC power. However, there are always differences in the temperature change caused by both power sources, which must be corrected in the microcalorimeter measurement process.

The microcalorimeter determines a measurement quantity of the transfer standard known as effective efficiency. Figure 2.2 illustrates the basic principle of microcalorimeter measurement. A bolometer element is controlled by a self-balancing bridge to maintain the operating resistance R_0 constant when RF power is applied. As the bolometer absorbs RF power, its resistance changes due to temperature variations. DC power is reduced to rebalance the bridge, and this reduction in DC power is proportional to the applied RF power.

Microcalorimeter measurements have long time constants because the balancing time of the bridge is relatively low. Furthermore, another measurement quantity, the thermopile voltage, needs to be measured. Measuring a single frequency point typically takes several minutes, sometimes more than an hour. Applying some repetitions for averaging and measuring across many frequency points can extend the measurement of a transfer standard to several weeks [6], [24], [36].

Effective efficiency η_e is defined as the ratio of the DC substituted power to the absorbed RF power in the transfer standard, as shown in Equation 2.3.

$$\eta_e = \frac{P_{DC}}{P_{RF_{abs}}} \tag{2.3}$$

Originally, effective efficiency was measured for the bolometer sensors [37]. For ideal measurements, η_e equals 1 (100 %) if the applied RF power is fully absorbed and the transfer standard exhibits identical thermal behavior for both DC and RF power. However, practical measurements yield η_e values less than 1 due to mount efficiency losses and RF-DC substitution errors. Power losses in the feeding line walls, transfer standard walls, and other components contribute to a measurement error known as mount efficiency. Additionally, RF-DC substitution error occurs when the transfer standard reacts differently to thermal distributions of RF and DC power [6].

A correction factor g is introduced to account for the fraction of heat that contributes to the temperature difference measured by the thermopile. It originates from RF losses in the feeding waveguide transition located in front of the reference plane, which lies between the transfer standard and the transmission line, as illustrated in Figure 1.2 [38]. Determining this correction factor is crucial for microcalorimeter development and is a key parameter in effective efficiency

measurement. The most significant source of uncertainty in effective efficiency measurements often comes from the uncertainty of the correction factor [25], [39].

Overall, microcalorimeter measurements of a transfer standard determine four parameters at each frequency: the DC voltage V_1 and thermopile output voltage e_1 without RF power, as well as the DC voltage V_2 and thermopile output voltage e_2 with applied RF power [40]. Furthermore, the microcalorimeter correction factor is determined through separate measurement processes using the foil short method. The effective efficiency of the transfer standard is calculated using Equation 2.4.

$$\eta_e = g\frac{1-\left(\frac{V_2}{V_1}\right)^2}{\frac{e_2}{e_1}-\left(\frac{V_2}{V_1}\right)^2} \tag{2.4}$$

Thermoelectric sensors are also suitable as transfer standards in microcalorimeter measurements, offering performance comparable to bolometer sensors. However, manufacturing

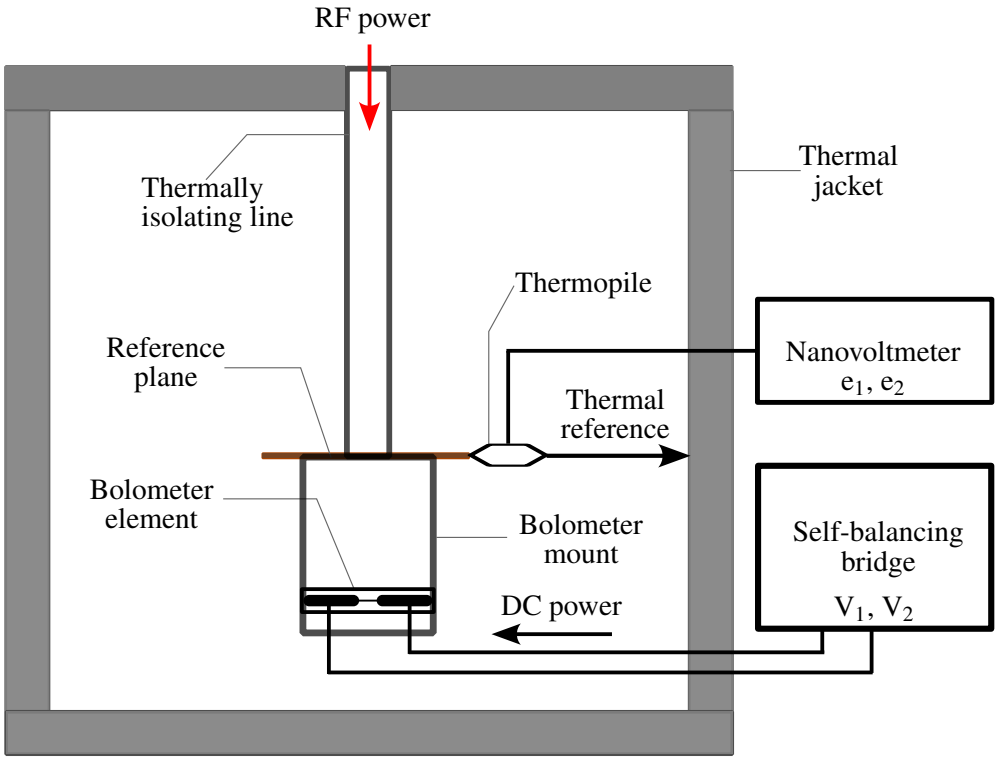

Figure 2.2: Principle of microcalorimeter measurement.

DOI: 10.7795/110.20250905

thermoelectric sensors for frequencies above 170 GHz remains challenging, and industries are developing new sensors for these ranges. Unlike bolometer sensors, RF power and DC power measurements with thermoelectric sensors are performed separately, as these devices are not equipped with a self-balancing bridge. Modifications to the RF-DC substitution method are required, especially for waveguide thermoelectric sensors [41].

2.2.2 Thermopile

Microcalorimeters use thermopiles to measure temperature changes in transfer standards. A thermopile is a device composed of multiple thermocouples connected in series to generate voltage in response to temperature differences. A thermocouple consists of two metals with different electrical conductivities that form a junction. The voltage is produced when there is a temperature difference at the junction of these materials. This physical effect is known as the Seebeck effect, a fundamental principle of thermoelectricity, where a temperature gradient across dissimilar conductors induces an electromotive force. Since the output of a single thermocouple is very small, adding more thermocouples in series increases the total voltage output and enhances the sensitivity of the thermopile. The thermopile operates based on the thermoelectric effect, where a voltage is produced at the junctions of two dissimilar metals when exposed to varying temperatures. The output voltage is proportional to the temperature difference or gradient. Thermopiles are highly sensitive and capable of measuring small temperature changes, making them ideal for applications in microcalorimeter measurements [42].

A set of thermopiles is used to measure the steady-state temperature difference between a transfer standard and a temperature reference. The thermopile is positioned between the transfer standard and the temperature reference [4]. It is located in a reference plane between the feeding line and the transfer standard. The temperature deviations between the feeding and the dummy transmission line are converted into voltage by the thermopile [43].

2.2.3 Transmission line

Transmission lines are designed to efficiently transmit RF power from a signal source to a load. However, in reality, losses are inevitable. To minimize these losses, the transmission line with the lowest attenuation is selected as the feeding line in a microcalorimeter measurement system.

Coaxial lines and rectangular waveguides are two types of transmission lines commonly used in microcalorimeters. In the millimeter-wave region, waveguides are preferred as feeding

lines due to the challenges of fabricating thermal isolation sections in coaxial technology. Most NMIs develop twin-type microcalorimeters with two transmission lines [16].

Waveguides can generally be classified into metal waveguides and dielectric waveguides, as shown in Figure 2.3. A metal waveguide is a hollow structure in the form of a metallic tube with a rectangular, circular, or elliptical cross-section. In contrast, a dielectric waveguide is a rod-shaped structure made of dielectric material [44].

NMIs utilize rectangular metal waveguides as transmission lines in microcalorimeters. These waveguides support either transverse electric (TE) or transverse magnetic (TM) modes. The rectangular cross-section operates in single mode, allowing only one mode to propagate. The dominant and fundamental mode of propagation in rectangular metal waveguides is the TE_{10} mode, which has the lowest cut-off frequency [45]. The dimensions of the waveguide determine its operating frequency range [46]. Figure 2.4 illustrates the field lines of the TE_{10} mode.

In addition to metal waveguides, dielectric waveguides can be used as an alternative for feeding lines in microcalorimeters. Dielectric waveguides offer advantages such as lower losses at higher frequencies, inherent temperature isolation, and greater mechanical flexibility compared to metal waveguides. They have been applied to the development of several devices and are suitable as feeding lines in waveguide microcalorimeters [47].

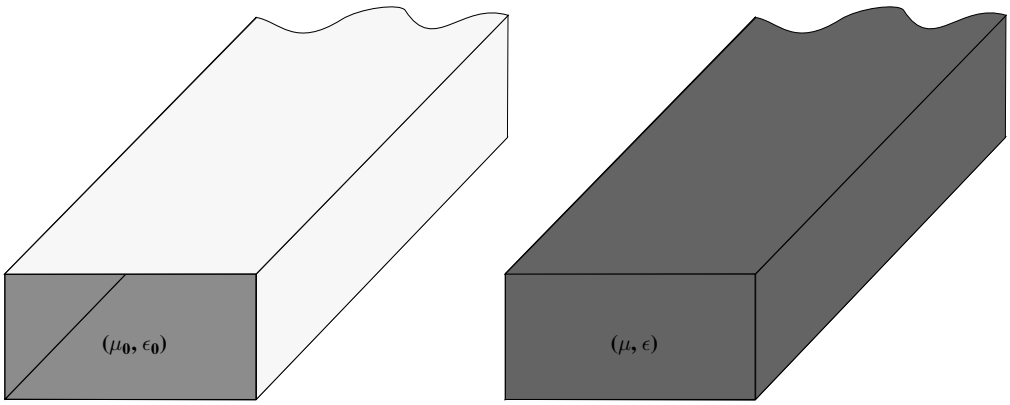

Figure 2.3: Structure of metal and dielectric waveguides.

DOI: 10.7795/110.20250905

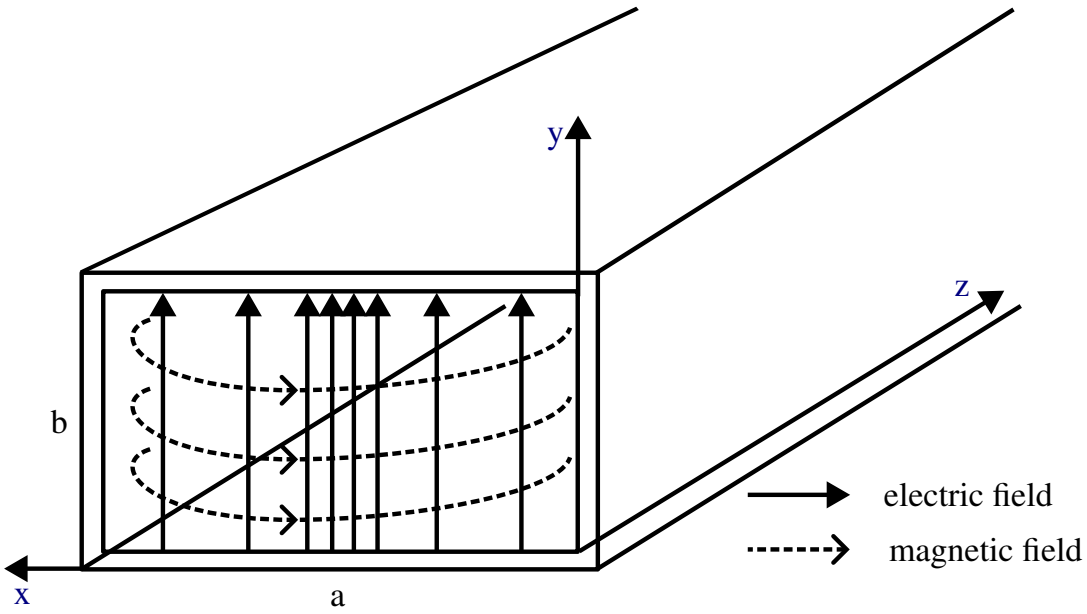

Figure 2.4: Field lines of TE_{10} mode in a rectangular metal waveguide [48].

2.2.4 Thermal Isolation Section

Metallic waveguides generally present poor heat insulation. Thermal isolation sections are implemented to suppress heat conduction. In a microcalorimeter, thermal isolation sections are used to insulate the transfer standard from external heat sources. These sections are positioned between the input transmission line of the microcalorimeter and the transfer standard.

Thermal isolation sections often consist of plastic disks, such as acrylonitrile butadiene styrene (ABS) or Polyetheretherketone (PEEK). These materials are chosen for mechanical strength, low thermal conductivity, and the possibility to apply thin metal layers. Most microcalorimeters are equipped with two to three thermal isolation sections, depending on the required level of precision and the length of the transmission line [6], [19]. The purpose of the thermal isolation section is to keep the fraction of heat contributing to the temperature differences between the measuring and reference lines as low as possible. As a critical component in the development of microcalorimeters, the thermal isolation section must be able to demonstrate excellent thermal isolation capabilities [49].

2.2.5 Thermal Jacket

Thermal jackets are designed and manufactured to fit a microcalorimeter, providing an external covering. Their main functions are to keep thermal stability within the microcalorimeter and minimize the impact of ambient temperature fluctuations. To achieve effective insulation, the microcalorimeter can be enclosed in a double-walled or multi-walled jacket. Plastic is used for the outer layer to isolate the microcalorimeter from external disturbances, while copper is used for the inner jacket. Since the transfer standard is a thermal power sensor, such as a bolometer or thermoelectric sensor, fluctuations in ambient temperature significantly affect its measurement stability. The use of thermal jackets helps in overcoming this problem [20].

Some NMIs combine the thermal jacket with a controlled water bath to monitor and regulate the temperature inside the microcalorimeter [24]. However, using a water bath requires careful handling to prevent water from leaking into the microcalorimeter, as this could cause significant damage to the instrument. To avoid the risks associated with water, insulating materials like polymeric foam can be used as an alternative for maintaining thermal stability. The thermal performance of polymeric foam is comparable to that of a water bath [50].

2.2.6 Transfer Standard and Dummy Load

A microcalorimeter with a twin-line arrangement includes two identical loads: one functions as the transfer standard, and the other is referred to as the dummy load. The dummy load acts as a temperature reference and is designed to have the same thermal and electrical characteristics as the transfer standard, including mass, geometry, thermal conductivity, and heat capacity. Matching the weight ensures that both loads exhibit similar heat absorption and dissipation behavior. Matching the electrical characteristics, such as impedance, minimizes reflection and ensures symmetrical signal propagation in both lines. These design considerations are critical because they ensure that any temperature difference measured by the thermopile is attributable only to the applied RF power, not to intrinsic differences between the two loads. The use of identical power sensors for both the transfer standard and the dummy load ensures that the same characteristics are met [36]. The schematic diagram of the twin-type microcalorimeter loads is depicted in Figure 2.5.

The effective efficiency of a transfer standard is independent of the reflection coefficient of the power sensor. For further measurement of RF devices, another parameter, the calibration factor, is determined during the calibration process. The calibration factor K accounts for both the effective efficiency and the reflection coefficient of the power sensor. It is defined as the ratio of the DC substituted power to the incident RF power on the reference standard, as expressed

 DOI: 10.7795/110.20250905

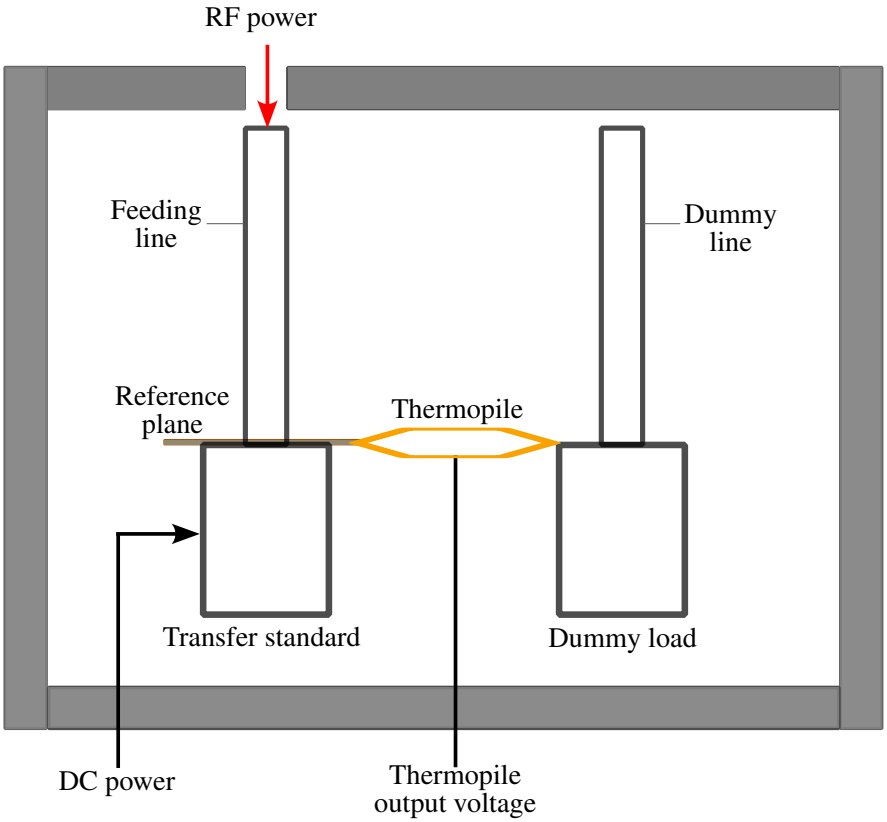

Figure 2.5: Schematic diagram of the twin loads in a microcalorimeter.

in Equation 2.5. The relationship between the calibration factor and the effective efficiency is shown in Equation 2.6.

$$K = \frac{P_{DC}}{P_{RF_{in}}} \tag{2.5}$$

$$K = \eta_e \left(1 - |\Gamma|^2\right) \tag{2.6}$$

The quantity Γ represents the input reflection coefficient of the transfer standard, measured using a vector network analyzer (VNA). In some cases, the calibration factor of the transfer standard is more relevant to users, as it is frequently used in calibrating commercial power sensors [4].

DOI: 10.7795/110.20250905

2.3 Dielectric Waveguide

A dielectric waveguide is a transmission medium made of dielectric materials that guide electromagnetic waves, often used in the frequency range of millimeter waves and sub-millimeter waves. Unlike conventional metal waveguides, dielectric waveguides have no metallic boundaries, eliminating conduction losses and potentially reducing transmission losses. This property makes dielectric waveguides particularly advantageous in high frequency and low loss applications [51].

Fabricating rectangular dielectric waveguides for millimeter-wave transmission lines with very small cross-sections is a challenge, but not more difficult than manufacturing rectangular metal waveguides. Dielectric materials have the capability to guide electromagnetic fields while isolating heat energy [18], [44]. This characteristic is particularly important for microcalorimeters, which are essentially instruments designed to measure heat.

The dielectric rod waveguide (DRW) offers advantages over conventional rectangular hollow metal waveguides, particularly at millimeter-wave and sub-millimeter-wave frequencies. One of the main benefits is the significantly lower propagation loss achievable with dielectric waveguides at higher frequencies. Metal waveguides suffer increasing conductor losses due to the skin effect, where current is confined to a very thin surface layer of the conductor. Additionally, surface roughness at high frequencies contributes to further losses, particularly above 100 GHz. These effects result in increased loss with frequency for metal waveguides. In contrast, dielectric rod waveguides minimize these issues by utilizing low-loss dielectric materials, enabling more efficient signal transmission and improved performance. Instead of conductor losses, their losses are dominated by dielectric absorption, which tends to scale more gradually with frequency [52]. Table 2.2 shows the comparison of the dielectric waveguide and the metal waveguide as transmission lines for the microcalorimeter.

2.3.1 Type of Dielectric Waveguides

There are two main types of dielectric waveguides: dielectric rod waveguide and optical waveguide. Dielectric waveguides are applicable for millimeter-wave applications and optical communications. Dielectric rod waveguides with rectangular or circular cross-sections are utilized in the millimeter-wave band, while optical waveguides, such as optical fibers, are used to transmit light in optical communication systems. Optical fiber waveguides have been extensively applied as a medium for long-distance transmission in telecommunications [44]. The propagation mechanism in dielectric waveguides relies on total internal reflection at the interface be-

 DOI: 10.7795/110.20250905

Table 2.2: Comparison of dielectric waveguides and metal waveguides as transmission lines for the microcalorimeter [18], [52], [53].

Feature	**Dielectric waveguide**	**Metal waveguide**
Propagation losses	Lower losses	Higher losses at frequencies above 100 GHz
Thermal isolation	No need for additional thermal isolation	Requires thermal isolation
Manufacturing tolerances	Wider tolerance	Tight tolerance
Flexibility	Flexible	Rigid

tween the dielectric material and air. This reflection confines the electromagnetic wave within the dielectric structure, allowing efficient guiding with minimal radiation loss. This dissertation focuses on dielectric rod waveguides with rectangular cross-section, often referred to simply as dielectric waveguides, for use as transmission lines in microcalorimeters.

Dielectric waveguides are rods of specific thickness that function as unshielded transmission line structures, allowing guided waves to propagate along their axial direction. This structure ensures the propagation of guided modes with minimal energy loss. Additionally, dielectric waveguides offer a broader operating frequency bandwidth and can be integrated with active or passive devices, including rectangular metal waveguides [54].

Minimizing losses in dielectric waveguides can be achieved by reducing the size of the rod base. A smaller rod size decreases the fraction of power propagating outside the dielectric core. However, if the rod becomes too small, electromagnetic waves can experience radiation losses. Therefore, the rod size is optimized by balancing these factors. Furthermore, for applications such as microcalorimeter transmission lines, the dielectric rod waveguide usually fits the cross-sectional size of the rectangular metal waveguide [47].

Table 2.3 provides the properties of various dielectric materials at a frequency of 140 GHz. Dielectric waveguides can be made from low-permittivity materials like Teflon or polyethylene, and high-permittivity materials such as silicon and sapphire. Materials with a high dielectric constant are often more fragile than those with a low dielectric constant. Losses in dielectric materials are characterized by the loss tangent $tan\ \delta$ [18], [55].

Table 2.3: Properties of dielectric materials [47], [51].

Material	**Relative permitivity** ϵ_r	**Loss tangent** $\tan\delta$
Gallium arsenide	13.0	3×10^{-4}
Silicon	11.6 - 11.8	0.03×10^{-4}
Sapphire	9.39 - 11.56	$1.1 - 2.1 \times 10^{-4}$
Polyethylene	2.3 - 2.8	0.4×10^{-4}
Teflon	2.0 - 2.1	$3 - 4 \times 10^{-4}$

2.3.2 Propagation Modes of Dielectric Waveguides

Propagation modes can be characterized by the patterns of the electromagnetic field distribution. They depend on the geometry and material properties of the waveguide. While rectangular metal waveguides support two types of propagation modes, TE and TM modes, dielectric waveguides mainly support hybrid modes. Hybrid modes are characterized by the presence of both electric and magnetic field components along the propagation direction (z-axis). There are two sets of hybrid modes, namely E^x_{mn} and E^y_{mn} [52], [56]. The indices x and y denote the primary polarization direction of the electric field, while the symbol of m and n indicate the number of extrema in the field distribution along the horizontal (x) and vertical (y) axes, respectively. In the E^y_{mn} mode, the electric field is predominantly polarized along the y-direction, whereas in the E^x_{mn} mode, the electric field is dominant in the x-direction [18], [51].

The modes E^x_{11} and E^y_{11} are the fundamental modes in rectangular dielectric waveguides. Among these, the E^y_{11} mode is typically recommended for rectangular dielectric waveguides because it is relatively easier to excite using transitions from metallic waveguides. Figure 2.6 illustrates the field line distribution of the E^y_{11} mode, which closely resembles the TE_{10} mode of rectangular metal waveguides, as shown in Figure 2.4. The cut-off frequency of dielectric waveguides depends on the waveguide cross-section and the dielectric constant of the rod. Simulation or measurement is needed to estimate the exact cut-off. The E^y_{11} mode in the dielectric rod waveguide connected to a WR-5 metal waveguide propagates effectively above a certain frequency [57].

DOI: 10.7795/110.20250905

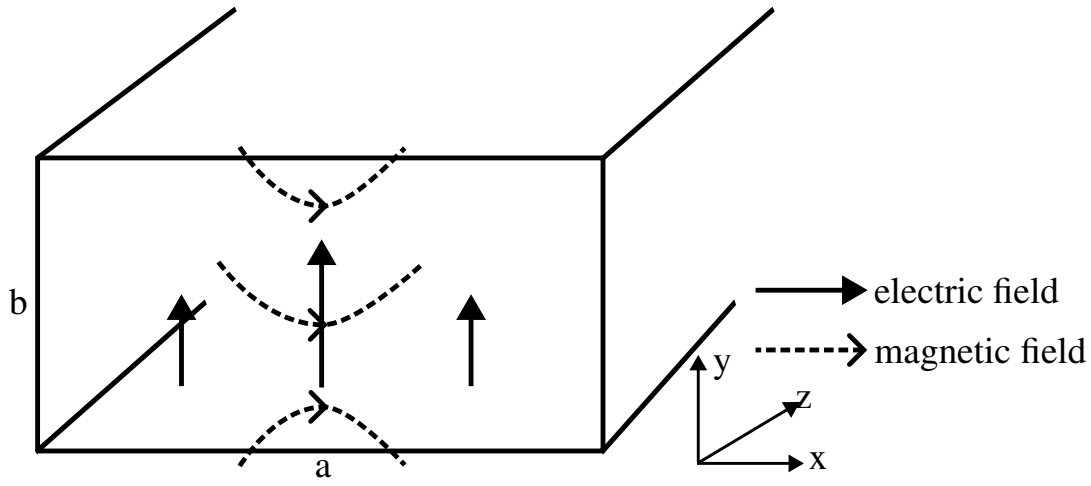

Figure 2.6: Field lines of the E_{11}^{y} mode in a rectangular dielectric waveguide [57]–[59].

2.3.3 Dielectric to Metal Waveguide Transitions

The transition between a dielectric waveguide and a rectangular metal waveguide is a critical interface in certain millimeter-wave applications, where efficient power transfer and minimal reflection are desired. In microcalorimeter systems, these transitions are necessary for connecting dielectric waveguides with standardized rectangular waveguide (WR) devices. Proper transitions between the two waveguide types are crucial for minimizing losses. Techniques to reduce losses include constructing horn structures in the transition region, tapering the terminal end of dielectric rods, or employing a combination of both [51], [60].

In addition to impedance matching, the transition should convert the millimeter-wave signal from the dominant mode of the rectangular metal waveguide to the dominant mode of the dielectric waveguide and vice versa, i.e., the TE_{10} mode of the rectangular metal waveguide directly excites the E_{11}^{y} mode in the rectangular dielectric waveguide. Design and optimization of the transition further enhance this mode transformation, resulting in reliable performance in high frequency applications [61].

DOI: 10.7795/110.20250905

DOI: 10.7795/110.20250905

3 Design and Simulation of Waveguide Microcalorimeter

The microcalorimeter designed in this work is based on a twin-line structure with a transfer standard and a dummy load. Figure 3.1 shows a schematic diagram of the waveguide microcalorimeter measurement system. The dummy load serves as a temperature reference, minimizing the effects of ambient temperature variations. Both the feeding line and the dummy (reference) line are constructed using dielectric waveguides. However, metal waveguides are still required to connect the dielectric waveguide to standardized interfaces, such as the signal source and the transfer standard.

Conventional microcalorimeter systems always require thermal isolation sections. However, in this system, the dielectric line itself serves to isolate the microcalorimeter from external heat disturbances, thereby eliminating the need for additional thermal isolation sections. Thermoelectric waveguide power sensors are utilized for both the transfer standard and the dummy load. A thermopile, composed of multiple thermocouples connected in series, measures the temperature difference between the transfer standard and the dummy load. The microcalorimeter is enclosed within three layers of shielding to maintain thermal stability, which contributes to a reliable millimeter-wave power measurement system.

3.1 Waveguide Structure Design for the Microcalorimeter Transmission Line

CST Microwave Studio was used for the design and simulation to optimize the transmission line of the waveguide microcalorimeter. The waveguide structure is one of the key components in designing the transmission line for the microcalorimeter. In this system, the metal waveguide is employed as a transition section, with the dielectric rod waveguide inserted into the hollow metal waveguide. The transition section clamps the dielectric rod waveguide at both ends, ensuring proper alignment and connectivity.

In addition to the metal waveguide, PEEK is utilized as the base material for the transition section. PEEK is a high performance polymer that can substitute metal in certain waveguide components due to its lightweight, flexibility, and durability in harsh environments [62]. In the microcalorimeter transmission line, a solid metal waveguide is utilized as the transition section at one port, while PEEK is employed at the other port to extend the thermal isolation

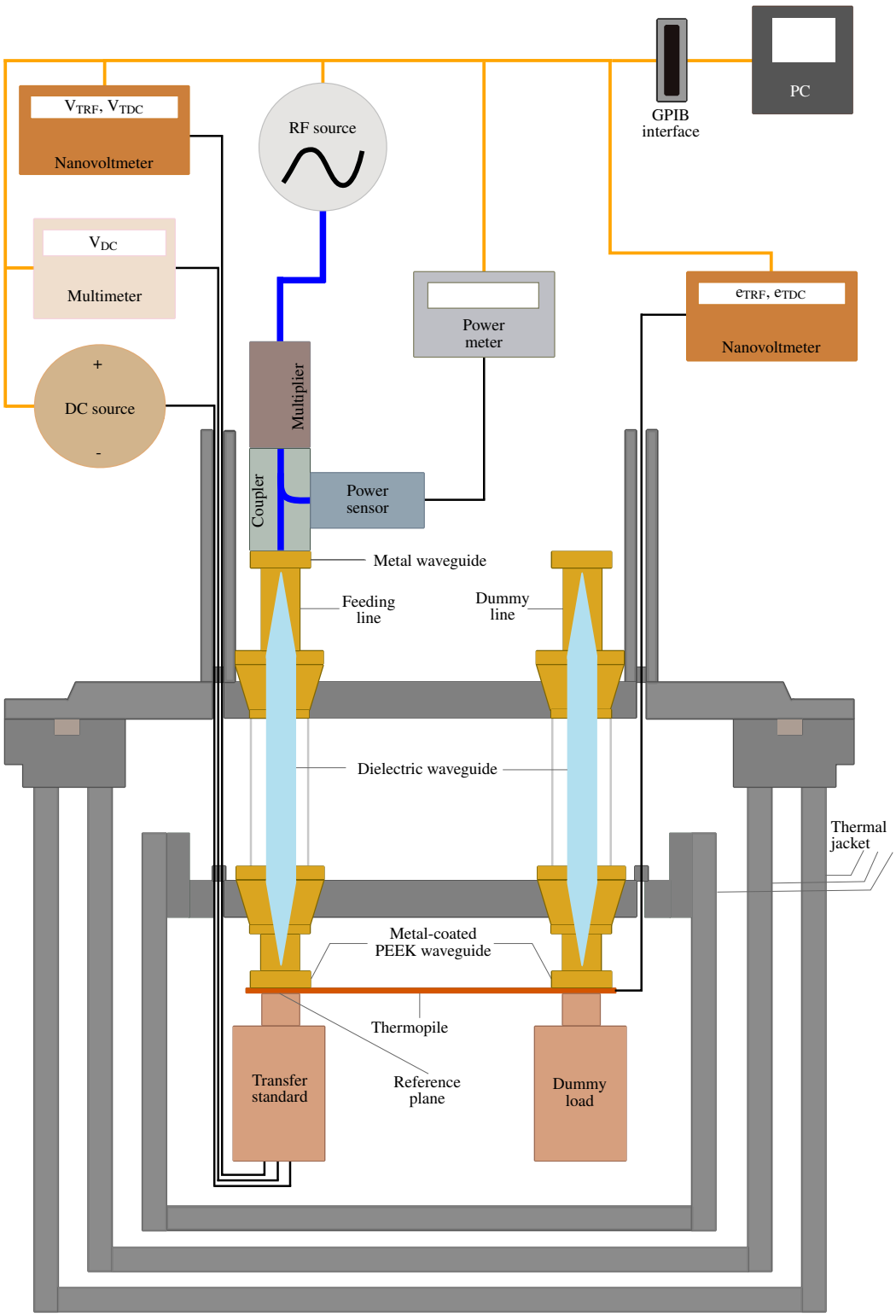

Figure 3.1: Schematic diagram of the microcalorimeter measurement system [14].

DOI: 10.7795/110.20250905

section. Both the metal waveguide and PEEK have the same cross-sectional dimensions to assure compatibility within the microcalorimeter transmission line [63], [64].

The design of the dielectric waveguide for the microcalorimeter transmission line involves determining the dimensions of the rod and the dielectric properties of the material. Selecting the appropriate dielectric waveguide material depends on its relative permittivity. A rigid material with a specific dielectric constant is selected to maintain long-term reliability. The dielectric waveguide dimensions are set to 1.295 mm x 0.648 mm to match the cross-section of the standardized WR-5 waveguide.

To enhance transition efficiency and minimize signal reflections in the transmission line, the dielectric rod waveguide is tapered into a wedge shape at both tips. Furthermore, a trumpet-shaped structure is integrated into the hollow metal waveguide, providing a smooth transition interface between the dielectric waveguide and the metal waveguide and minimizing signal loss.

3.1.1 Design of the Tapering Section of the Dielectric Waveguide

The tapering section of the dielectric waveguide plays a critical role in ensuring efficient coupling between the dielectric waveguide and the standard rectangular metallic waveguide. Both ends of the dielectric rod feature identical tapering sections in shape and size. Key parameters for optimizing the taper design include the geometry of the tapering section, the tapering section length, and the diameter of the taper tip.

The performance of the interface between the dielectric waveguide and the metal waveguide can be further enhanced by increasing the length of the tapering sections [65]. However, fabricating a longer taper in the dielectric waveguide presents significant challenges due to the fragility of the material. Consequently, the length of the tapering section is optimized to ensure an efficient transition within the frequency range of the microcalorimeter.

Various types of wedge shapes can be designed for dielectric waveguides, including vertical taper (x-taper), horizontal taper (y-taper), and a combination of vertical and horizontal taper (pyramidal taper) [66]. Figure 3.2 illustrates the three types of tapering sections for dielectric waveguides.

- The vertical taper occurs in the vertical plane. It is relatively easy to fabricate and effective in coupling the E_{11}^{y} mode due to good field alignment with the TE_{10} mode in rectangular metal waveguides.

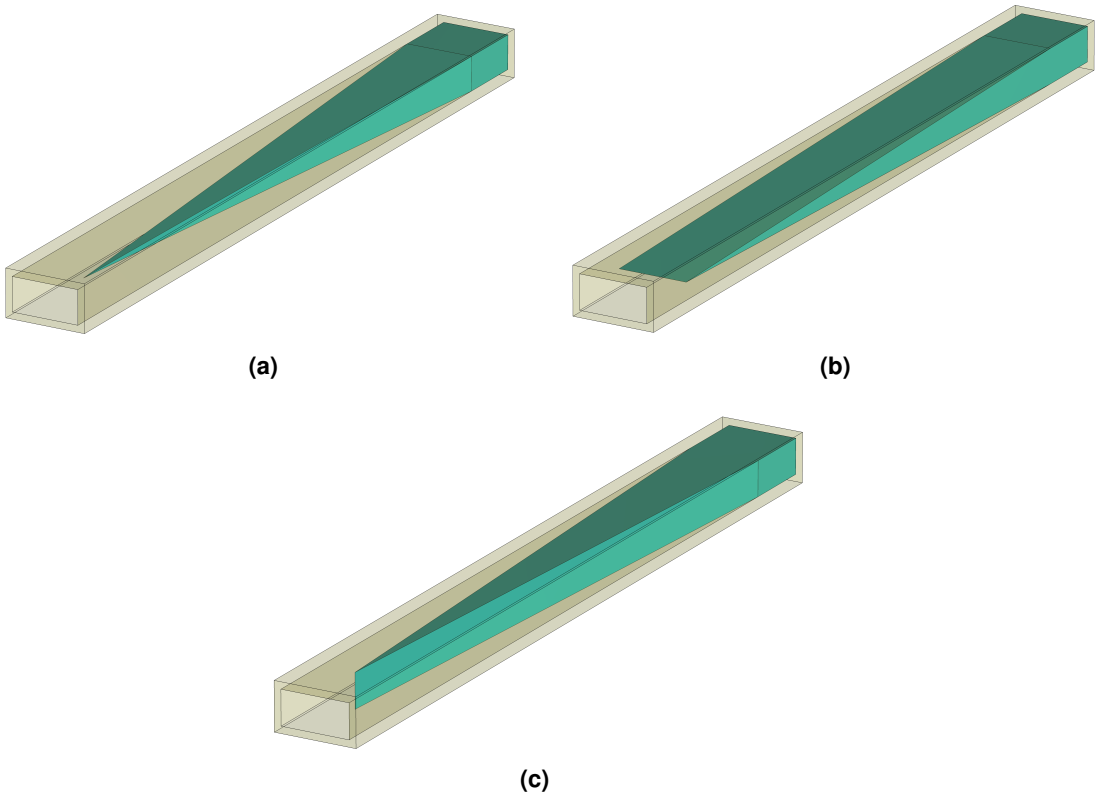

Figure 3.2: Types of tapering sections for dielectric waveguides. (a) Pyramidal taper. (b) Horizontal taper. (c) Vertical taper [14].

- The horizontal taper involves tapering in the horizontal plane. It can improve side-mode suppression but may present alignment challenges during integration.

- The pyramidal taper offers the most symmetric field distribution and potentially the best performance for hybrid modes like E_{11}^{y}. However, it is structurally fragile and very challenging to manufacture with precision.

The E_{11}^{y} mode is a hybrid mode in which the electric field is predominantly polarized in the y-direction, similar to the dominant TE_{10} mode in rectangular metallic waveguides. The taper facilitates a gradual transformation of the field distribution and impedance from the metal waveguide to the dielectric rod. Among the taper types, the pyramidal taper theoretically provides the most efficient coupling to the E_{11}^{y} mode due to its symmetric field transformation along both axes. However, due to its mechanical weakness, especially in small-scale imple-

DOI: 10.7795/110.20250905

mentations, it is not practical for long-term stable applications. In this dissertation, the vertical taper is selected as the optimal design. It balances performance and manufacturability by:

- Providing sufficient coupling efficiency to the E_{11}^{y} mode, as the major electric field component aligns well vertically with the TE_{10} mode field from the metallic waveguide.
- Allowing simpler and more robust fabrication, thereby minimizing the risk of structural failure.

Compared to the horizontal taper and pyramidal taper designs, the vertical taper provides better practical efficiency, making it the optimal choice for the dielectric waveguide tip.

Producing a sharply tapered tip, as shown in Figure 3.2(c), is nearly impossible in practice due to the extremely small size of the dielectric rods used in this frequency range. To address this, the tip of the tapering section is given a rounded shape, as shown in Figure 3.3, making it feasible to fabricate while maintaining good performance. The rounded tip design involves modifying the tapering end with specific diameters to create a smooth tip.

3.1.2 Design of the Trumpet Structure in the Metal Waveguide

The transition between dielectric waveguides with low permittivity and metal waveguides is more challenging, making it difficult to achieve good matching. This difficulty arises because

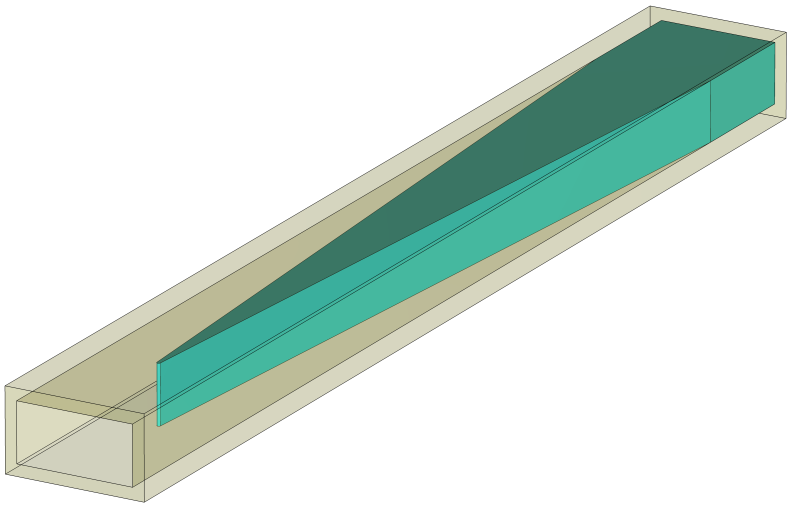

Figure 3.3: Rounded tip of the tapering section of the dielectric waveguide.

electromagnetic fields in low dielectric constant materials propagate partially outside the dielectric rod waveguide [51]. In contrast, materials with high dielectric constants can more effectively confine RF power within the rod, but they are more fragile and difficult to fabricate as transmission lines. Therefore, a trumpet structure is applied to improve the transition between the dielectric rod waveguide with low permittivity and the hollow metal waveguide, as depicted in Figure 3.4.

In the developed design, the trumpet structure was implemented in CST as a circular-arc flare. The flare profile follows the geometry of a circular arc, which can be mathematically described by the general circle equation. The geometry is uniquely defined by the input radius r_0 at the metallic waveguide aperture, the output radius r_L at the dielectric rod interface, and the total flare length L. From these parameters, the arc radius R is determined. The use of a circular-arc flare provides a smooth, continuous curvature that enables a gradual impedance transition while maintaining mechanical simplicity.

The optimization parameters of the trumpet structure include its radius and length, which are adjusted to achieve optimal matching between the dielectric waveguide and the metal waveguide. This structure is integrated into the metal waveguide by truncating a portion of the metal waveguide to create the trumpet shape. The trumpet begins with a circular cross-section and gradually transitions into the rectangular cross-section of the WR-5 metal waveguide. This

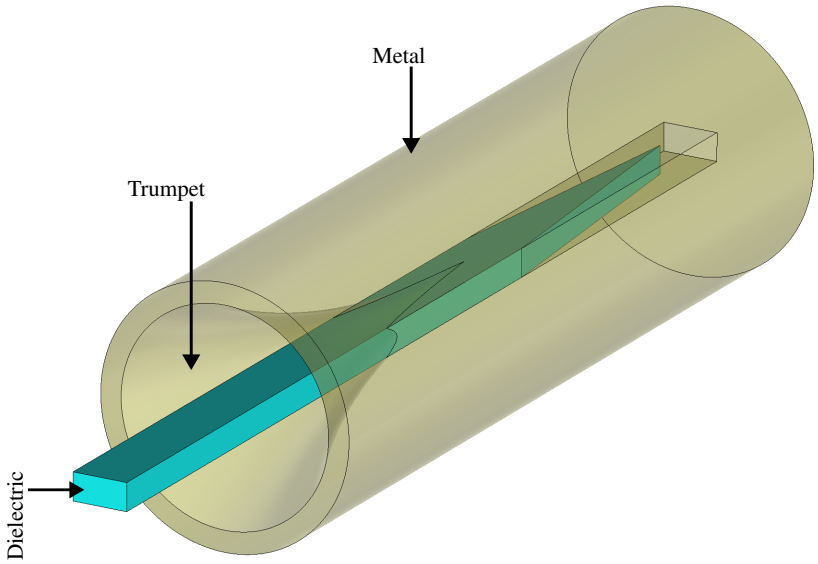

Figure 3.4: Trumpet structure in the metal waveguide [26].

DOI: 10.7795/110.20250905

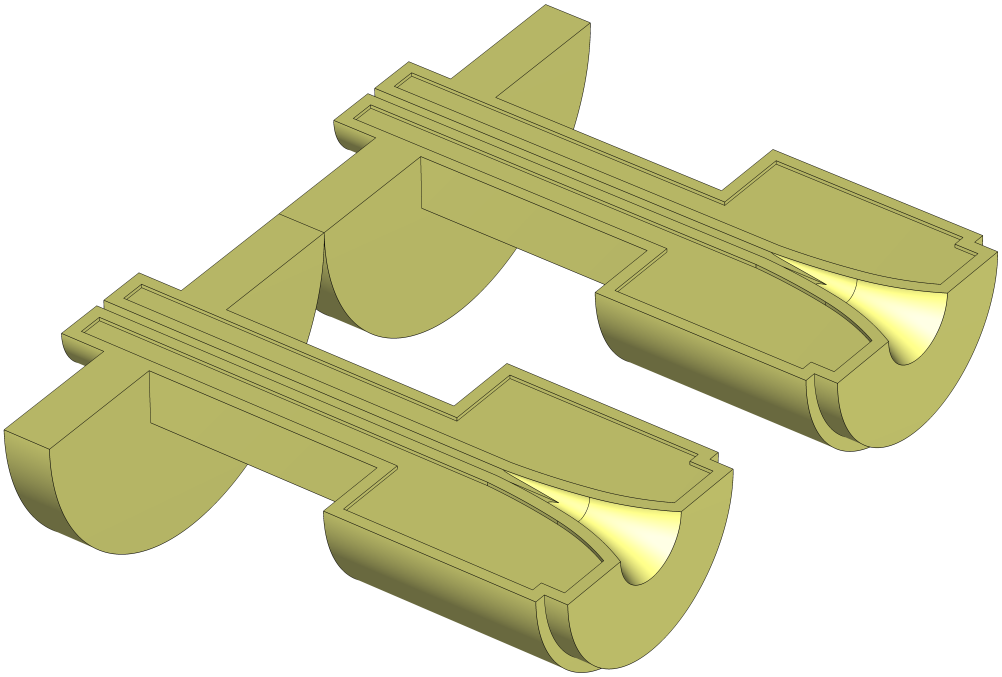

Figure 3.5: Construction drawing of the metal waveguide with the trumpet structure.

smooth geometric transformation facilitates impedance matching, ensuring efficient coupling between the dielectric rod and the metallic waveguide. In the microcalorimeter transmission line, this structure forms a cavity resembling a trumpet. The trumpet geometry significantly improves the transition between the metal waveguide and the dielectric waveguide by enhancing the propagation of electromagnetic fields.

Figure 3.5 shows construction drawing of the metal waveguide with the trumpet structure. The metal waveguide is manufactured using a split-block design. One of the ports features a smooth, gradually expanding flared structure, resembling a trumpet shape. This transition serves as a matching section for coupling electromagnetic waves into or out of the waveguide.

3.1.3 Design of the Transmission Line of the Microcalorimeter

Transmission lines in microcalorimeters must efficiently guide electromagnetic waves from the source to the detector while minimizing losses, reflections, and impedance mismatches. A complete design of the transmission line for the microcalorimeter is shown in Figure 3.6. The design employs a hybrid approach that combines dielectric and metal waveguides, utilizing the

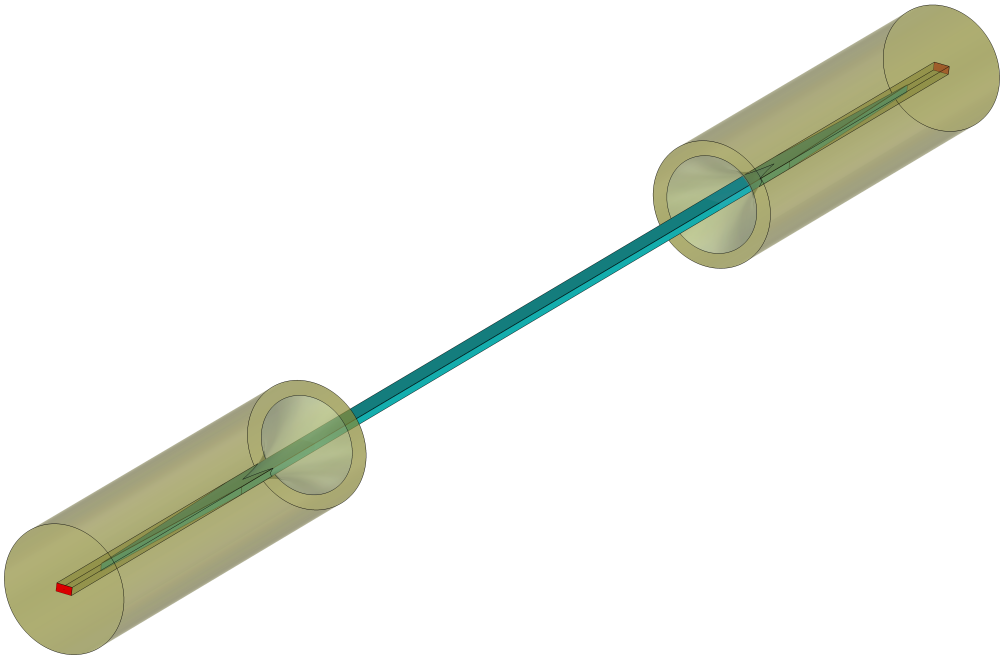

Figure 3.6: Design of the transmission line of the microcalorimeter.

advantages of both to achieve optimal performance. The dielectric waveguide provides low-loss feeding, while the metal waveguide ensures standardized interfacing with WR-5 devices [67].

The microcalorimeter transmission line has an overall length of 178 mm, which is adjusted to align with the overall mechanical design of the microcalorimeter [14], [26]. Tapered sections with rounded shapes are applied to both ends of the dielectric waveguide. Both transitions at the metal waveguide incorporate a trumpet-shaped structure, enhancing the efficiency of wave transmission.

3.2 Simulation of the Microcalorimeter Transmission Line Performance

Comprehensive simulations were carried out using CST Microwave Studio to evaluate the integration of the dielectric waveguide with the metal waveguide, which together form the transmission line of the microcalorimeter. The simulations, performed over the frequency range of 140 GHz to 220 GHz, utilized the finite element method (FEM) with a frequency-domain

DOI: 10.7795/110.20250905

solver. A perfect electric conductor (PEC) was assumed for the metal waveguide, while a lossless dielectric material with a relative permittivity of 2.3, corresponding to the material used in the fabrication of the dielectric waveguide, was employed for the dielectric section. The studies focused on optimizing the transition and impedance matching between the dielectric and metal waveguides by analyzing the impact of the tapering section of the dielectric rod waveguide and the trumpet structure in the hollow metal waveguide.

The tapering sections of the dielectric waveguide were simulated by analyzing three groups of parameters: the geometry of the tapering section, the rounded shape of the tapering section tip, and the length of the tapering section. Furthermore, simulations examined the effects of the trumpet structure and determined the efficient trumpet diameter in the metal waveguide. The main objective of these simulations was to identify the optimal waveguide structure for fabricating the microcalorimeter transmission line.

3.2.1 Simulation of the Geometry of the Tapering Section in the Dielectric Waveguide

This study investigated three types of tapering geometries: tapering in the vertical plane, tapering in the horizontal plane, and pyramidal tapering, as illustrated in Figure 3.2. The simulations aimed to evaluate the performance of the tapering geometry before fabrication, considering production simplicity and the transmission characteristics of the dielectric rod waveguide. All tapering types were simulated using identical parameters, including a tapering section length of 10 mm, a total dielectric rod length of 12 mm, and a relative permittivity of 2.3 for the lossless dielectric material. The only difference among the designs was the geometry of the tapering section.

Figure 3.7 presents the simulation results of the scattering parameters (S-parameters), S_{11} and S_{21}, for all tapering geometries. The results indicate that all three tapering types outperform the non-tapered configuration. The transmission coefficient at the lower end of the frequency range is significantly reduced in the absence of tapering, as the electromagnetic field tends to spread out from the dielectric waveguide. Consequently, tapering the dielectric rod improves the transmission line performance of the microcalorimeter.

Among the tapering geometries, the vertical taper structure exhibited the best performance in the simulations. The return loss of the vertical taper showed the greatest improvement over the other geometries. Additionally, the insertion loss of the vertical taper demonstrated a better transmission coefficient compared to the horizontal taper and performed comparably to the pyramidal taper. This can be attributed to the electromagnetic field being more concentrated

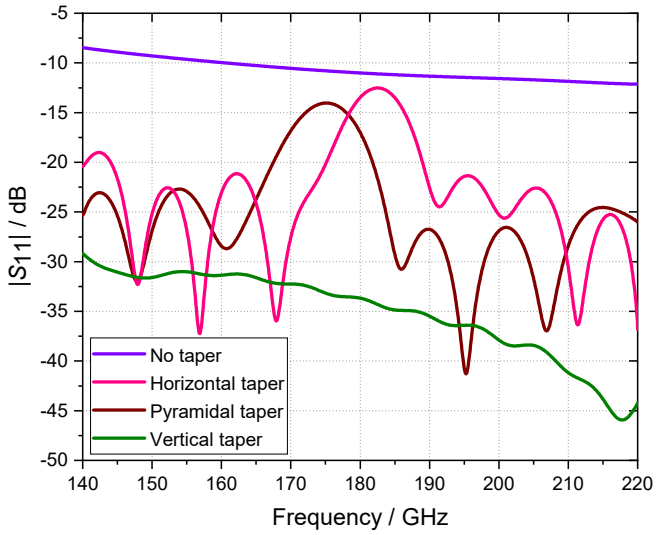

(a)

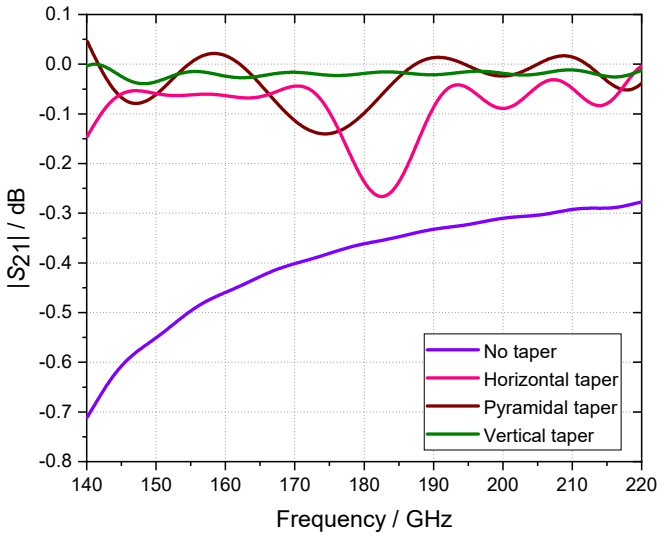

(b)

Figure 3.7: Simulation results for different tapering geometries in the dielectric waveguide [14]. (a) S_{11}. (b) S_{21}.

DOI: 10.7795/110.20250905

in the vertical direction (E-plane) than in the horizontal direction (H-plane) within the metal waveguide. As a result, the vertical taper delivers better performance than the horizontal taper. Moreover, the simulation results for the horizontal taper and pyramidal taper displayed significant fluctuations across the frequency range, whereas the vertical taper provided a smooth response throughout the frequency range. Based on these simulation results, the dielectric waveguide in this study was fabricated with a vertical taper at the tip of the dielectric rod. The vertical plane tapering section was used for subsequent simulations and further analysis.

3.2.2 Simulation of the Round-Shaped Tip Tapering Section in the Dielectric Waveguide

The tip of the tapering section adopted a rounded shape instead of a sharp one. Since achieving a perfectly sharp tip for the tapering section, as shown in Figure 3.2(c), is challenging in practice, simulations were conducted to analyze the effects of a rounded shape at the tapering section tip. These simulations aimed to evaluate the impact of a rounded tip at the end of the dielectric waveguide, as depicted in Figure 3.3. The tapering section was modeled using the Blend Edges function in CST Microwave Studio, with tip radius (r_t) ranging from 0 mm to 0.1 mm. While a radius of 0 mm (a perfectly sharp tip) serves as a theoretical reference, such sharp tips are nearly impossible to fabricate due to their mechanical fragility. In practical terms, a minimum tip radius of approximately 0.05 – 0.1 mm can be achieved using high-precision machining. The total length of the tapering section of the dielectric waveguide in this simulation was approximately 12 mm, with no rounding at the tip (r_t = 0 mm).

The simulation results for the rounded tip of the tapering section are presented in Figure 3.8. As expected, the tapering tip without a rounded shape provided the best simulation results. The reflection coefficient increases with the radius of the tapering tip, with the largest radius (r_t = 0.1 mm) yielding the highest reflection coefficient. However, reflection coefficients for tapered ends with radius of 0.06 mm or less were found to be acceptable.

There was no significant difference in the transmission coefficient between the tapering tip without a rounded shape and the tapering tip with a radius of 0.02 mm. Both configurations also exhibited similar transmission coefficients to a tapering tip with a radius of 0.04 mm, particularly at frequencies above 160 GHz. In contrast, the transmission coefficient decreased significantly for tapering tips with radius of 0.08 mm or larger.

The tapering tip with a radius of 0.04 mm demonstrated a reflection coefficient of less than -20 dB, and its transmission coefficient was nearly equivalent to that of the perfectly sharp tapering tip. Therefore, a tapering section with a rounded tip radius of 0.04 mm is considered

the best option for fabricating the dielectric rod waveguide. By cutting the tip of the tapering section to a radius of approximately 40 μm, the transmission line retains good performance while remaining feasible for fabrication.

3.2.3 Simulation of the Tapering Section Length in the Dielectric Waveguide

The simulation results for the tapering section length can be seen in Figure 3.9. Studying the proportional length of the tapering section is necessary because a long tapering section is neither practical nor durable. Several taper lengths of the dielectric rod waveguide were simulated to determine the optimum dimensions. The values of taper lengths (l_t) were varied from 1 mm to 12 mm. This range was selected to cover both the practical limits of taper fabrication and the expected coupling performance. Although longer tapers (e.g., >12 mm) may offer improved impedance matching, they introduce fabrication challenges due to mechanical fragility.

The matching between the dielectric waveguide and the metal waveguide enhances with a longer tapering section. The reflection coefficients show significant improvement as the taper length increases from 1 mm to 6 mm across the entire frequency range. Tapering sections shorter than 4 mm exhibit relatively high reflection coefficients. However, taper lengths of 6 mm and above demonstrate good and acceptable performance. Only slight improvements in the reflection coefficient are observed for taper lengths longer than 10 mm.

The observation results indicate that increasing the length of the tapering section generally leads to an improvement in the transmission coefficient. However, the transmission coefficients for tapering section lengths between 10 mm and 12 mm were found to be nearly identical, suggesting that extending the taper beyond 10 mm provides negligible additional benefit. Consequently, further increasing the tapering section length would be unnecessary and could introduce practical drawbacks, such as increased fabrication complexity. Based on these observations, a tapering section length of 10 mm is identified as the most efficient choice for the dielectric waveguide in this work.

3.2.4 Simulation of the Effect of the Trumpet Structure in the Metal Waveguide

The trumpet structure was investigated in this research to optimize the transition between the metal waveguide and the dielectric waveguide. To evaluate the effectiveness of the trumpet structure, simulations were performed to analyze its influence on the microcalorimeter transmission line. In these simulations, the trumpet section was modeled as air to accurately repre-

 DOI: 10.7795/110.20250905

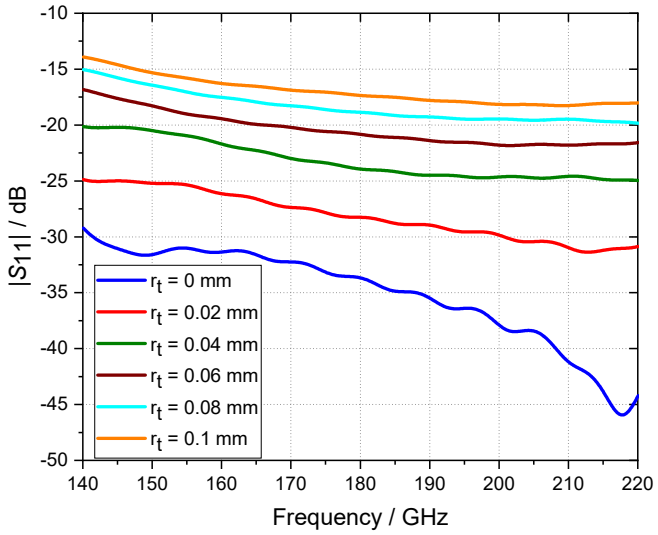

(a)

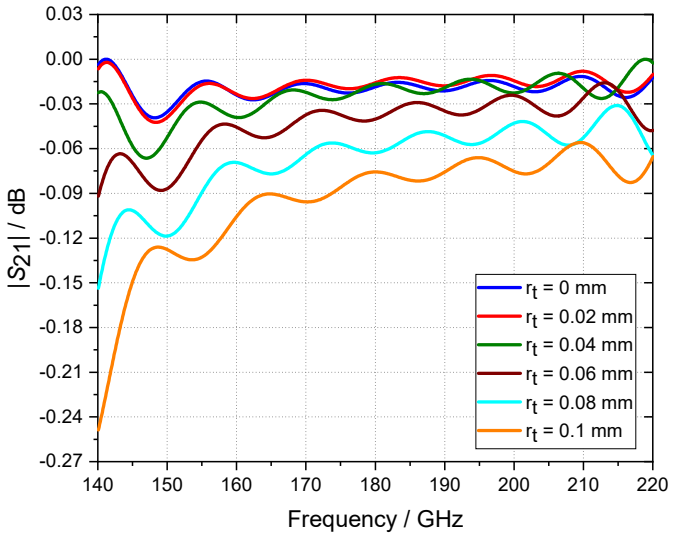

(b)

Figure 3.8: Simulation results of tapering tips with rounded shapes in the dielectric waveguide. (a) S_{11}. (b) S_{21}.

DOI: 10.7795/110.20250905

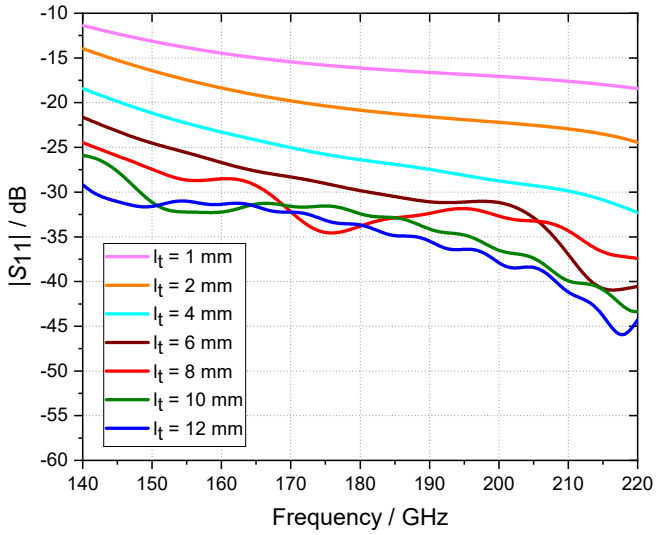

(a)

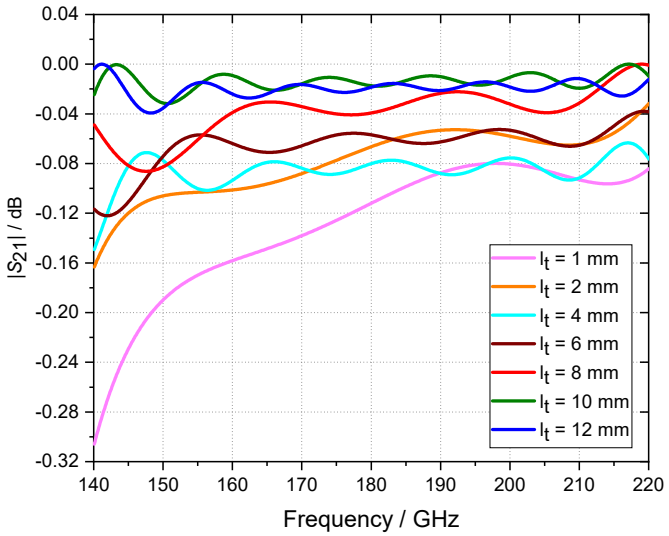

(b)

Figure 3.9: Simulation results for different tapering section lengths in the dielectric waveguide. (a) S_{11}. (b) S_{21}.

DOI: 10.7795/110.20250905

sent the gap between the metal waveguide walls and the dielectric rod throughout the transition. The diameter of the trumpet structure was set to 5 mm. At the start of the trumpet, the wall thickness of the metal waveguide was 1 mm, gradually increasing to 3 mm at the end of the metal waveguide. This configuration provides a smooth transition consistent with the trumpet-shaped geometry, as illustrated in Figure 3.4. In the corresponding simulation of the trumpet structure, the dielectric rod shown in Figure 3.4 was not included, in order to analyze only the effect of the trumpet structure.

Figure 3.10 presents the simulation results for the metal waveguide, both with and without the trumpet structure. For comparative purposes, a model of the metal waveguide without the trumpet structure was also simulated. In this case, the wall thickness of the metal waveguide was uniformly set to 3 mm to maintain similar overall dimensions to the metal waveguide with the trumpet structure. This design choice ensures that the performance differences observed in the simulations can be directly attributed to the presence or absence of the trumpet structure, rather than discrepancies in geometric dimensions.

The metal waveguide without the trumpet structure demonstrated higher reflection losses and less efficient transmission, indicating the need for improvement in its design. To address this issue, a trumpet structure is employed. This structure gradually transforms the cross-sectional dimensions and guiding properties of one waveguide to match those of another, minimizing impedance mismatches. The transmission line incorporating the trumpet structure showed significant enhancement.

3.2.5 Simulation of the Diameter of the Trumpet Structure in the Metal Waveguide

Figure 3.11 depicts the simulation results for trumpet structures with varying diameters of the trumpet opening (d_t), illustrating their impact on the transition between the metal waveguide and the dielectric waveguide. Diameters ranging from 1.5 mm to 6 mm were tested to evaluate their influence on the transmission efficiency and overall performance of the waveguide system. These simulations aim to identify the most suitable trumpet diameter that provides minimal reflections and optimal impedance matching at the transition interface. Since the width of the dielectric waveguide is 1.295 mm, it is a necessary design constraint that the diameter of the trumpet structure exceeds this value. This requirement assures that the trumpet properly encloses the dielectric waveguide, forming the gradual transition characteristic of the trumpet geometry.

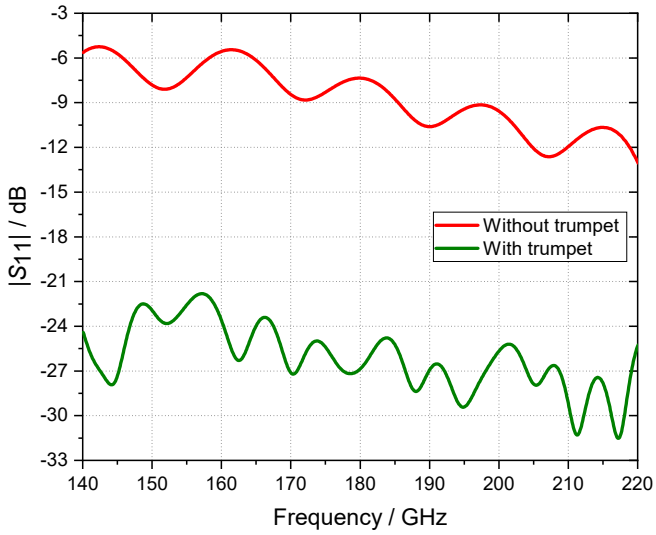

(a)

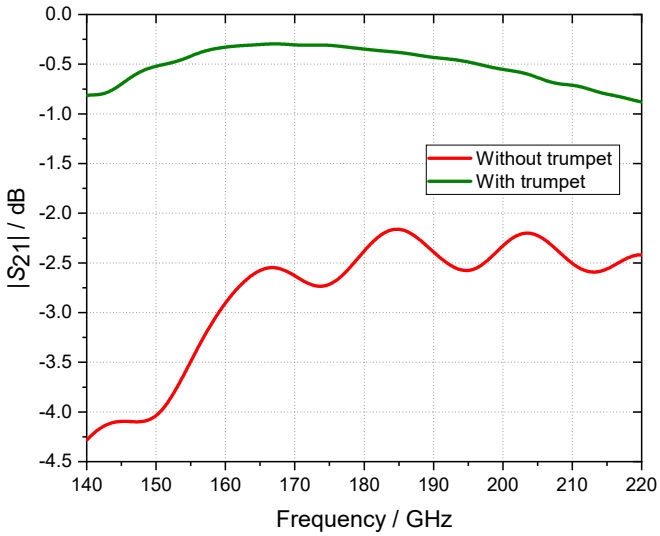

(b)

Figure 3.10: Simulation results of the metal waveguide with and without the trumpet structure. (a) S_{11}. (b) S_{21}.

DOI: 10.7795/110.20250905

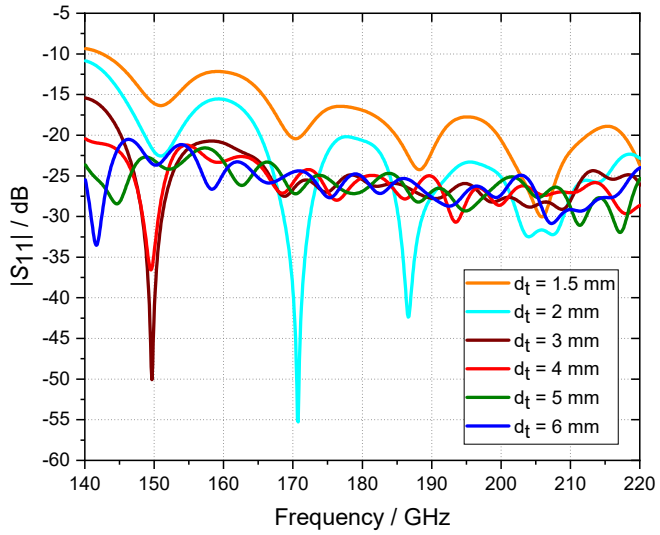

(a)

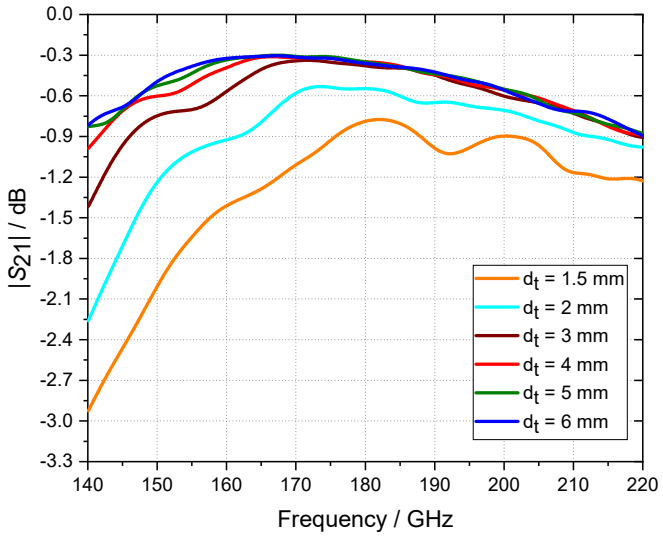

(b)

Figure 3.11: Simulation results of the metal waveguide for different diameters of the trumpet opening. (a) S_{11}. (b) S_{21}.

DOI: 10.7795/110.20250905

Trumpets with diameters smaller than 3 mm demonstrated poor performance, characterized by high reflection coefficients and low transmission coefficients. These results arise from an insufficient transition area, leading to significant reflections at the interface between the metal and dielectric waveguides. The performance is unsuitable for applications requiring high accuracy, such as millimeter-wave power measurement standards.

On the other hand, trumpets with diameters of 4 mm and larger exhibited satisfactory performance, with significantly improved transmission coefficients and reduced reflections. Among the tested configurations, the simulation results for trumpet diameters in the range of 4 mm to 6 mm were nearly identical, and further increases in diameter had minimal impact on overall performance. However, the 4 mm diameter trumpet showed greater variations in the reflection coefficient at certain frequencies. Trumpets with diameters between 5 mm and 6 mm demonstrated more stable performance across the frequency range, making them more reliable for use in microcalorimeter transmission lines. Based on these findings, this study recommends trumpet diameters in the range of 5 mm to 6 mm for the transition between the metal and dielectric waveguides.

The size of the trumpet structure is closely tied to the cross-sectional dimensions of the hollow rectangular metal waveguide to which it is coupled. This relationship ensures proper alignment and impedance matching between the metal and dielectric waveguides. Larger hollow metal waveguides with greater cross-sectional areas require proportionally larger trumpet diameters to maintain optimal transition performance. The diameter of the trumpet must be carefully scaled to accommodate the electromagnetic field distribution and minimize reflections at the interface between the waveguides. For instance, the dimensions of the trumpet structure for a WR-3 metal waveguide are inherently smaller than those required for a WR-5 metal waveguide. This is because the WR-3 waveguide has a smaller cross-section compared to the WR-5 waveguide, which demands a corresponding adjustment in the trumpet design to match the field propagation characteristics.

3.2.6 Simulation of the Transmission Line of the Microcalorimeter

The simulation of the complete microcalorimeter transmission line is performed by considering the optimal configuration obtained from simulations of the tapering section of the dielectric waveguide and the trumpet structure of the metal waveguide. The dimensional settings of the transmission line model, as shown in Figure 3.6, are based on these previous simulations. This approach balances achieving the best performance results while maintaining ease of fabrication for the transmission line.

 DOI: 10.7795/110.20250905

The simulation results for the transmission line of the microcalorimeter are characterized by the reflection coefficient and the transmission coefficient across the frequency range from 140 GHz to 220 GHz. The S_{11} parameter, as shown in Figure 3.12(a), measures the impedance mismatches along the transmission line. In this frequency range, the return loss is better than 20 dB, indicating good impedance matching.

The S_{21} parameter, presented in Figure 3.12(b), represents the transmitted power through the transmission line. The transmission coefficient remains close to 0 dB, with minor variations across the frequency band. This result demonstrates that the transmission line exhibits low insertion loss, allowing efficient power transfer across the specified frequency range. The flatness and stability of the insertion loss indicate consistent performance and minimal dispersion, which are critical for the operation of the microcalorimeter, where precise RF power measurements are required.

The combination of excellent reflection and transmission coefficients highlights the high efficiency and reliability of the transmission line design. These characteristics ensure that the transmission line delivers electromagnetic signals with minimal power loss, enabling accurate detection of thermal energy in microcalorimeter applications.

3.3 Thermal Simulation of Microcalorimeter Transmission Line

In this study, thermal simulations were conducted to examine heat distribution in the microcalorimeter transmission line. Understanding the thermal behavior of these materials and structures is essential to ensure reliable performance, as temperature variations can significantly affect the performance of the microcalorimeter.

Thermal simulations were performed using the EM-Thermal Coupling Simulation project in CST Microwave Studio, which integrates electromagnetic field analysis with thermal analysis. The thermal simulation was carried out using the finite element method in the frequency domain. Boundary conditions, such as ambient temperature, were also defined to simulate realistic operating conditions.

Both metal and dielectric waveguides are tested in the thermal simulation. The modeling structure for the thermal isolation section is designed according to the cross-section of the standardized WR-5 waveguide. Parameters of the thermal isolation section are simulated to determine optimal results. Additionally, comparisons between metal and dielectric waveguides

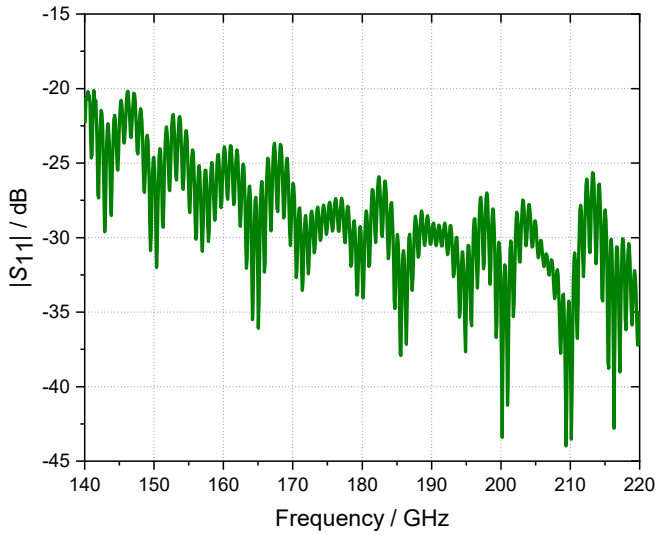

(a)

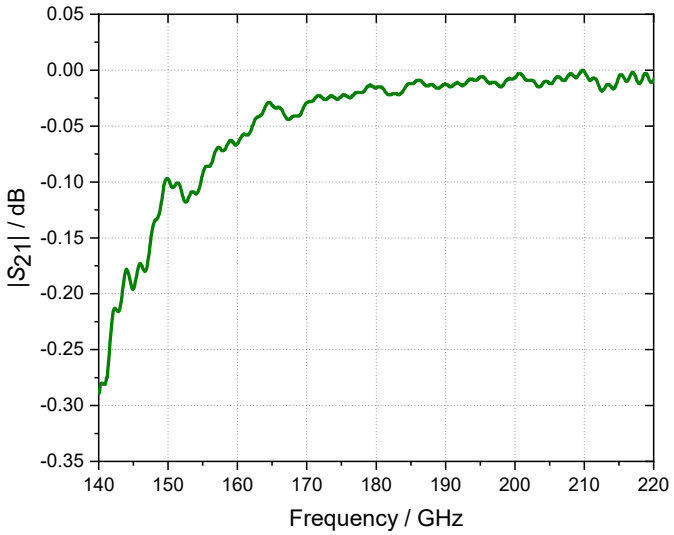

(b)

Figure 3.12: Simulation results of the transmission line of the microcalorimeter. (a) S_{11}. (b) S_{21}.

DOI: 10.7795/110.20250905

are conducted to confirm that dielectric waveguides do not require additional thermal isolation sections.

3.3.1 Thermal Simulation of Metal Waveguide without Thermal Isolation Section

Figure 3.13 shows the thermal simulation model of the metal waveguide without a thermal isolation section. Copper with a thermal conductivity of 400 W/(mK) is used as the material for the metal waveguide in the thermal simulation. The thermal condition of the transmission line is set at 23 °C. An external heating source with a temperature of 28 °C is added to the input port of the metal waveguide. This external temperature source is not part of the microcalorimeter measurement system and acts as an unwanted heat source. The purpose of this additional heating is to study how the external environment affects the measurement of RF power in the microcalorimeter system.

The simulation results for the metal waveguide without the thermal isolation section are shown in Figure 3.14. The temperature of the metal waveguide along its entire length, up to the output port, increases to 28 °C as external heating from the heat source is transferred into the waveguide. Consequently, this external heating is measured as part of the RF power, leading to inaccuracies in the measurement system. Therefore, a thermal isolation section is necessary to address this issue [68].

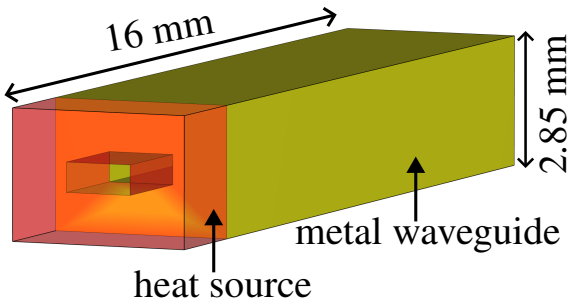

Figure 3.13: Thermal simulation model of a metal waveguide without a thermal isolation section.

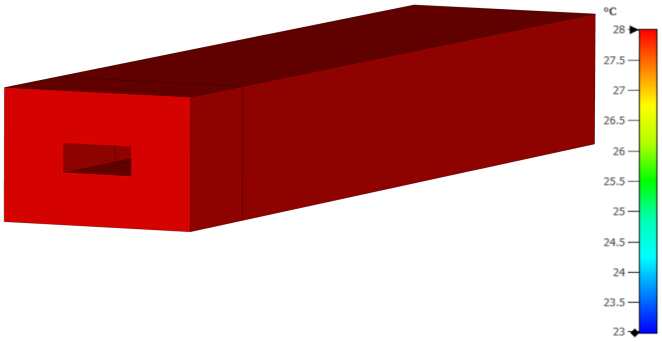

Figure 3.14: Thermal simulation results for the metal waveguide without a thermal isolation section.

3.3.2 Thermal Simulation of Metal Waveguide with Thermal Isolation Section

Custom-made thermal isolation sections are typically used in conjunction with commercial transmission lines to form the complete RF feeding line for a microcalorimeter. The thermal isolation section is constructed from ABS material (ϵ_r = 2.3) coated with a copper layer with a thickness of 0.01 mm.

Figure 3.15 illustrates the thermal simulation model of the metal waveguide with the thermal isolation section. A heating source with a temperature of 28 °C is applied to the metal waveguide. The thermal isolation section is positioned between the heating source and the input of the metal waveguide. The length of the thermal isolation section is specified as 1 mm.

As shown in Figure 3.16, the temperature of the metal waveguide behind the thermal isolation section remains stable at 23 °C, consistent with the thermal setting. The thermal isolation section successfully eliminates the external heating source of 28 °C, effectively isolating the metal waveguide from unwanted heating effects. As a result, only the RF signal from the source is delivered to the output port, without the unwanted additional heating. This demonstrates the importance of the thermal isolation section in providing effective heat-blocking performance.

3.3.3 Thermal Simulation of Parameters of Thermal Isolation Section in the Metal Waveguide

Key parameters of the thermal isolation section, such as its length and the thickness of the metallic coating on the waveguide wall, were simulated to determine the most effective design. The transmission line model used in these simulations is based on Figure 3.15, with adjust-

 DOI: 10.7795/110.20250905

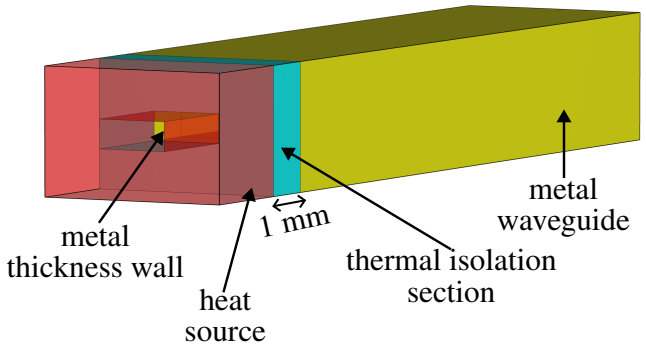

Figure 3.15: Thermal simulation model of a metal waveguide with a thermal isolation section.

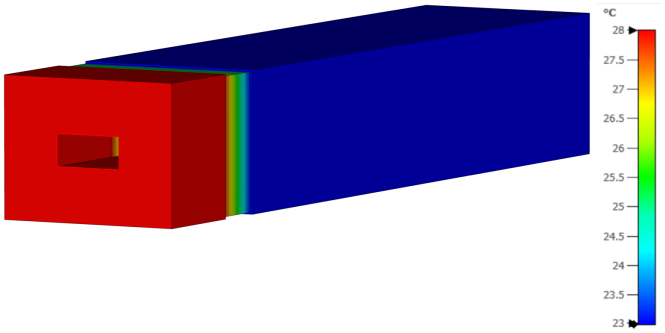

Figure 3.16: Thermal simulation results for the metal waveguide with a thermal isolation section.

ments made to specific parameters. By appropriately configuring the parameters of the thermal isolation section, the influence of the external heating can be effectively minimized.

The length of the thermal isolation section was varied from 0.1 mm to 2.5 mm to identify the optimal design. The total length of the transmission line was 16 mm. Figure 3.17 presents the simulation results for the length of the thermal isolation section. The temperature rises above 23 °C along the entire waveguide length, extending to the output port when the isolation section length is less than 1 mm. However, for lengths of 1 mm or more, the temperature remains stable at 23 °C. These results indicate that the transmission line does not require a long thermal isolation section, as a length of 1 mm or greater achieves the same thermal performance. Therefore, a thermal isolation section with a length of 1 mm is preferred for its efficiency.

The thickness of the metal waveguide wall in the isolation section was also investigated, with values ranging from 0.0005 mm to 0.3 mm. Figure 3.18 shows the simulation results for the wall thickness. During these simulations, the length of the thermal isolation section was fixed at 1 mm. In practice, wall thicknesses ranging from 0.01 mm to 0.03 mm offer a good

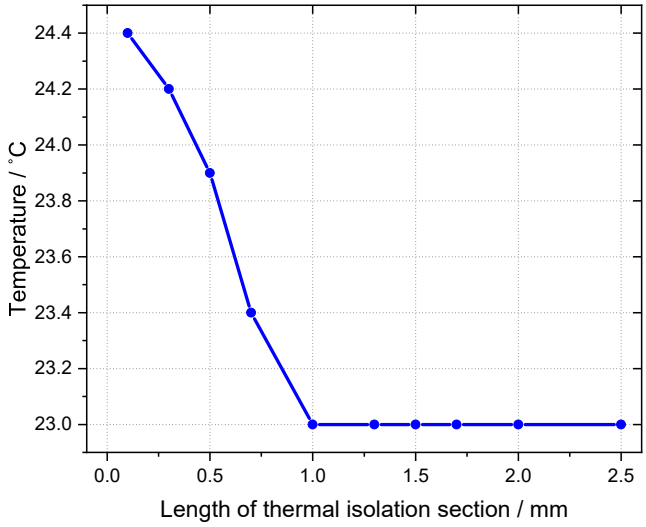

Figure 3.17: Thermal simulation results for the length of the thermal isolation section [68].

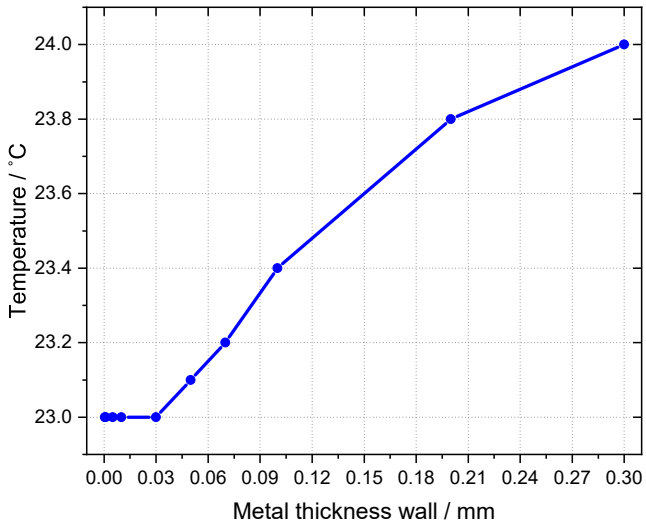

Figure 3.18: Thermal simulation results for the thickness of the metal coating on the waveguide walls in the thermal isolation section [68].

DOI: 10.7795/110.20250905

compromise between manufacturability and thermal isolation performance. A wall thickness of 0.03 mm or less keeps a stable temperature of 23 °C. However, as the wall thickness increases beyond 0.03 mm, the temperature rises due to the reduced effectiveness of the thermal isolation section. To simplify fabrication while maintaining thermal performance, a wall thickness of 0.01 mm is recommended. The coating is made of copper and then layered with gold.

3.3.4 Thermal Simulation of Dielectric Waveguide

Figures 3.19 and 3.20 present the thermal simulation model and results for the dielectric waveguide, respectively. All other simulation parameters, including transmission line dimensions, boundary conditions, ambient temperature, external heat source, and simulation settings, were kept identical to those used in the metal waveguide simulations. This ensures a direct and meaningful comparison of the performance between the metal waveguide with the thermal isolation section and the dielectric waveguides.

Unlike metal waveguides, the dielectric waveguide itself can act as a thermal isolation section, eliminating the need for an additional thermal isolation section. This simulation aims to verify that thermal isolation is unnecessary for dielectric waveguides. As in the simulations for the metal waveguide, the thermal condition inside the transmission line is set at 23 °C,

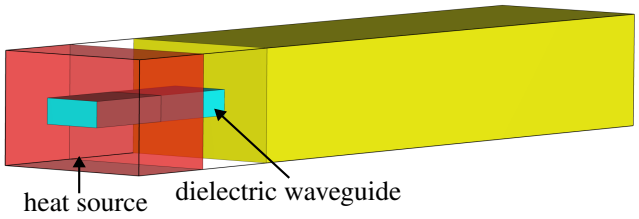

Figure 3.19: Thermal simulation model of the dielectric waveguide

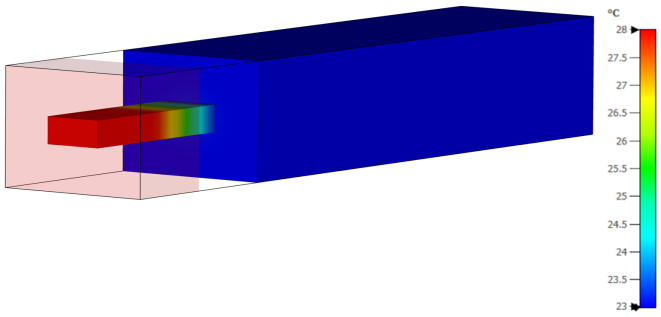

Figure 3.20: Thermal simulation results for the dielectric waveguide

with an external heat source of 28 °C applied to the model. The dielectric waveguide in this simulation is composed of ABS material. The thermal properties of ABS used in the simulation are: thermal conductivity of 0.2 W/m·K, specific heat capacity of 1300 J/kg·K, and density of 1080 kg/m³. These values were set in the CST material definition to accurately simulate the heat conduction behavior of the dielectric waveguide.

The simulation results show that the dielectric waveguide maintains a stable temperature of 23 °C at the output port of the transmission line, which is similar to the results for the metal waveguide with a thermal isolation section. As a result, the power-measuring section accurately detects only the RF signal. This confirms that dielectric waveguides do not require additional thermal isolation sections, offering a significant advantage when used as transmission lines for microcalorimeters. Therefore, the transmission line design in this study utilizes dielectric waveguides without additional thermal isolation sections.

 DOI: 10.7795/110.20250905

4 Fabrication of Waveguide Microcalorimeter

Fabrication of a waveguide microcalorimeter operating in the frequency range of 140 GHz to 220 GHz requires precise machining processes due to the small dimensions of the waveguide components at these high frequencies. Advanced machining techniques and specialized equipment are necessary to keep dimensional tolerances within acceptable limits. Maintaining these tolerances is essential for minimizing signal degradation and verifying the accuracy of the microcalorimeter measurement.

Construction of the transmission lines for the microcalorimeter is challenging due to the integration of extremely small hollow transition sections made of PEEK and metal waveguides, as well as the use of very thin dielectric rod waveguides. The feeding line and dummy line of the microcalorimeter are built from scratch at PTB, following the design and simulation process. The thermopile and thermal jacket have been modified for the new microcalorimeter. Transfer standards and dummy loads are manufactured in collaboration with Rohde & Schwarz. A signal source is integrated with other devices to generate a stable signal for the desired frequency measurement. All components are assembled to form a complete waveguide microcalorimeter measurement system.

4.1 Fabrication of the Metal Waveguide

The rectangular waveguide parts serve as the transition sections of the transmission line, manufactured in a split-block design using brass for one port and PEEK material for the other port. Trumpet-shaped structures with diameters of 5.5 mm are incorporated into the transition sections. Fabrication of the metal waveguide is particularly complex due to the small dimensions of the hollow waveguide (0.648 mm in height and 1.295 mm in width) and the high precision required for holes and dowels. In practice, a fabrication tolerance of approximately 1 % of the waveguide aperture width (around 13 µm) is maintained [69], [70]. This tight tolerance is essential to minimize discontinuities that could degrade measurement accuracy. The holes and dowels are necessary for assembling the standardized waveguide interfaces and establishing connections between the microcalorimeter transmission line, the RF signal source, and the transfer standard.

A computer numerical control (CNC) machine is the primary tool used for fabricating both metal and PEEK waveguide components. This versatile machine can shape and cut complex geometries with high precision. The CNC system employed in this process achieves a posi-

tional accuracy of up to ±1 µm [71], enabling the accurate formation of the rectangular hollow waveguide, dowel holes, and trumpet-shaped transitions. The CNC machine operates based on programmed instructions derived from computer-aided design (CAD) models of the waveguide components. CAD drawings of the metal and PEEK waveguides are loaded into the CNC machine, which executes the design instructions. The waveguide components are manufactured in half pieces and later joined together. While the brass waveguide can be directly employed as part of the microcalorimeter transmission line after adding a standard thin gold layer, the PEEK waveguide requires several metallization steps to assure conductivity.

The transition at the input port of the microcalorimeter transmission line is entirely constructed from metal. Metal waveguides are typically made from materials such as brass, aluminum, copper, or other low-resistivity metals. For this fabrication, brass is selected due to its high conductivity, strength, ductility, and excellent machinability [63], [72]. The metal waveguide is gold-plated to enhance durability and performance, resist chemical corrosion, and withstand high-temperature oxidation over time [73].

Figure 4.1 illustrates the mechanical fabrication process of the metal waveguide, starting with the preparation and cleaning of the brass block material. The block is cut to the size specified in the design and split into two halves, each forming one part of the waveguide. The hollow waveguide is precisely machined at the center of each part, with dimensions equal to half the standard size of the WR-5 waveguide.

The production process continues with the creation of the trumpet structure and joint holes, which are used to combine the two halves of the metal waveguide. The connecting parts of the standardized interface flanges are fabricated to enable the metal waveguide to interface with other devices. The flanges are designed to be compatible with commercially available connectors.

The completed metal waveguide is shown in Figure 4.2, with a total length of 48 mm. The aperture of the fabricated waveguide matches the dimensions of the WR-5 waveguide, ensuring the efficient delivery of electromagnetic waves in the 140 GHz to 220 GHz frequency range. To form a complete microcalorimeter transmission line, the two halves of the metal waveguide are combined during the assembly process with the dielectric rod waveguide and the PEEK waveguide.

The transition at the output port of the microcalorimeter transmission line (located inside the thermal jacket) is fabricated from PEEK coated with a thin gold layer. The gold was applied using sputtering, with a thickness of approximately 1 µm, which is equivalent to about five times the skin depth at the WR-5 frequency band. This metallization enables the PEEK substrate to support electromagnetic wave propagation. PEEK is utilized to extend thermal insulation to the

 DOI: 10.7795/110.20250905

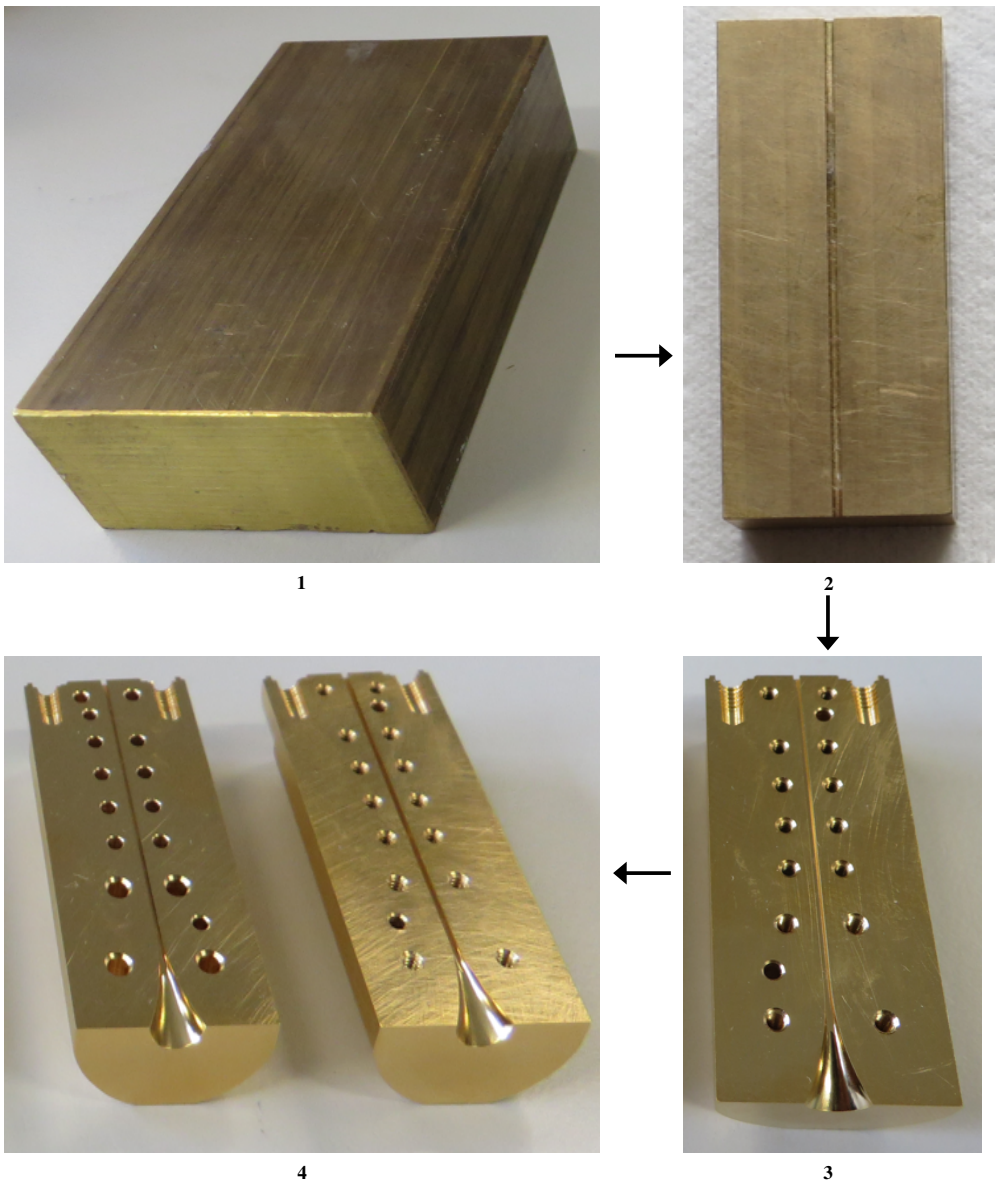

Figure 4.1: Manufacturing process of the metal waveguide.

microcalorimeter reference plane. Additionally, PEEK offers structural flexibility, enabling it to accommodate bending in the microcalorimeter transmission line [74].

PEEK is particularly suited for applications where thermal stability is critical [75]. Since the microcalorimeter is fundamentally a temperature-measuring device, PEEK serves as an ideal material for the transmission line. Its low thermal conductivity helps minimize heat trans-

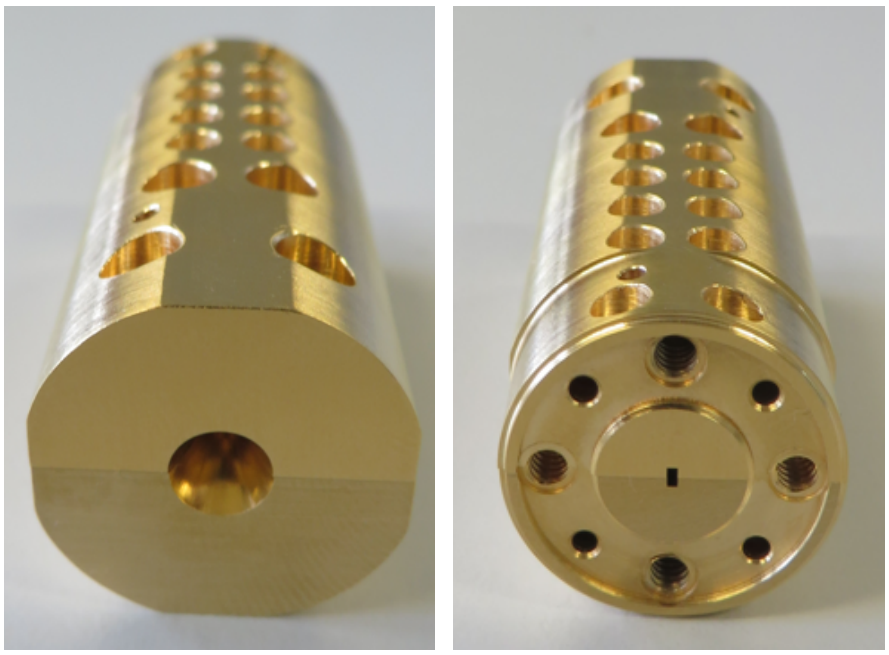

Figure 4.2: Metal waveguide at both ports (left and right sides of the figure).

fer to surrounding components. With a thermal conductivity of approximately 0.29 W/m·K [62], [76], which is significantly lower than that of metals such as brass or gold, PEEK effectively limits heat conduction within the transmission line, ensuring that RF power measurements remain accurate.

The mechanical fabrication process for the PEEK waveguide is similar to that of the metal waveguide, with the additional step of metallizing the PEEK waveguide. The PEEK material block is processed into individual pieces to form the transmission line of the microcalorimeter, as illustrated in Figure 4.3. The dimensions of the PEEK waveguide match those of the metal waveguide; however, its flange design differs to accommodate thermal insulation functions. Figure 4.4 presents the final metallized PEEK waveguide.

4.2 Fabrication of the Dielectric Waveguide

The fabrication process of the dielectric waveguide, which functions as the feeding line in the microcalorimeter transmission line, is illustrated in Figure 4.5. A dielectric material with a low dielectric constant ($\epsilon_r = 2.3$), namely high-density polyethylene (HDPE), is used to fabricate the dielectric waveguide. HDPE exhibits low dielectric loss and high mechanical stability.

DOI: 10.7795/110.20250905

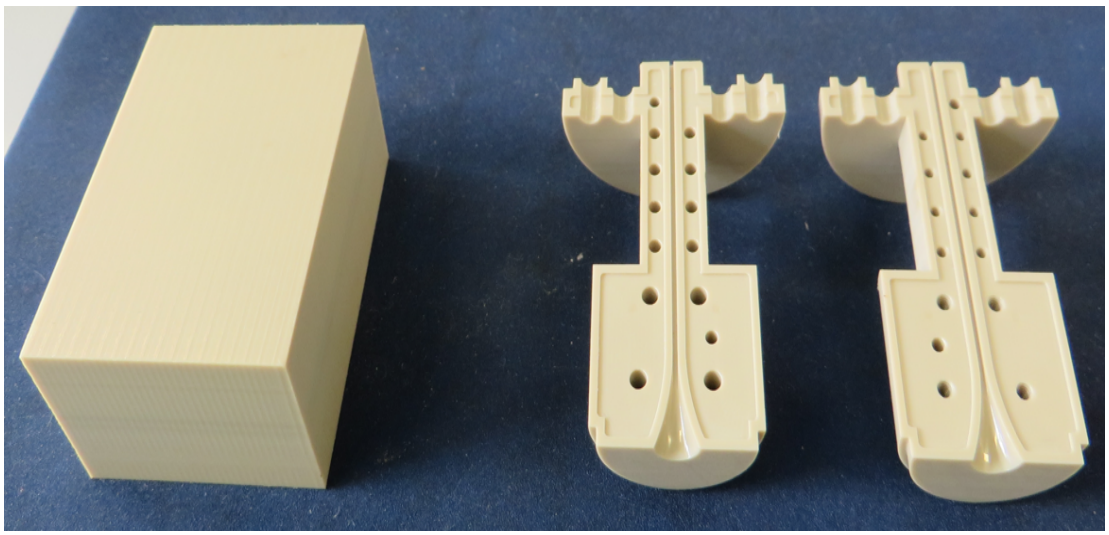

Figure 4.3: Manufacturing process of the metal-coated PEEK hollow waveguide.

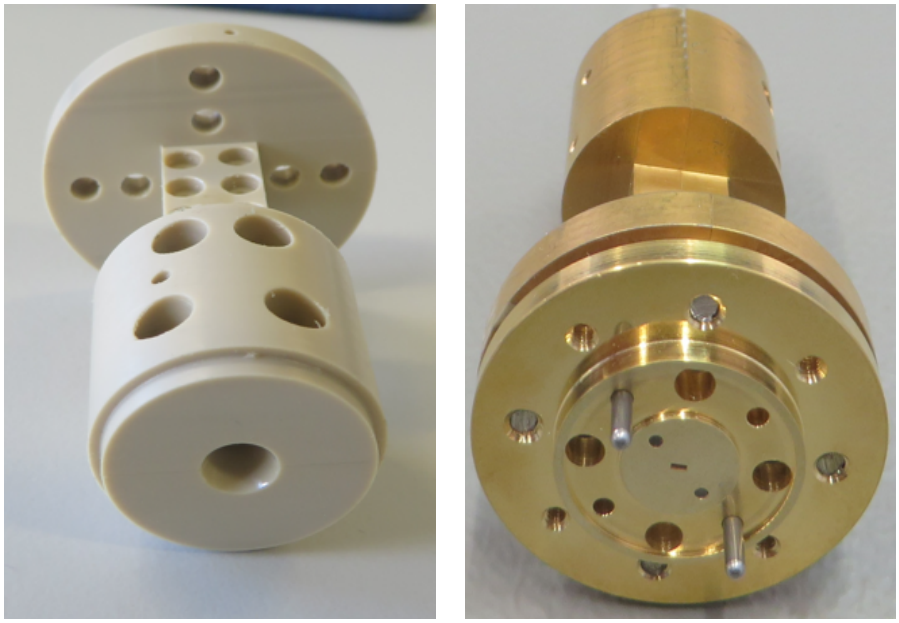

Figure 4.4: Metal-coated PEEK hollow waveguide. The left side of the figure shows the-uncoated PEEK waveguide, while the right side shows the metallized PEEK waveguide.

DOI: 10.7795/110.20250905

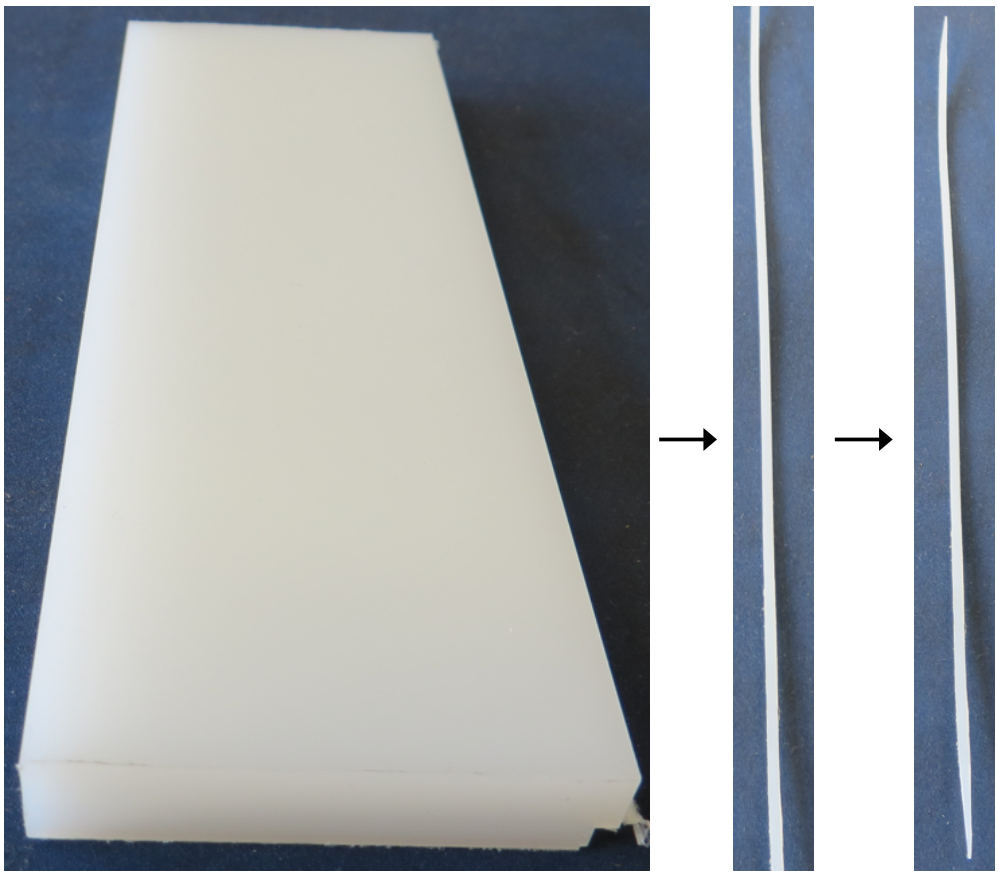

Figure 4.5: Step by step fabrication process of the dielectric waveguide from HDPE. From left to right: raw HDPE block, machined rod shape, and final tapered dielectric waveguide.

Furthermore, HDPE has demonstrated its effectiveness as a substrate material in various microwave components [77], [78]. Consequently, HDPE is chosen as the material for the dielectric waveguide in the microcalorimeter transmission line.

The HDPE material is first prepared by cutting it into a uniformly shaped rod. This initial shaping verifies that the material matches the inner dimensions of the waveguide opening in the metal waveguide, thereby ensuring structural integrity and optimal performance within the microcalorimeter transmission line. Precision machining techniques, including CNC micromachining and laser cutting, are employed to achieve the required dimensional accuracy. The fabrication of the dielectric waveguide requires high dimensional precision to ensure a proper fit within the metal waveguide and to maintain consistent electromagnetic performance. In

DOI: 10.7795/110.20250905

particular, the CNC micromachine used in this work must achieve tight tolerances on both the cross-sectional dimensions of the dielectric rod and the geometry of its tapered ends.

Both ends of the dielectric waveguide are tapered on the vertical sides. According to the simulation results, the tapered section is manufactured with a length of 10 mm at each tip. The total length of the dielectric waveguide, from end to end, is approximately 174 mm. After fabrication, the dielectric waveguide is assembled with the metal waveguide to form a complete microcalorimeter transmission line. Alignment tools and fixtures are utilized during assembly to confirm precise positioning.

4.3 Construction of the Transmission Line for the Microcalorimeter

In this work, the construction of the microcalorimeter transmission line involves the integration of three main components: a dielectric rod waveguide, a metal-coated PEEK hollow waveguide, and a metal waveguide. The dielectric rod waveguide is utilized as the primary transmission medium due to its superior performance in propagating millimeter-wave signals with low losses. The metal-coated PEEK hollow waveguide and the metal waveguide serve as transition elements, facilitating smooth transitions between the dielectric rod waveguide and other devices.

One end of the dielectric rod waveguide is inserted into the metal waveguide, while the other end is connected to the metal-coated PEEK hollow waveguide. The tapered tips of the dielectric rod waveguide are joined to the transition sections through a trumpet structure at one port of each transition section, as shown on the left side of Figures 4.2 and 4.4. The right sides of these figures are connected to other devices, such as the RF source and the transfer standard.

To protect the dielectric rod waveguide and extend its durability, a plastic tube equipped with holders is used as a protective cover. This tube provides physical protection against external forces or environmental factors that could potentially damage the waveguide. To ensure that the plastic protective tube does not interfere with the propagating modes of the dielectric rod waveguide, its inner diameter must be sufficiently larger than the width of the dielectric waveguide. It is recommended that the inner diameter be at least three times the width of the dielectric rod to minimize interaction with the electromagnetic field. For mechanical purposes in this design, the inner diameter of the protective tube is set equal to the diameter of the trumpet structure in the metal waveguides, which is significantly larger than the diameter of the dielec-

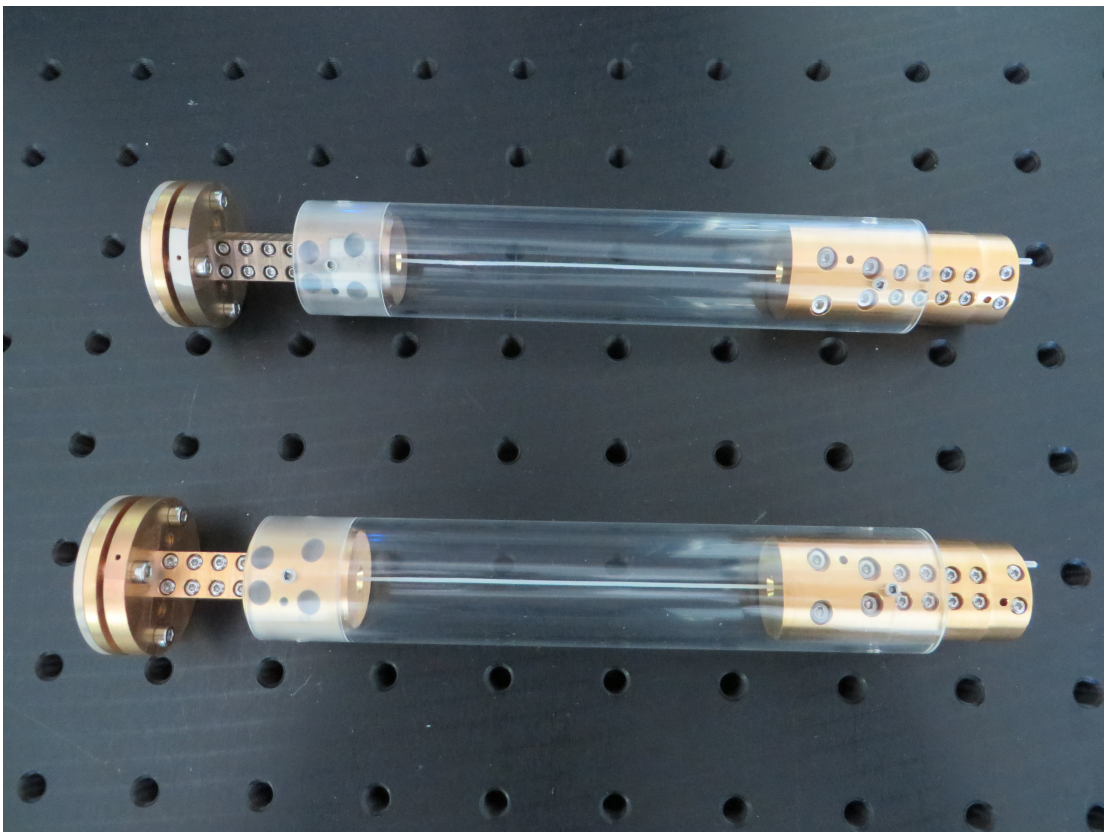

Figure 4.6: The complete transmission line used in the waveguide microcalorimeter, consisting of one feeding line and one reference line. The assembly includes a dielectric waveguide with tapered transitions, trumpet-shaped metal waveguide connectors at both ends, and a plastic protective tube.

tric waveguide. The holders within the tube secure the dielectric rod waveguide in position within the transmission line.

Figure 4.6 shows the complete transmission line of the microcalorimeter. The dummy line of the microcalorimeter is constructed identically to the feeding line. The metal waveguide, which forms one port of the transmission line, is positioned at the top of the microcalorimeter and connected to the millimeter-wave signal source. The metal-coated PEEK hollow waveguide, forming the second port, is located at the bottom of the microcalorimeter and linked to the power sensor.

The precise geometrical dimensions of the various components that constitute the microcalorimeter transmission line are listed in Table 4.1. This table serves as a comprehensive

 DOI: 10.7795/110.20250905

Table 4.1: Geometrical dimensions and recommended tolerances for the components of the microcalorimeter transmission line.

Component	Dimension	Tolerance	Notes
Overall transmission line	178 mm	±0.5 mm	Total length of the microcalorimeter transmission line.
Dielectric waveguide	174 mm	±0.5 mm	Includes 10 mm tapered sections at both ends; dielectric constant = 2.3.
Metal waveguide	48 mm	±0.1 mm	Trumpet structure incorporated; transition section as the input port.
Metal-coated PEEK hollow waveguide	48 mm	±0.1 mm	Trumpet structure incorporated; transition section as the output port.
Tapered sections	10 mm	±0.05 mm	Both ends of the dielectric waveguide are tapered on the vertical sides.
Trumpet structure	5.5 mm	±0.05 mm	Diameter of the trumpet structure in the transition section.
Hollow waveguide	0.648 mm (height) 1.295 mm (width)	±0.005 mm	Cross-section of the hollow waveguide [79].

reference for understanding the structural design of the transmission line of the microcalorimeter in the frequency range of 140 GHz to 220 GHz.

4.4 Assembly of the Waveguide Microcalorimeter

The assembly of the waveguide microcalorimeter involves the integration of multiple components, including the millimeter-wave power source module, transmission lines, transfer standard, dummy load, thermopile, thermal jacket, and DC devices. These components are carefully positioned and precisely interconnected to build optimal system performance. The assembly process starts with positioning the transmission line on the microcalorimeter base extension. The microcalorimeter base extension comprises two distinct parts, as depicted in Figure 4.7. This base extension provides the foundation for the entire system, assuring stability and proper alignment of all subsequent components while being designed to offer structural support and accommodate the symmetrical layout of the twin-line configuration.

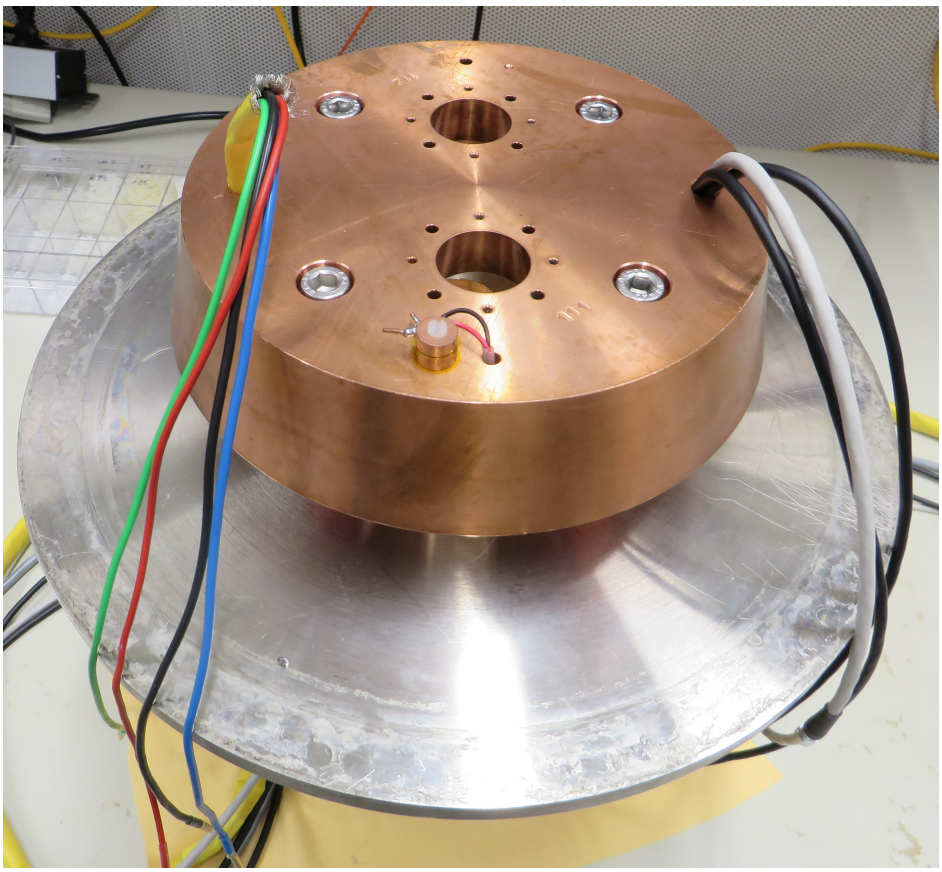

Figure 4.7: Microcalorimeter base extension.

A stable millimeter-wave power source is essential for the development of the waveguide microcalorimeter. To ensure this stability, the source must provide a consistent output with minimal power fluctuations. This is accomplished by integrating additional stabilization devices with the signal source to maintain a steady millimeter-wave signal throughout operation. The power source module comprises a signal generator, multiplier, isolator, filter, directional coupler, power sensor, and power meter. The signal generator operates at frequencies up to 67 GHz. A multiplier with a multiplication factor of 6 extends the frequency range to 140 GHz–220 GHz. The waveguide filter minimizes harmonic signals generated by the multiplier. An isolator reduces unwanted influences from the signal generation parts on the power sensor, such as a poor or varying source match.

The combination of a directional coupler, thermoelectric sensor, and power meter ensures precise leveling control of the signal generator. The incident power at the reference plane of the

 DOI: 10.7795/110.20250905

microcalorimeter is consistently controlled through a power leveling system. The integration setup for determining the millimeter-wave power source is similar to Figure 3.1, with monitoring instruments connected to the side arm of the directional coupler.

The waveguide thermoelectric sensor serves as both the transfer standard and the dummy load for the waveguide microcalorimeter. This choice arises due to the unavailability of commercial thermistor mounts. The waveguide thermoelectric sensor was developed in collaboration with Rohde & Schwarz.

RF-DC power substitution cannot be applied directly to the waveguide thermoelectric sensor, necessitating additional devices such as DC sources and meters. The sensor includes two absorbers: the RF termination (first heater) for RF power absorption and the DC resistive heater (second heater) for DC power absorption [80].

The twin-type waveguide microcalorimeter features a symmetrical arrangement of the feeding line and the dummy line. The transfer standard connects to the feeding line, while the dummy load connects to the dummy line. This twin-line structure minimizes the effects of ambient temperature drift, improving measurement repeatability.

The feeding line, dummy line, transfer standard, dummy load, and microcalorimeter thermopile are enclosed within copper-walled thermal jackets, as presented in Figure 4.8, to reduce

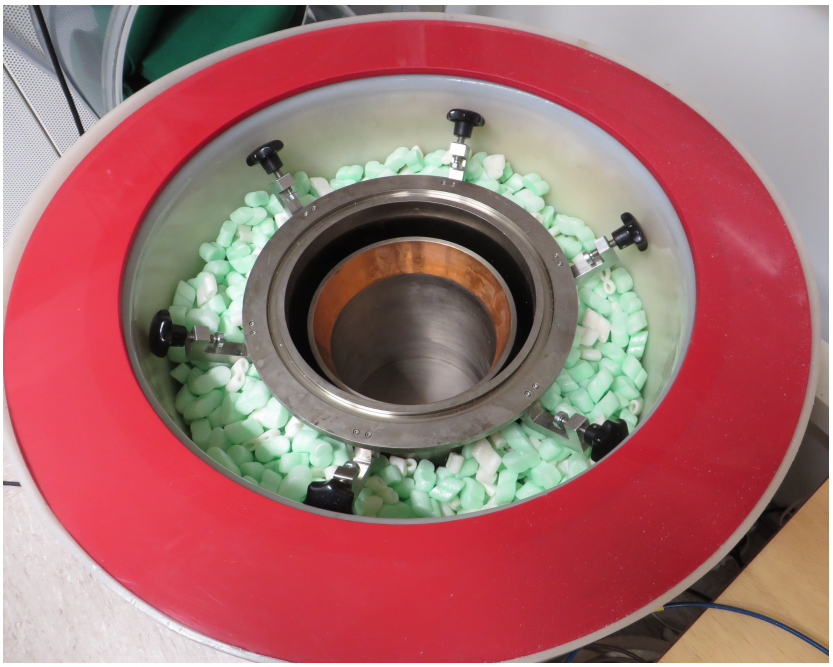

Figure 4.8: Thermal jacket.

DOI: 10.7795/110.20250905

temperature fluctuations. The two outer layers made of plastic are combined to form the outer thermal jacket, while the remaining layer, made of copper, serves as the inner thermal jacket. A large number of polymeric foams are placed between the outer and inner thermal jackets to improve the long-term stability of temperatures [14]. Custom fasteners confirm precise alignment and secure the components within the jackets during measurements.

The microcalorimeter thermopile, as depicted in Figure 4.9, is mounted at the reference plane to measure the temperature difference between the transfer standard and the dummy load

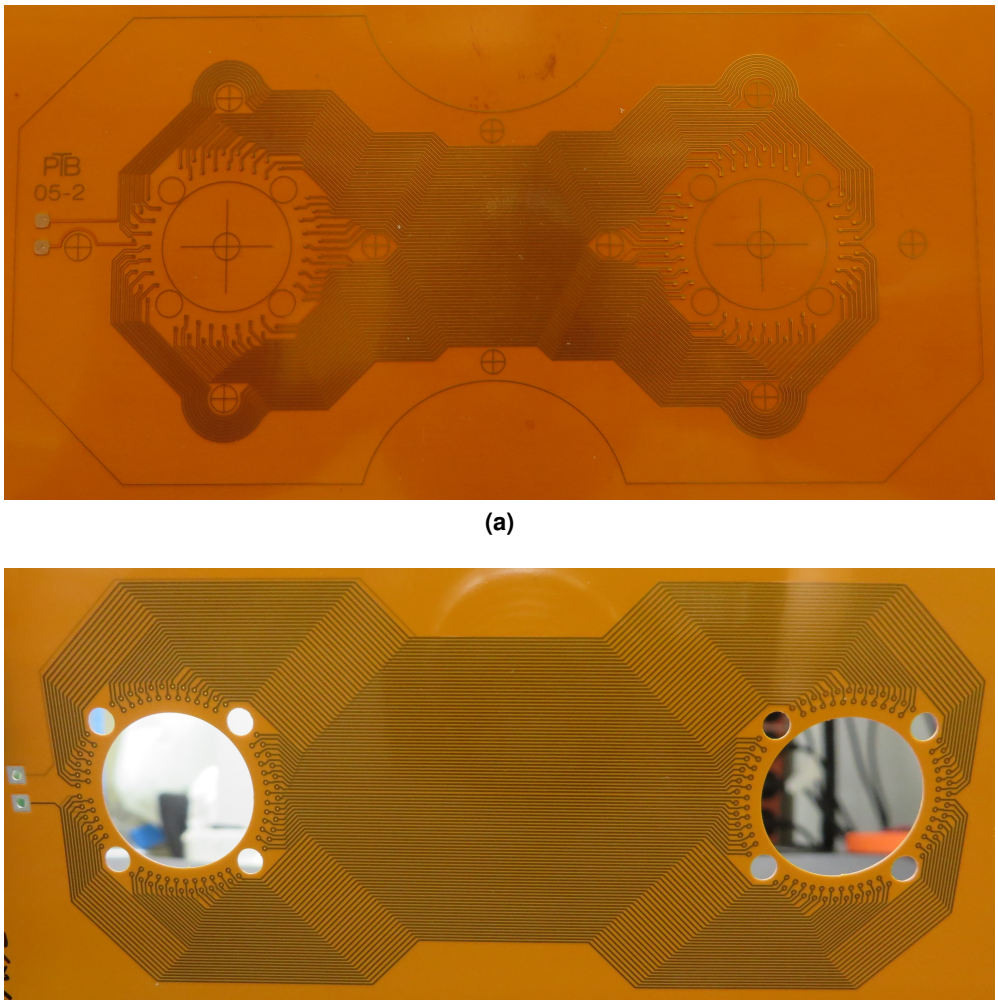

(a)

(b)

Figure 4.9: Microcalorimeter thermopile. (a) 60 thermocouple pairs. (b) 90 thermocouple pairs.

DOI: 10.7795/110.20250905

in the microcalorimeter measurement. This thermopile is custom-designed for the waveguide microcalorimeter and measures 80 mm in length from one terminal to the other. It is fabricated using type T (copper–constantan) thermocouples and generates an output voltage proportional to the temperature difference.

The previous generation of the thermopile consisted of 60 thermocouple pairs connected in series (Figure 4.9(a)). Recently, a new thermopile was developed with approximately 90 thermocouple pairs (Figure 4.9(b)). Constructed also from copper and constantan (ISOTAN) and covered with a polyimide film (Kapton), the thermopile provides mechanical rigidity, excellent insulation, and high tensile strength [81], [82].

The construction of the waveguide microcalorimeter incorporates a variety of custom-built mechanical components to achieve precise alignment of the system. Components such as holders, clamps, rings, cones, and feedthrough connectors were specifically designed for this purpose, as shown in Figure 4.10. Each component is manufactured with micrometer-level tolerances to ensure precise alignment of the microcalorimeter for accurate millimeter-wave power measurements.

Figure 4.10: Mechanical components of waveguide microcalorimeter.

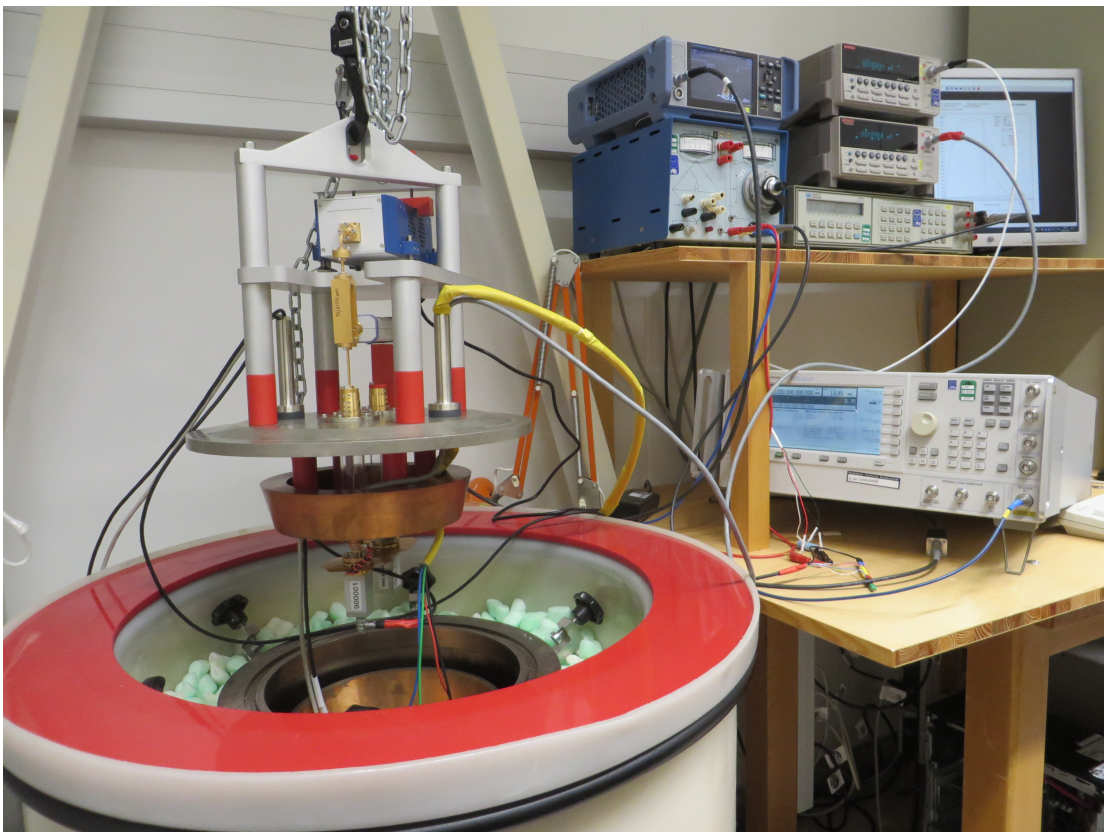

Figure 4.11: Waveguide microcalorimeter for millimeter-wave power standard and system (140 GHz–220 GHz).

To enable connectivity between RF devices and measurement instruments, specialized cables with custom connectors were installed and routed through the top lid of the microcalorimeter. These cables provide reliable connections for DC measurement instruments, facilitating the integration of external devices such as thermoelectric sensors and power meters. Specialized feedthroughs are employed to ensure that the cables maintain signal integrity while also providing mechanical robustness during operation. These connection interfaces offer reliable sealing, contributing to the long-term stability of the microcalorimeter. The fully assembled WR-5 waveguide microcalorimeter, shown in Figure 4.11, serves as a primary standard and measurement system for millimeter-wave power within the frequency range of 140 GHz to 220 GHz.

DOI: 10.7795/110.20250905

5 Characterization of Waveguide Microcalorimeter

Characterization of the waveguide microcalorimeter is performed to validate its functionality and verify its suitability as the primary standard for millimeter-wave power measurements within the frequency range of 140 GHz to 220 GHz. This process involves assessing the performance of each individual component to verify that their combined operation yields accurate and reliable power measurements. Key factors include the evaluation of the power source level, transmission line characteristics, and the microcalorimeter correction factor, all of which contribute to the overall measurement accuracy. Furthermore, measurement of the waveguide thermoelectric sensor transfer standard confirms traceability and completes the evaluation process of the waveguide microcalorimeter.

5.1 Measurement of Power Source Levels

The stability of the power source impacts the consistency of the power delivered to the microcalorimeter, making it an essential parameter for accurate measurements. To monitor power source levels, a power meter is typically connected to the output waveguide of the millimeter-wave power source, providing feedback on power levels as illustrated in Figure 5.1. In this configuration, a Rohde & Schwarz NRP220TWG power sensor, along with a Rohde & Schwarz

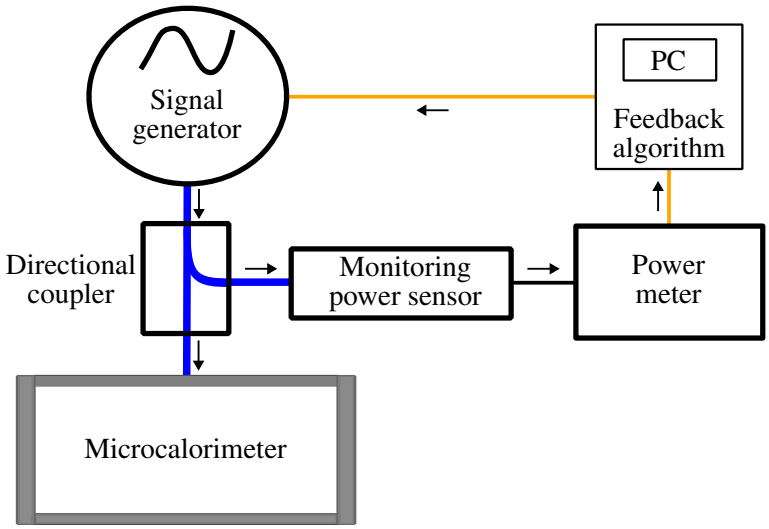

Figure 5.1: Schematic of the power source stabilization process.

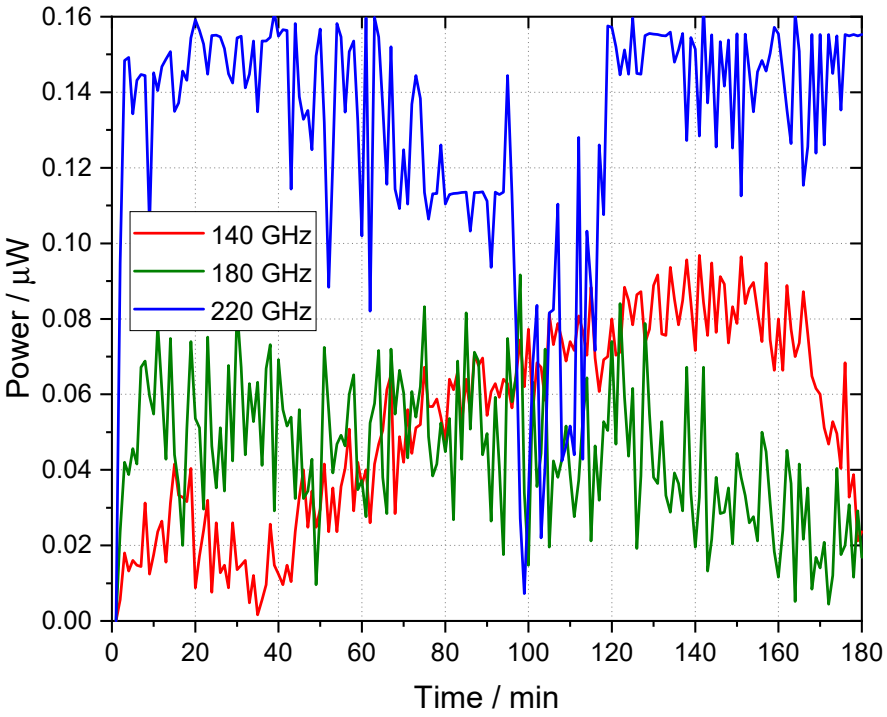

Figure 5.2: The stability of the millimeter-wave signal generator (fluctuation relative to the initial value at time = 0). The initial values were 87 µW, 58 µW, and 42 µW at frequencies of 140 GHz, 180 GHz, and 220 GHz, respectively.

NRX power meter, is attached to the side arm of a directional coupler, which isolates the forward traveling wave from any reflected power. This isolation ensures that the power meter captures the true output power stability without interference from reflections. By observing the output power, any fluctuations in the output of the signal generator can be detected and adjusted to maintain a stable power source.

Figure 5.2 presents the fluctuation of power measurements relative to the initial value (time = 0), highlighting the stability of the millimeter-wave signal generator. The initial powers were 87 µW, 58 µW, and 42 µW at frequencies of 140 GHz, 180 GHz, and 220 GHz, respectively. The graph illustrates the output power stability at the start, middle, and end of the frequency range of the waveguide microcalorimeter with the same power set at the reference plane. The minor fluctuations observed in the output power are well within acceptable limits.

DOI: 10.7795/110.20250905

If significant power fluctuations are detected, a feedback loop is activated. The feedback mechanism operates as follows: the power meter continuously monitors the forward power. If a deviation from the preset reference level is detected, the system sends a control signal back to the signal generator through a feedback algorithm in the custom LabVIEW program, adjusting its output power to restore the desired level. This adjustment ensures that the incident power at the reference plane of the microcalorimeter remains stable across all frequency measurements. This controlled setting assures consistent input power to the microcalorimeter, providing a reliable reference for accurate millimeter-wave power measurements.

5.2 Measurement of the Transmission Line for the Waveguide Microcalorimeter

The main measurement parameters of the transmission line to be determined include insertion loss (IL) and return loss (RL) across the operational frequency range. These parameters were measured using a vector network analyzer connected to the input and output ports of the transmission line, as shown in Figure 5.3. High return loss and low insertion loss are desirable characteristics for waveguide components. For waveguides operating in the 140 to 220 GHz band, acceptable return loss values typically range from 10 dB to 20 dB or better. Insertion loss specifications vary depending on the component and application, but are often between 1 dB and 4 dB [83]–[86]. Return loss and insertion loss are linked to the S-parameters, as shown in Equations 5.1 and 5.2.

$$RL = -20\ \log(|S_{11}|) \tag{5.1}$$

$$IL = -20\ \log(|S_{21}|) \tag{5.2}$$

Figure 5.4 shows the measurement results of the S_{11} parameter for the microcalorimeter transmission line across the operational frequency range of 140 GHz to 220 GHz, compared with the simulation results. A return loss better than 16 dB was observed throughout this frequency range, indicating good impedance matching. This is essential for the precise determination of millimeter-wave power, as reflections can introduce uncertainties into the measurement process.

Furthermore, the measured results align with simulation predictions, validating the design and the simulation models employed during the development process. The agreement between

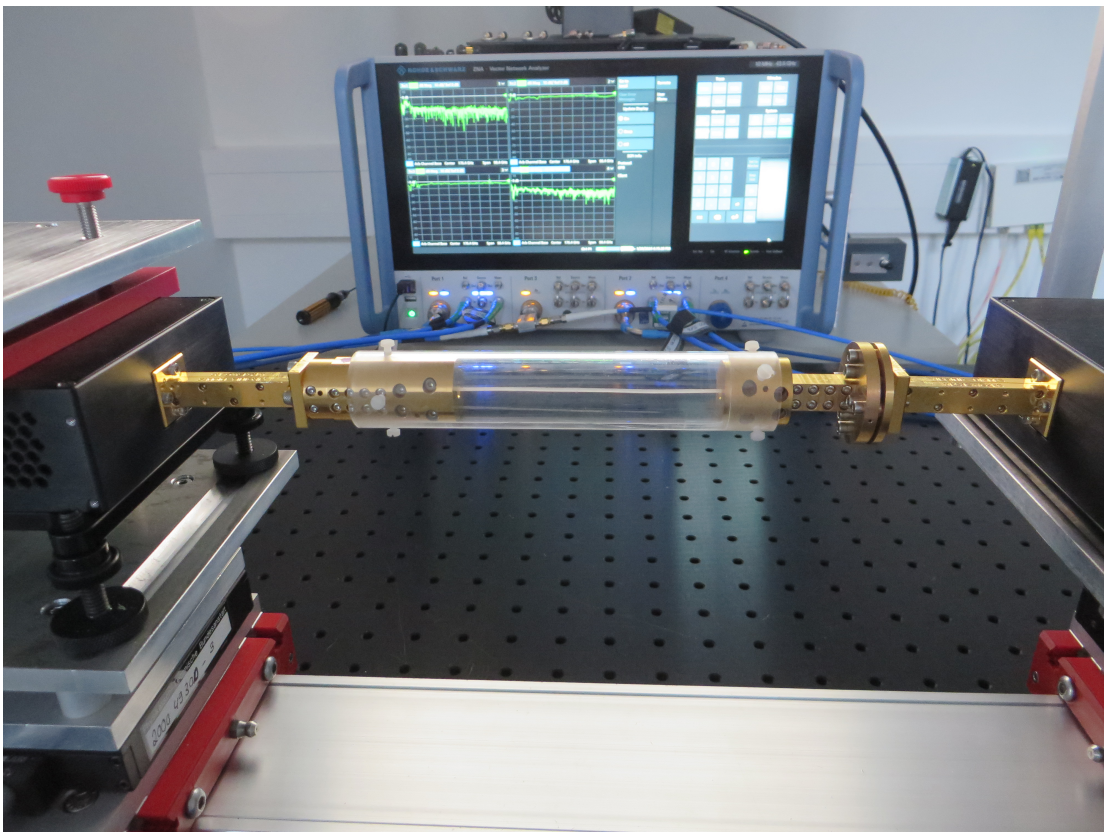

Figure 5.3: Measurement setup for the transmission line of the microcalorimeter.

measured and simulated results also highlights the reliability of the transmission line design in maintaining consistent performance across a wide operational bandwidth.

Figure 5.5 depicts both the measurement and simulation results for the S_{21} parameter of the microcalorimeter transmission line within the frequency band of 140 GHz to 220 GHz. Across the specified frequency range, the insertion loss ranges between approximately 2.9 dB and 3.8 dB. These values indicate a reasonable and acceptable level of loss for a transmission line operating at these frequencies, where achieving low losses presents significant challenges [26]. Compared to microcalorimeters operating in lower frequency bands, such as WR-10 (75 to 110 GHz) or WR-15 (50 to 75 GHz), insertion losses are typically in the range of 1.0 to 2.0 dB. At even lower frequencies, such as below 18 GHz, insertion losses can be less than 0.5 dB due to reduced conductor losses. Although the measured loss in this system is higher, it aligns with expectations at 140 to 220 GHz, where both dielectric and conductor losses naturally increase with frequency. The simulation results show nearly perfect performance, with insertion loss

DOI: 10.7795/110.20250905

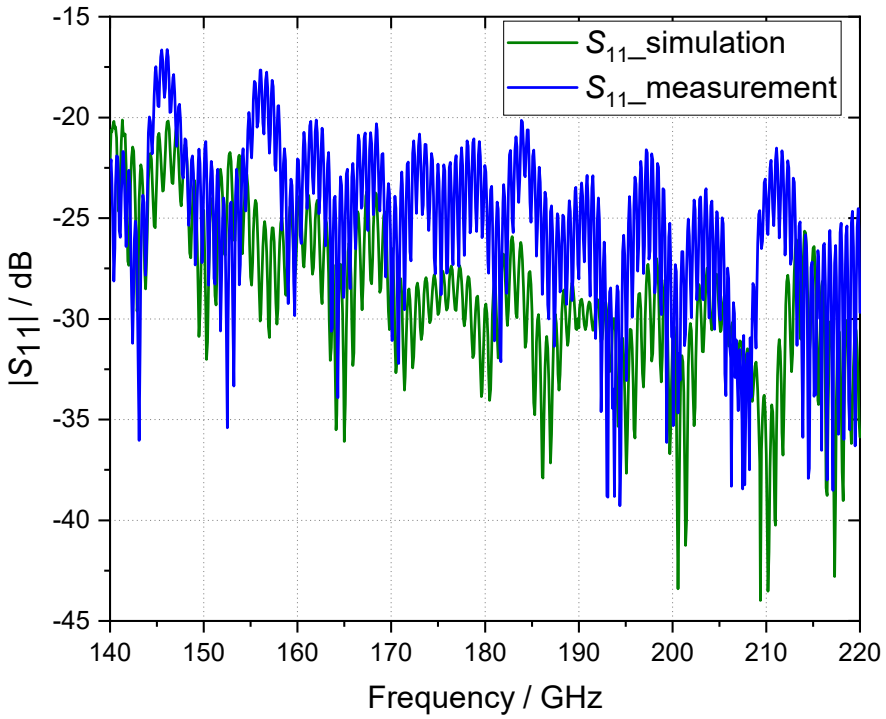

Figure 5.4: S_{11} parameter of the microcalorimeter transmission line.

close to zero, as they were conducted using a PEC for the metal waveguide and a lossless dielectric material, while the measurement results come from a lossless transmission line.

Insertion loss is influenced by several factors, including the materials and design of the transmission line. One major contributor to the observed losses is the loss tangent of the dielectric material used in the transmission line. At millimeter-wave frequencies, even materials with relatively low loss tangents can exhibit losses due to the increased sensitivity of these systems to material properties [87]. In this work, the dielectric material has a loss tangent of approximately 0.005 to 0.010 [26]. Achieving sufficiently low insertion loss allows the transmission line to support accurate and reliable power measurements in the waveguide microcalorimeter.

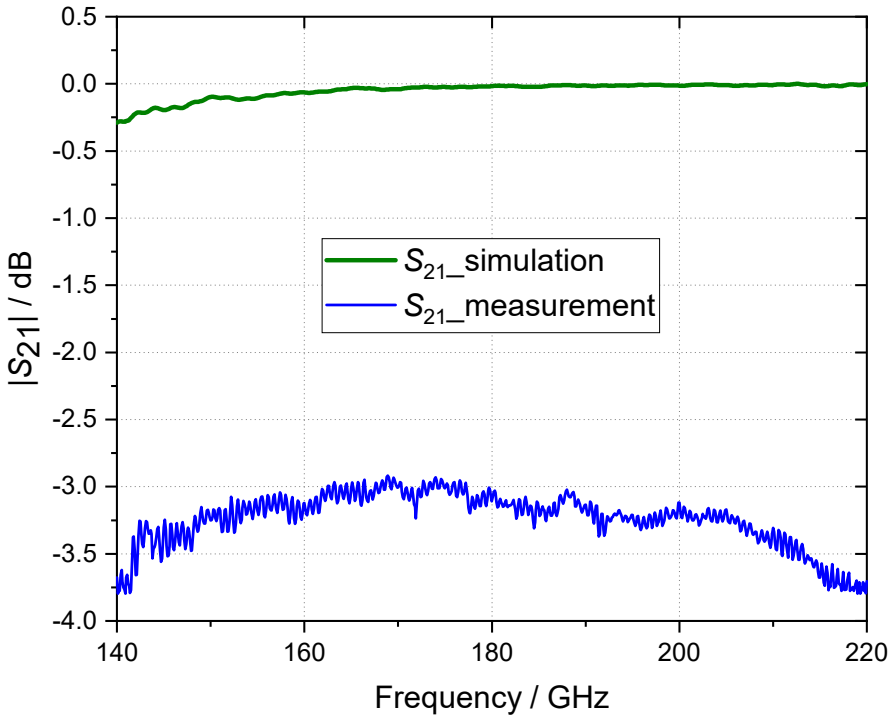

Figure 5.5: S_{21} parameter of the microcalorimeter transmission line.

5.3 Measurement Procedure for the Power of the Waveguide Microcalorimeter

The measurement procedure for the waveguide microcalorimeter involves a sequence of steps, including thermal stabilization, RF power measurement, and DC power measurement. Since the NTS220TWG waveguide thermoelectric device is used as the transfer standard, RF power and DC power measurements are performed alternately to enable RF-DC substitution. The measurement process is automated using a custom software program developed in LabVIEW.

5.3.1 Thermal Stabilization

Prior to conducting power measurements, the waveguide microcalorimeter must be thermally stabilized. This step is crucial because millimeter-wave power is measured based on the heat

DOI: 10.7795/110.20250905

generated within the microcalorimeter, and even slight variations in ambient temperature can introduce significant errors.

The thermal stabilization process involves monitoring the temperature of the microcalorimeter system. This is achieved using the microcalorimeter thermopile connected to a nanovoltmeter, which measures the voltage generated by the thermopile in response to temperature changes. A low voltage (in the range of hundreds of nanovolts) and stable voltage reading indicates that the temperature difference between the sensors is minimal, signifying that the system has reached thermal equilibrium and is adequately stabilized.

The thermopile is highly sensitive to small temperature variations, making it an ideal instrument for monitoring the thermal environment within the microcalorimeter. The thermal stability of the system can be continuously assessed by observing the voltage readings from the nanovoltmeter.

After completing the measurement setup, as illustrated in Figure 3.1, the thermal stabilization process is initiated to ensure a stable environment for accurate power measurements. This process is typically completed within one day. During this period, the system components, including the waveguide microcalorimeter and its surrounding environment, gradually adjust to eliminate any residual thermal gradients or fluctuations.

Figure 5.6 shows the thermopile voltage output from the moment the microcalorimeter is immersed in the thermal jacket until thermal stabilization is achieved over a 24-hour period. A significant drop in thermopile voltage occurs within the first hour of immersion. The abrupt deviation at around 1.3 hours can be explained by the measurement setup. During the initial phase, the thermal jacket of the microcalorimeter was open while the device was being immersed, which allowed the ambient temperature to have a strong influence on the system. This is reflected in the large difference in the thermopile output voltage, indicating a temperature difference between the thermal reference and the transfer standard. After the thermal jacket was closed, the system began to stabilize, accompanied by a significant decrease in temperature.

However, fluctuations in the voltage continue until the system stabilizes after approximately 18 hours, as shown in Figure 5.7. Beyond this point, the thermopile voltage remains relatively stable, with fluctuations within ±50 nV. The results further exhibit an initial fluctuation, followed by small but regular oscillations. This behavior can be interpreted as the system gradually reaching a thermal equilibrium state while compensating for the influence of the ambient temperature. The presence of the thermal jacket minimizes these external effects and supports the stabilization of the temperature inside the microcalorimeter.

Once the thermal environment has reached equilibrium and stable voltage readings are observed on the nanovoltmeter, the microcalorimeter is ready to perform measurements. The

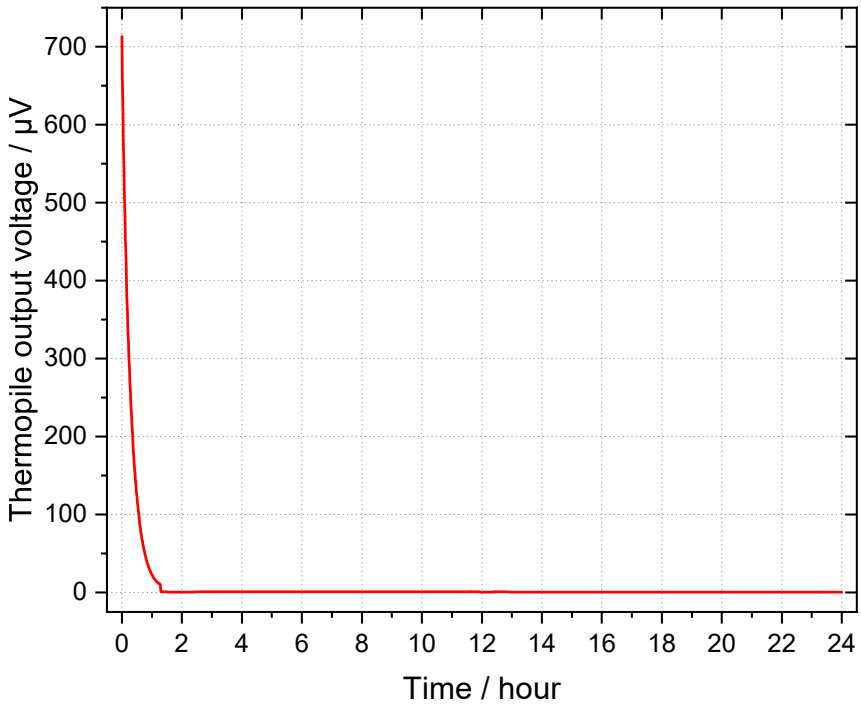

Figure 5.6: Thermopile voltage output of the microcalorimeter over 24 hours, starting from initial immersion in the thermal jacket until thermal stabilization is achieved. The gradual decrease in voltage fluctuation indicates the system reaching thermal equilibrium, which is necessary for accurate RF power measurements.

stability achieved during this process assures that the heat detected by the microcalorimeter is solely due to the incident millimeter-wave power, without external temperature influences. This careful preparation establishes the foundation for reliable power measurements.

5.3.2 RF Power Measurement

Microcalorimeter measurements are carried out in two main sequential steps: the RF power measurement and the DC power measurement. The process begins with the RF power measurement, where the microcalorimeter receives the incident RF signal. Throughout this phase, the DC heater circuit is left unbiased, and the DC source is completely disconnected from the measurement system [14].

DOI: 10.7795/110.20250905

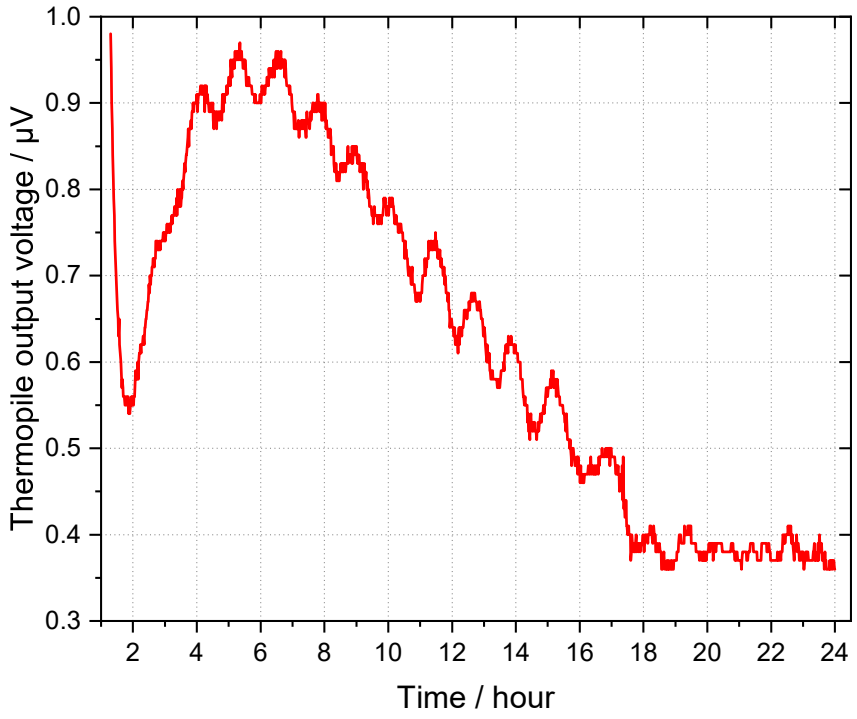

Figure 5.7: Thermal stabilization is achieved after the microcalorimeter is immersed in the thermal jacket for 18 hours.

RF power is determined by precisely measuring the heat dissipated in the load of a waveguide thermoelectric sensor. When RF power from the signal generator is applied to the transmission line, it is absorbed by the RF load within the sensing region of the transfer standard, converting the RF signal into heat. The sensor thermopile inside the thermoelectric sensor measures the temperature rise due to the applied RF power, as illustrated in Figure 5.8. Simultaneously, the microcalorimeter thermopile at the reference plane measures the temperature difference between the transfer standard and the dummy load.

During the RF power measurement, the output voltages of the sensor thermopile, denoted as V_{TRF}, and the output voltages of the microcalorimeter thermopile, represented as e_{TRF}, are recorded using nanovoltmeters, as shown in Figure 3.1. These voltages are directly associated with the temperature increase at the reference plane of the microcalorimeter, resulting from

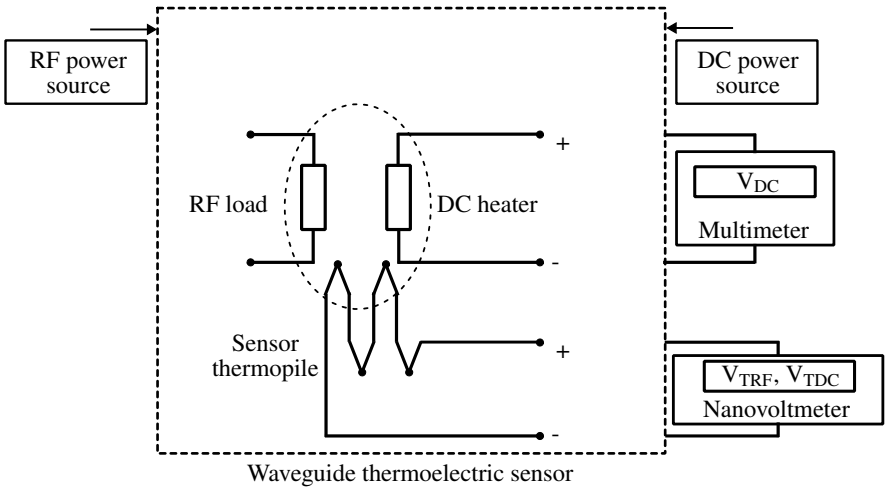

Figure 5.8: Wiring diagram of waveguide thermoelectric sensor [35].

the absorption of RF power in the RF termination. The voltages are subsequently used in calculating the generalized efficiency of the transfer standard.

5.3.3 DC Power Measurement

DC power measurement provides a reference for the accurate determination of RF power using the RF-DC substitution technique in the microcalorimeter measurement. This approach involves comparing the thermal response induced by RF power to the equivalent thermal response generated by a known DC power. The ability to establish this direct correlation ensures that RF power measurements are traceable to fundamental electrical standards.

In a waveguide thermoelectric sensor, the two loads can be designed to have identical electrical and thermal characteristics, but they do not have to be. For example, the RF heater could be 50 Ω, while the DC heater is 1 kΩ, and the thermopile does not have to be completely symmetrical. Thus, unlike bolometer sensors, the efficiency value can be larger than 1. This is due to differences in electrical resistance and thermal coupling between the RF and DC loads, which can result in a stronger thermopile response to RF heating compared to DC heating, making it possible for the efficiency to exceed 1. When RF power is applied to the first load, it is absorbed and dissipated as heat, resulting in a measurable temperature increase. Similarly, when DC power is applied to the second load, it produces an equivalent thermal effect. The DC power is adjusted until the thermal response matches that of the RF power.

During the DC power measurement, the RF source is switched off to make sure that the thermal response is only due to the applied DC power. In this process, the output voltage

DOI: 10.7795/110.20250905

of the sensor thermopile is denoted as V_{TDC}, and the output voltage of the microcalorimeter thermopile is represented as e_{TDC}. These voltages represent the temperature rise in the sensing region caused by the DC power dissipated in the heater element. The DC source is controlled with the goal of matching V_{TDC} as closely as possible to V_{TRF}. When V_{TDC} matches V_{TRF}, it indicates that the thermal response from the DC power is equivalent to that produced by the absorbed RF power. Once the matching condition is achieved, the nanovoltmeter records the values of V_{TDC} and e_{TDC}, which are then used to determine the generalized efficiency of the transfer standard.

The DC substituted power P_{DC} is calculated using the output voltage of the thermoelectric sensor V_{DC}, and the resistance of the DC heater, R_{DC} as expressed in Equation 5.3. In this calculation, V_{DC} is measured using a multimeter, as depicted in Figure 5.8. The resistance R_{DC} is a known and stable parameter, typically determined through prior characterization of the DC heater. In this work, the resistance R_{DC} is measured to be 994.5 Ω. The DC substituted power is considered equivalent to the RF power absorbed P_{RFabs}.

$$P_{\mathrm{DC}} = \frac{V_{\mathrm{DC}}^2}{R_{\mathrm{DC}}}. \tag{5.3}$$

5.4 Measurement of the Correction Factor for the Waveguide Microcalorimeter

Determination of the correction factor for a microcalorimeter is a significant step in the development of the new microcalorimeter. An ideal microcalorimeter is modeled by Equation 2.4 with g being 1. The correction factor should account for all relevant non-ideal factors, including losses in the feeding line and sensor input section (both contributing to variability in the heating constant), as well as RF radiation, where a portion of the incident RF power is emitted from the system as electromagnetic radiation instead of being absorbed by the sensor load. Additionally, this correction factor is utilized to calculate the generalized efficiency of the NTS220TWG thermoelectric sensors [88].

5.4.1 Measurement Methods for the Correction Factor of Microcalorimeters

Several methods exist for calculating the correction factor of microcalorimeters. These include the line method, through method, offset short method, foil short method, and a newer method involving a vector network analyzer [19], [21], [25], [39]. Most NMIs determine the correction

factors for their microcalorimeters using one of these methods. It has been reported in [39] and [88] that comparisons of these measurement methods show good agreement. In this study, the correction factor was determined using the foil short method. This technique is particularly advantageous because of its simplicity and effectiveness in identifying RF losses during microcalorimeter measurements.

Figure 5.9 shows a custom-made foil short, constructed from copper, which is used as a flush short in the foil short measurement method. The foil short is designed to be as thin as possible to maintain a similar thermal response when measuring the transfer standard with and without the foil short. It was fabricated with a thickness of 0.05 mm. This foil short is placed between the reference plane and the transfer standard to characterize the correction factor of the dielectric waveguide microcalorimeter.

There are two measurement steps involved in calculating the correction factor using the foil short method. First, the microcalorimeter measures the foil short with the transfer standard, followed by a measurement of the transfer standard alone. An isolator is used during measurements of the transfer standard with the foil short to protect the signal generator from reflected power caused by the foil short. The correction factor of the microcalorimeter is analyzed in relation to RF power losses and the variability of thermal paths (the nonlinearity effect) in the microcalorimeter-transfer standard combination. Generally, the correction factor is used

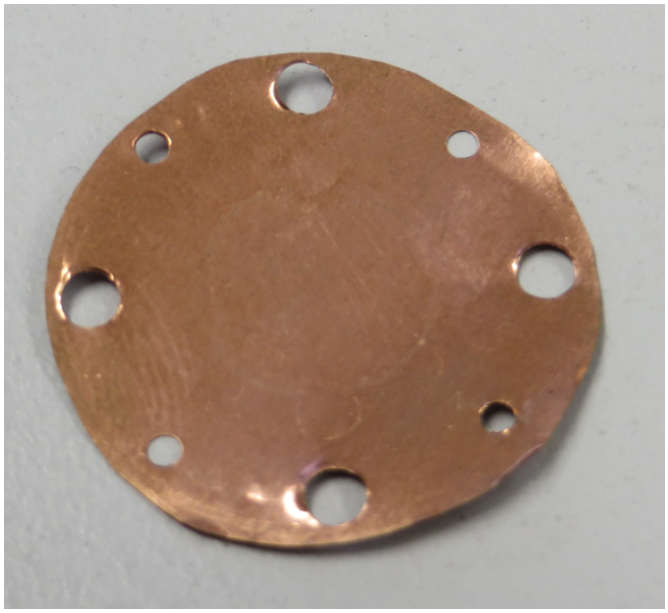

Figure 5.9: Foil short for the determination of the microcalorimeter correction factor [88].

DOI: 10.7795/110.20250905

to account for the contribution of losses due to imperfections in the thermal isolation section of the microcalorimeter, which can be characterized using the foil short. The correction factor quantifies the difference between an ideal heat measurement, in which no heat is lost, and the actual measurement, in which a portion of the heat is lost. In this microcalorimeter setup, the dielectric waveguide and the metal-coated PEEK hollow waveguide at the reference plane act as the thermal isolation section [88], [89].

To quantify deviations from ideal behavior and determine the correction factor g, the foil short method is employed. Equation 5.4 presents a model for calculating the correction factor. The value 1 reflects the baseline ideal case (no correction needed), while the remaining terms account for deviations from this ideal condition.

$$g = 1 + M_S \cdot (Measured\ deviation\ from\ ideal\ reflection) \tag{5.4}$$

In this method, a foil short with reflection coefficient Γ_{FS} is placed at the reference plane. The short causes all incident RF power to be reflected back toward the source, while dissipation occurs through Ohmic losses at the foil short. When RF power is delivered to the microcalorimeter, the corresponding change in thermopile output voltage Δe_{FS}, is detected. This voltage is measured using a nanovoltmeter and can be expressed as a function of the incident power at the foil short P_{iFS}, the reflection coefficient Γ_{FS} and a proportionality constant k_{S}. This constant, which depends on the fraction of power passing through the thermopile and its sensitivity [14], characterizes the sensitivity and efficiency of the thermopile in detecting thermal changes and converting them into a measurable voltage output. The resulting voltage represents the thermal response of the microcalorimeter.

In practice, the transfer standard connected to the microcalorimeter may not perfectly match the characteristic impedance of the microcalorimeter system, resulting in partial reflections and standing waves. These standing waves alter the thermal loading pattern at the reference plane and, consequently, affect the heat transfer to the thermopile. The degree of mismatch is described by the reflection coefficient of the transfer standard Γ_{S}. To account for the influence of these reflections, a mismatch correction factor M_{S} is introduced, as shown in Equation 5.5. This term models how the presence of standing waves modifies the power absorbed compared to the perfectly matched case.

$$M_S = \frac{1 + |\Gamma_{\mathrm{S}}|^2}{1 - |\Gamma_{\mathrm{S}}|^2} \tag{5.5}$$

By combining the adjusted thermal response from the foil short measurement and correcting for the mismatch introduced by the transfer standard, the complete expression for the correction factor g is formulated in Equation 5.6. This factor includes three terms: the baseline ideal value of 1, a mismatch scaling term, and the difference between the measured thermal response and the expected ideal response with the foil short (the bracketed term). This equation compensates for relevant non-idealities, including reflection mismatches and partial power loss, therefore enabling precise microcalorimeter measurements.

$$g = 1 + \frac{1 + |\Gamma_{\mathrm{S}}|^2}{1 - |\Gamma_{\mathrm{S}}|^2} \cdot \left(\frac{\Delta e_{\mathrm{FS}}}{k_{\mathrm{S}} P_{\mathrm{iFS}} \left(1 + |\Gamma_{\mathrm{FS}}|^2\right)} - \frac{1 - |\Gamma_{\mathrm{FS}}|^2}{1 + |\Gamma_{\mathrm{FS}}|^2} \right) \tag{5.6}$$

The value P_{iFS} is determined through a directional coupler experiment and represents the RF power reaching the foil short, as described in [6], [89]. This involves measuring the incident power at the main port and the side-arm powers when the power sensor and the foil short with the sensor connected to the microcalorimeter. The reflection coefficients Γ_{S} and Γ_{FS} are measured using a VNA. The proportionality constant k_{S} is influenced by the physical properties of the thermopile, such as its thermal conductivity, electrical resistivity, and structural design. This constant is derived from the linearity of the thermopile, as shown in Figure 5.10, and is calculated using Equation 5.7. The thermopile output voltage increases proportionally with the applied DC power, indicating a highly linear response over the measured range. This linear behavior confirms the suitability of the thermopile for precise thermal power detection in microcalorimeter applications.

$$k_{\mathrm{S}} = \frac{\overline{P}_{DC}}{\overline{e}_{\mathrm{DC}}} \tag{5.7}$$

The value $\overline{e}_{\mathrm{DC}}$ denotes the average thermopile output voltage when only the power sensor is attached to the microcalorimeter. This voltage results from the heating effect of several applied DC power levels $\overline{P}_{\mathrm{DC}}$.

5.4.2 Correction Factor of the Dielectric Waveguide Microcalorimeter

Figure 5.11 shows the correction factor associated with the newly developed dielectric waveguide microcalorimeter, which uses a thermoelectric sensor as the transfer standard. This plot presents a combination of measured data points for the correction factor values and a second-degree (quadratic) polynomial fit that has been applied to the data. The data points show significant variability because each frequency results in a different standing wave pattern, leading to slightly different thermal conditions at the reference plane. The polynomial fit helps account for

DOI: 10.7795/110.20250905

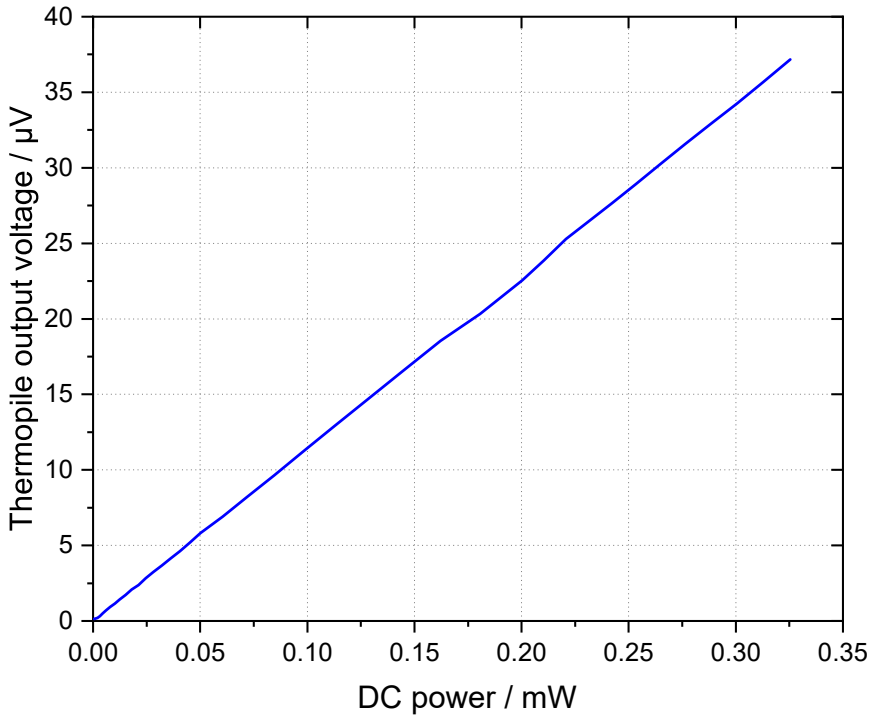

Figure 5.10: Linearity characterization of the microcalorimeter thermopile.

these standing wave patterns as described in [25]. The fitted curve is a quadratic polynomial of the form: correction factor = 0.00001022 f^2 - 0.003755 f + 1.387. The second-degree polynomial was used because the correction factor varies smoothly with frequency and exhibits slight curvature. The quadratic fit captures this behavior effectively. In contrast, higher-order polynomials would introduce unnecessary complexity without physical justification, while a linear (first-degree) fit may not adequately represent the curvature across the frequency band.

This expression was chosen to strike a balance between fitting accuracy and avoiding overfitting. It effectively captures the general trend and fluctuations in the correction factor over the 140–220 GHz frequency range while reducing the impact of noise caused by standing wave effects. Although higher-order polynomials were considered, they did not offer significant improvements in fit quality and introduced unnecessary oscillations.

The correction factor values for the dielectric waveguide microcalorimeter range from 1.041 to 1.062 over the frequency span of 140 GHz to 220 GHz. These values, which con-

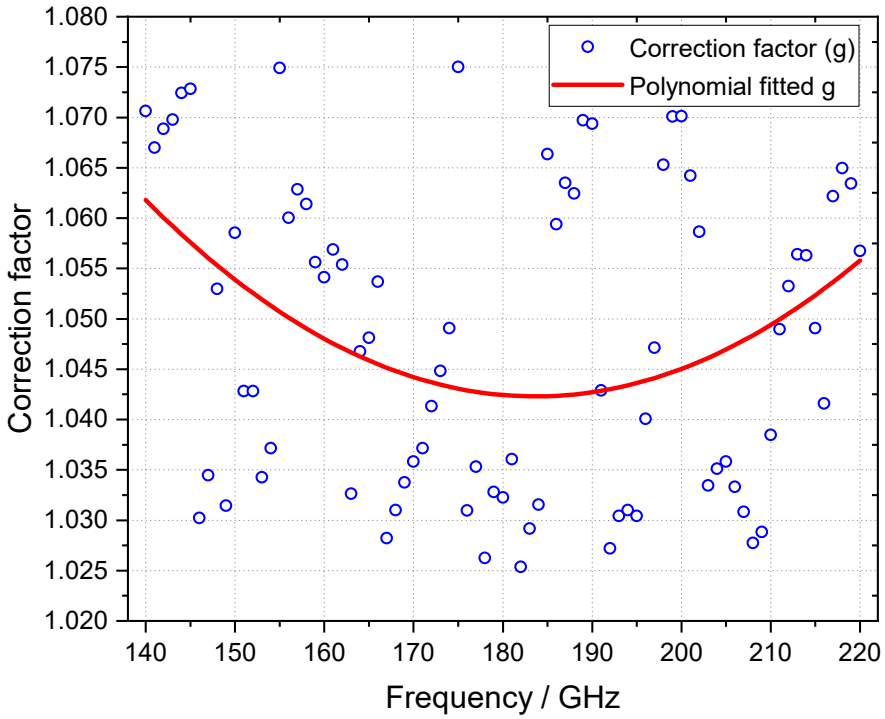

Figure 5.11: Correction factor g of the new dielectric waveguide microcalorimeter.

sistently exceed 1, indicate the presence of RF losses in the microcalorimeter transmission line. To ensure accurate measurement results, the raw data obtained from the microcalorimeter measurement must be multiplied by the corresponding correction factor to compensate for these losses.

In the foil short method, the calculation of the correction factor relies on thermopile voltages, and the reflection coefficients of the foil short and the transfer standard. Measurement results demonstrate some variations in the correction factor as a function of frequency, mainly due to imperfections in the measured reflection coefficients of the foil short. Ideally, a foil short reflects nearly all incident RF power ($|\Gamma_{\mathrm{FS}}| = 1$). However, in practice, it may be slightly less due to imperfect construction or material properties. The frequency dependence of the correction factor is further influenced by reflections from the transfer standard, although RF loss is the dominant factor overall. Furthermore, variability in the thermal path within the microcalorimeter contributes to the correction factor.

DOI: 10.7795/110.20250905

5.4.3 Comparison of Correction Factors of Microcalorimeters Over Time

PTB has built a series of microcalorimeters as RF power standards for different frequency bands over the years. These microcalorimeters have developed from the first generation N-type coaxial microcalorimeter to the recently established WR-5 waveguide microcalorimeter. Every version represents a step forward in extending frequency coverage. For each newly developed microcalorimeter, determining the correction factor is a crucial step in the measurement process.

Table 5.1 provides a comparative overview of the correction factor values for several microcalorimeters developed at PTB. The table includes eleven microcalorimeters with various connector types, each designed to operate within specific frequency ranges. The measurement frequency range of these microcalorimeters spans from 10 MHz to 220 GHz. The increasing correction factor highlights the challenges associated with RF losses at higher frequencies, as demonstrated by comparing the correction factors across different microcalorimeters.

Microcalorimeters designed to operate at higher frequencies exhibit larger correction factors compared to those operating at lower frequencies. This trend is primarily due to the increased RF losses and variations in thermal response associated with millimeter-wave and sub-

Table 5.1: Comparison of correction factors for microcalorimeters at PTB [90].

Type of microcalorimeter	Frequency range	Correction factor values
N type coaxial	10 MHz — 18 GHz	1.00079 — 1.0034
WR-90	8.2 GHz — 12.4 GHz	1.0011 — 1.0020
WR-62	12.4 GHz — 18 GHz	1.0012 — 1.0022
WR-42	18 GHz — 26.5 GHz	1.0015 — 1.0037
WR-28	26.5 GHz — 40 GHz	1.0016 — 1.0044
WR-22	33 GHz — 50 GHz	1.0019 — 1.0058
WR-19	40 GHz — 60 GHz	1.0083 — 1.013
WR-15	50 GHz — 75 GHz	1.012 — 1.016
WR-10	75 GHz — 110 GHz	1.015 — 1.026
WR-7	110 GHz — 170 GHz	1.020 — 1.040
WR-5	**140 GHz — 220 GHz**	**1.041 — 1.062**

DOI: 10.7795/110.20250905

millimeter-wave measurements. Among the microcalorimeters developed at PTB, the new dielectric waveguide microcalorimeter demonstrates the highest correction factor. As the operating frequency increases, the heat distribution generated by RF dissipation within the waveguide becomes less uniform. This variability in thermal distribution amplifies nonlinearities in the thermopile response. These inconsistencies further impact the correction factor, demonstrating the importance of precise measurement techniques.

5.5 Measurement of the Transfer Standard

For the first time, a waveguide thermoelectric sensor of type NTS220TWG was utilized as a transfer standard in the WR-5 dielectric waveguide microcalorimeter. This milestone represents a significant advancement in the calibration of millimeter-wave power sensors within the frequency range of 140 GHz to 220 GHz. The transfer standard establishes a connection between primary power standards and secondary measurement systems.

5.5.1 Generalized Efficiency of the Transfer Standard

In the characterization of waveguide thermoelectric sensors, a measurement quantity known as generalized efficiency is introduced instead of effective efficiency, which is commonly used for thermistor mounts. This shift from effective efficiency to generalized efficiency is necessary due to fundamental differences in the measurement processes between thermistor mounts and waveguide thermoelectric sensors. Unlike thermistor mounts, which have a single absorber where the RF-DC substitution technique can be directly applied, waveguide thermoelectric sensors contain two absorbers. As a result, the RF-DC substitution technique cannot be applied directly. Instead, it is implemented indirectly to determine the generalized efficiency of a waveguide thermoelectric sensor [14], [16].

The generalized efficiency η_{gen} is defined as the ratio of the DC substituted power in the DC resistive heater to the RF power absorbed in the RF termination. This ratio is determined under the condition that the output voltage of the sensor thermopile remains equal for both RF and DC power measurements. This definition ensures that the efficiency parameter correctly accounts for the thermal and electrical characteristics of waveguide thermoelectric sensors. The expression for generalized efficiency is given in Equation 5.8, providing a quantitative basis for

 DOI: 10.7795/110.20250905

comparing sensor performance across a frequency measurement range.

$$\eta_{\text{gen}} = \left.\frac{P_{\text{DC}}}{P_{\text{RFabs}}}\right|_{V_{\text{TRF}}=V_{\text{TDC}}} . \tag{5.8}$$

The generalized efficiency establishes the relationship between the DC substituted power and the RF power absorbed for a waveguide thermoelectric sensor. This efficiency characterizes the performance of the waveguide thermoelectric sensor for RF power measurements. Since waveguide thermoelectric sensors rely on thermal conversion principles, their efficiency must be evaluated by considering heat distribution and thermopile response within the sensor.

Heating coefficients describe the sensitivity of the thermopiles used in both the microcalorimeter and the transfer standard. The heating coefficient of the microcalorimeter, denoted as m, is determined using Equation 5.9. This coefficient quantifies the response of the microcalorimeter thermopile to a given amount of applied RF power and DC power. Similarly, the heating coefficient of the transfer standard, represented as n, is determined using Equation 5.10. This coefficient identifies the sensitivity of the sensor thermopile to thermal energy generated by both RF absorption and DC substitution.

Determination of the generalized efficiency of the transfer standard is based on the RF power absorbed by the sensing element of the thermoelectric sensor. However, in practical implementations, not all of the incident RF power is absorbed by the sensing element. A portion of the RF power spreads beyond the absorption region, dissipating into surrounding areas within the sensor structure or the waveguide itself. To address this issue, the correction factor of the microcalorimeter, as quantified using Equation 5.6, is incorporated into the calculation of the generalized efficiency. By applying this correction, the determination of the generalized efficiency of the transfer standard becomes more precise [14]. Finally, the generalized efficiency of the waveguide thermoelectric sensor is calculated using Equation 5.11.

$$m = \frac{P_{\text{DC}}}{e_{\text{TDC}}} \tag{5.9}$$

$$n = \frac{P_{\text{DC}}}{V_{\text{TDC}}} \tag{5.10}$$

$$\eta_{\text{gen}} = g \cdot \frac{n}{m} \cdot \frac{V_{\text{TRF}}}{e_{\text{TRF}}} \tag{5.11}$$

DOI: 10.7795/110.20250905

The calibration factor of the transfer standard, which is derived from the generalized efficiency, is determined using Equation 5.12.

$$K = \eta_{\text{gen}} \left(1 - |\Gamma|^2\right) \tag{5.12}$$

This approach to determining the calibration factor is consistent with the conventional method based on the effective efficiency.

5.5.2 Measurement of Generalized Efficiency of the Waveguide Thermoelectric Sensor

Figure 5.12 presents the generalized efficiency of the NTS220TWG waveguide thermoelectric sensor (serial number 900001) measured in the WR-5 dielectric waveguide microcalorimeter.

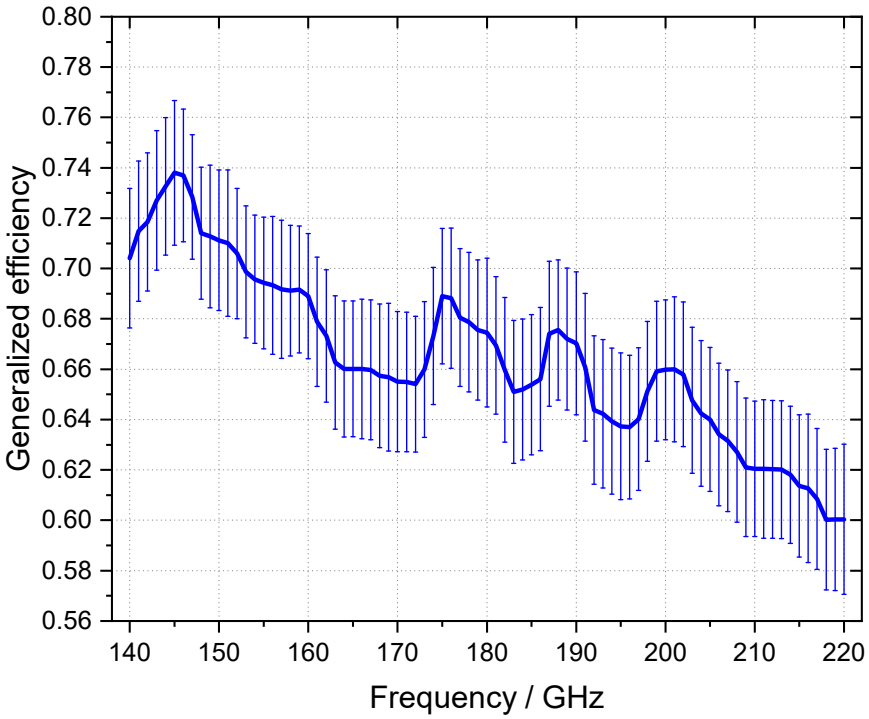

Figure 5.12: Generalized efficiency of the NTS220TWG waveguide thermoelectric sensor (serial number 900001).

DOI: 10.7795/110.20250905

In addition to the generalized efficiency values, the figure also illustrates the associated expanded uncertainty with a coverage factor of k = 2, representing a 95 % confidence level. The results indicate that the generalized efficiency of the NTS220TWG transfer standard varies between 60 % and 74 % across the frequency range of 140 GHz to 220 GHz. The generalized efficiency range is considered acceptable to good for this millimeter-wave frequency band. The frequency-dependent variation in the generalized efficiency can be attributed to factors such as changes in RF absorption characteristics of the RF load, thermal dissipation properties, and waveguide losses at different frequencies.

Several sources contribute to the uncertainty in the measurement of generalized efficiency, including uncertainty in the correction factor, bias voltage measurement uncertainty, thermopile voltage measurement uncertainty and measurement repeatability. Equation 5.11 serves as the model equation to calculate the contribution of each uncertainty source.

The uncertainty in the correction factor primarily arises from reflections, thermal variability, and imperfections in the foil short. It is evaluated based on external measurement data and is classified as a Type B uncertainty. This uncertainty is assumed to follow a normal (Gaussian) distribution, due to the nature of the calibration process. The relatively high sensitivity coefficient for this input indicates that uncertainty in the correction factor significantly impacts the final result of the generalized efficiency.

The bias voltage, measured by a digital voltmeter, represents the electrical output of the thermoelectric sensor when exposed to RF power. Its uncertainty stems from noise and the resolution limits of the digital voltmeter. This is also a Type B uncertainty, assumed to follow a normal distribution, with a sensitivity coefficient that indicates a moderate influence on the overall uncertainty.

The thermopile voltage reflects the thermal response of the microcalorimeter to the absorbed RF power. Uncertainty in this measurement is due to variations in thermal conduction, and limitations in nanovoltmeter resolution and noise. It is classified as a Type B uncertainty, assumed to follow a normal distribution. Its sensitivity coefficient indicates an inverse relationship with generalized efficiency, meaning that as the thermopile voltage increases, the calculated efficiency decreases.

Measurement repeatability accounts for the variability in four repeated measurements under identical conditions. It is categorized as a Type A uncertainty and is statistically estimated from the standard deviation of the repeated measurements. The sensitivity coefficient for repeatability is unity, as it directly reflects changes in the output quantity, which is the generalized efficiency.

DOI: 10.7795/110.20250905

Table 5.2: Uncertainty budget for the generalized efficiency at frequency of 220 GHz [14].

Quantity	**Probability distribution**	**Type**	**Standard uncertainty** $u(x_\mathbf{i})$	**Sensitivity coefficient** $c(x_\mathbf{i})$	**Uncertainty contribution** $\mathbf{\lvert}c(x_\mathbf{i})\mathbf{\rvert} \cdot u(x_\mathbf{i})$
Repeatability	Normal	A	0.004812	1	0.004812
Bias voltage	Normal	B	0.004591	0.1283	0.000589
Thermopile voltage	Normal	B	0.060982	-0.0326	0.001988
Correction factor	Normal	B	0.022640	0.5656	0.012805
Combined standard uncertainty, u_c					0.013836
Expanded uncertainty (k = 2), U					0.028

All these input uncertainties are combined into a combined standard uncertainty using the root-sum-square (RSS) method, in accordance with the Guide to the Expression of Uncertainty in Measurement, which provides a standardized framework for these calculations [23], [91]. The expanded uncertainty of the generalized efficiency of the NTS220TWG waveguide thermoelectric sensor has been determined to be approximately 3 % within its operating frequency range, up to 220 GHz. The dominant contributor to this overall uncertainty is the correction factor, emphasizing the importance of its accurate characterization in the waveguide microcalorimeter system. Table 5.2 presents the uncertainty budget for the generalized efficiency at a frequency of 220 GHz.

 DOI: 10.7795/110.20250905

6 Dissemination of Transfer Standard

A transfer standard that has been measured in a microcalorimeter is further used to disseminate measurement results through the calibration process in the direct comparison method. In this work, the NTS220TWG transfer standard establishes a link between the primary RF power standard and working measurement standards, building measurement traceability across the 140 GHz to 220 GHz frequency range. This confirms that RF power measurements conducted by laboratories remain consistent, reliable and traceable to the primary standard. The approach contributes to the expansion of the metrological framework for RF power measurements at higher frequencies, supporting a broader range of millimeter-wave applications [92].

6.1 Direct Comparison Transfer Method

The direct comparison transfer method is a fundamental technique for measuring RF power based on alternating connections between a calibrated power sensor and an unknown power sensor to an RF power source. This method allows for a direct comparison of an unknown RF signal with a calibrated reference power sensor, enabling accurate power measurement with minimal complexity [29], [93]. The RF power source used in this method can take various forms, including:

- A signal generator, which serves as a power source.
- A signal generator with an isolator or attenuator, which helps mitigate reflections and stabilize power output.
- A setup incorporating a directional coupler (power splitter), which provides monitoring of the signal generator output while ensuring a controlled measurement process.

The direct comparison method is widely used in calibration laboratories and RF applications due to its speed, simplicity, and effectiveness. This technique provides a straightforward and efficient approach for transferring measurement traceability from a primary standard to an unknown sensor, making it ideal for routine calibration procedures in industry. Higher accuracy implementations include high-directivity waveguide directional couplers for waveguide-based RF power measurements or precision power splitters for coaxial RF power measurements. The use of a highly directive directional coupler helps stabilize the forward-traveling signal component, effectively providing a matched and stable signal source [94].

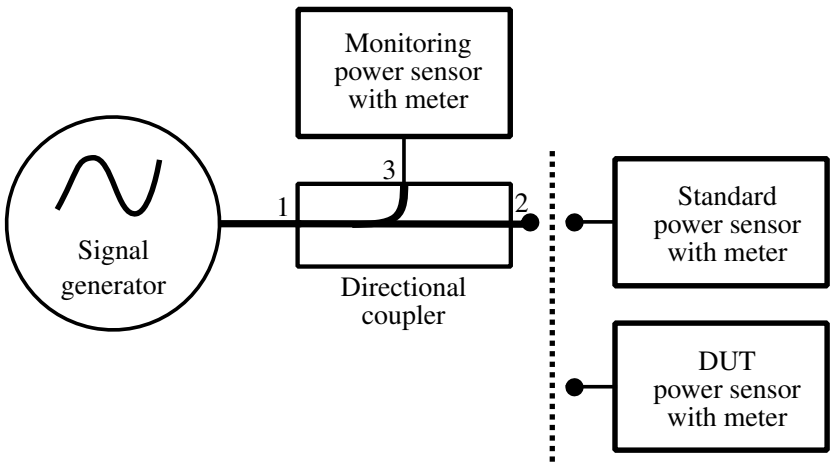

Figure 6.1: Simplified block diagram of RF power sensor calibration using the direct comparison transfer method with a directional coupler.

Figure 6.1 presents a block diagram illustrating the calibration process of an RF power sensor using the direct comparison transfer method with a directional coupler. In this setup, the effective signal source comprises the following elements: a signal generator, a directional coupler, and a monitoring power sensor. The output reflection coefficient of this source setup is known as the equivalent source reflection coefficient (equivalent source mismatch) Γ_{GE}, which represents the reflection characteristics of the effective signal source at the output terminal of the directional coupler [95].

The directional coupler plays a crucial role in the calibration system by providing power monitoring. It assures that the RF power delivered to both the standard sensor and the unknown sensor remains stable by compensating for any fluctuations in the signal generator output. A dedicated monitoring power sensor measures the power at the coupled port (side arm of the directional coupler), allowing real-time adjustments to the generator output to maintain a constant power level. To achieve high measurement accuracy, a feedback loop is implemented between the monitoring power sensor and the signal generator [4]. The main role of this feedback loop is to stabilize the output power from the generator in real time. In practice, this is accomplished by continuously sampling the power at the coupled port using the monitoring sensor and feeding that measurement into a control system, which dynamically adjusts the output level of the signal generator. This is implemented using a software-based feedback algorithm integrated into the measurement system. Any deviation in the monitored power, caused by generator drift, triggers an immediate correction signal to the generator, maintaining a constant power level at the measurement port.

DOI: 10.7795/110.20250905

In the millimeter-wave waveguide band, the performance of the feedback loop is enhanced by using high-directivity directional couplers with stable coupling ratios and low-reflection monitoring sensors with fast response times. These directional couplers allow accurate signal sampling through the coupled port and provide consistent coupling performance across frequencies. This ensures that power fluctuations are detected quickly and corrected effectively. The approach significantly improves measurement repeatability and minimizes errors caused by power instability in millimeter-wave calibration setups.

The signal generator is typically connected to port 1 of the directional coupler, with port 2 serving as the measurement port and port 3 used for monitoring. The standard power sensor and the DUT power sensor are alternately connected to the measurement port for comparative power measurement, while the monitoring power sensor remains continuously connected to port 3 (side arm) of the directional coupler. The standard power sensor has been calibrated in advance using a microcalorimeter measurement to determine its calibration factor K_{S}. When the standard power sensor is connected to the measurement port, the power of the standard power sensor P_{S}, and the monitoring power sensor P_{MS} are measured. Similarly, when the DUT power sensor is connected, the power of the DUT power sensor P_{D}, and the monitoring power sensor P_{MD} are measured. By continuously monitoring power measurements (P_{MS} and P_{MD}), fluctuations in the RF power source can be accounted for, ensuring that the measured power values are accurately corrected. This approach minimizes errors caused by source instability, mismatch reflections, or signal generator drift, thereby enhancing the accuracy of RF power measurement.

To accurately account for mismatch effects in the direct comparison transfer method, the reflection coefficient of the standard power sensor Γ_{S}, the reflection coefficient of the DUT power sensor Γ_{D}, and the equivalent source reflection coefficient must be measured. These measurements are conducted separately using a VNA to characterize impedance mismatches in the system. The equivalent source reflection coefficient of the directional coupler, which is a three-port device, is determined using the one-port VNA calibration technique as outlined in [95]. For this measurement, port 1 of the directional coupler is connected to port 1 of the VNA, while port 3 is connected to port 2 of the VNA. Once the connections are established, a one-port VNA calibration is applied to port 2 of the directional coupler. This calibration process involves measuring the reflection coefficient at port 2 of the directional coupler, representing the equivalent source reflection coefficient [96].

Calibration quantities used to characterize power sensors commonly include effective efficiency, generalized efficiency and the calibration factor. The latter quantifies how much of the applied RF power is effectively utilized by the power sensor to produce a corresponding

output signal. It provides a direct means of correcting measured power values and represents the incident power at the reference plane of the power sensor. The calibration factor of the DUT power sensor K_{D} can be calculated using Equation 6.1.

$$K_{\mathrm{D}} = K_{\mathrm{S}} \cdot \frac{P_{\mathrm{D}}}{P_{\mathrm{S}}} \cdot \frac{P_{\mathrm{MS}}}{P_{\mathrm{MD}}} \cdot \frac{|1 - \Gamma_{\mathrm{GE}}\Gamma_{\mathrm{D}}|^2}{|1 - \Gamma_{\mathrm{GE}}\Gamma_{\mathrm{S}}|^2} \tag{6.1}$$

6.2 Calibration of the Millimeter-Wave Power Sensor

Calibration of millimeter-wave power sensors using a transfer standard is carried out through the direct comparison transfer method. A waveguide thermoelectric sensor with a known calibration factor serves as a transfer standard in this calibration process. This approach ensures measurement traceability for commercial power meters operating at millimeter-wave frequencies. The waveguide thermoelectric sensor is utilized to calibrate various types of commercially available power sensors, including bolometers, diode detectors, and thermal power meters.

Dissemination of the transfer standard to commercial power sensors through the direct comparison transfer method is significantly faster compared to microcalorimeter measurements. Unlike microcalorimeter measurements, which require long stabilization times, the direct comparison transfer method allows for rapid calibration with minimal setup adjustments. This is one advantage of using the direct comparison method, although somewhat higher measurement uncertainties must be accepted [97].

Since a waveguide thermoelectric sensor is used as a transfer standard, RF power and DC power measurements must be performed separately to determine the DC substituted power. This process involves first measuring the RF power absorbed by the sensor and then performing a separate DC substitution measurement to determine the equivalent power required to produce the same sensor thermopile response. In contrast, other types of power sensors, such as thermistors or diode sensors, allow for power measurement in a single setup. These sensors often have built-in circuitry to directly measure the incident RF power without requiring a separate DC substitution step. This simplifies the calibration process and reduces the number of measurements needed.

A PM5B calorimetric power meter with serial number 785V is used as the DUT power sensor in this direct comparison measurement. The PM5B is designed for millimeter-wave and sub-terahertz frequency measurements. Its sensor head features a WR-10 waveguide input for power measurement across a frequency range of 75 GHz to 110 GHz. A variety of waveguide tapers are available to accommodate measurements beyond this range. The PM5B is capable

DOI: 10.7795/110.20250905

of RF power measurement across an extended frequency range from 75 GHz up to 3 THz by utilizing appropriate waveguide tapers that match the sensor head to different frequency bands. A WR-5 waveguide taper is employed for this measurement, enabling the system to operate within the frequency range of 140 GHz to 220 GHz [98].

Figure 6.2(a) presents a schematic diagram of the calibration of an RF power sensor using the direct comparison transfer method when a waveguide thermoelectric sensor is used as the standard power sensor. In this calibration process, both RF power and DC power measurements are performed to achieve the same thermopile output voltage. During RF power measurement as shown in Figure 6.2(a), the waveguide power sensor and the PM5B power meter are alternately connected to the RF power source. The thermopile output voltage of the standard power sensor during RF measurement V_{TRF}, and the power P_{MS} are measured first. Subsequently, the powers P_{D} and P_{MD} are measured.

To determine the power P_{S}, the DC measurement is performed only for the waveguide thermoelectric sensor, as shown in Figure 6.2(b). The DC source is adjusted through a Burster 4530 precision resistance temperature detector (RTD) simulator until the thermopile output voltage of the standard power sensor during DC measurement V_{TDC} is closely similar to the V_{TRF}. The voltages of the DC resistive heater V_{DC} is recorded when this condition is reached. The DC substituted power which represents P_{S} is determined using Equation 5.3. This calculation involves the known resistance of the DC resistive heater R_{DC}. Finally, the calibration factor of the DUT PM5B is determined using Equation 6.1.

The calibration process is conducted automatically using a measurement program built with LabVIEW. If the standard power sensor is a different type rather than a waveguide power sensor (e.g., a thermistor mount), the calibration of the DUT power sensor requires only a single setup as shown in Figure 6.2(a). In such cases, the power measurement can be performed directly without the need for a separate DC substitution step.

Figure 6.3 shows the measurement setup used for the direct comparison transfer method in calibrating the WR-5 power sensor. The calibration factor of the PM5B calorimetric power meter equipped with a WR-5 waveguide taper is presented in Figure 6.4. The PM5B exhibits a relatively flat calibration factor over the frequency range of 140 GHz to 220 GHz, with values varying between 91 % to 93 %. This stability indicates that the power meter maintains consistent measurement accuracy across the entire operational bandwidth, minimizing frequency-dependent variations. In the millimeter-wave and sub-terahertz regions, sensor efficiency can often fluctuate due to impedance mismatches, waveguide losses, and thermal effects. However, the PM5B demonstrates a stable frequency response effectively reducing these potential variations.

DOI: 10.7795/110.20250905

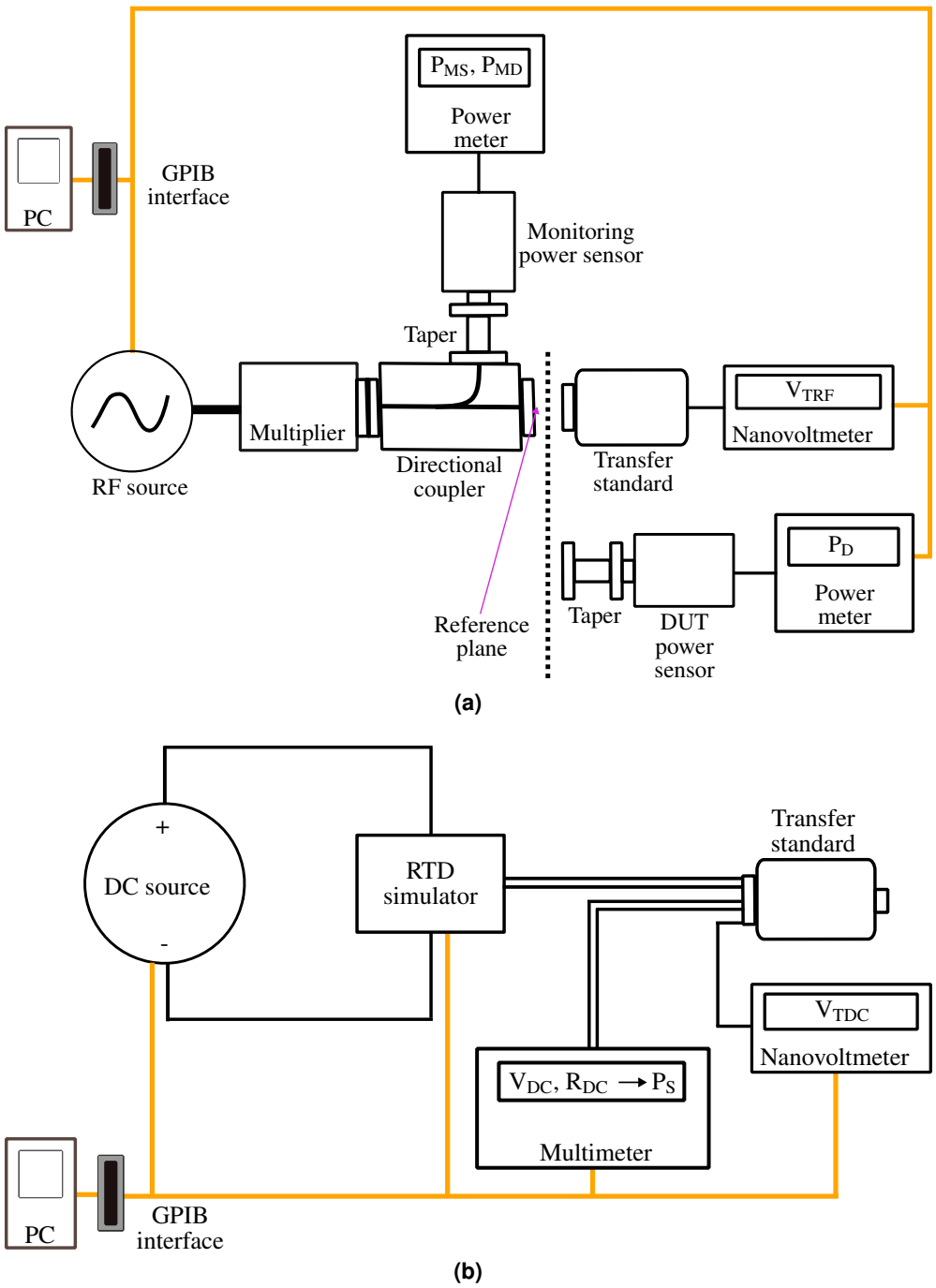

Figure 6.2: Schematic diagram of calibration of RF power sensor in the direct comparison transfer method. (a) RF power measurement. (b) DC power measurement.

DOI: 10.7795/110.20250905

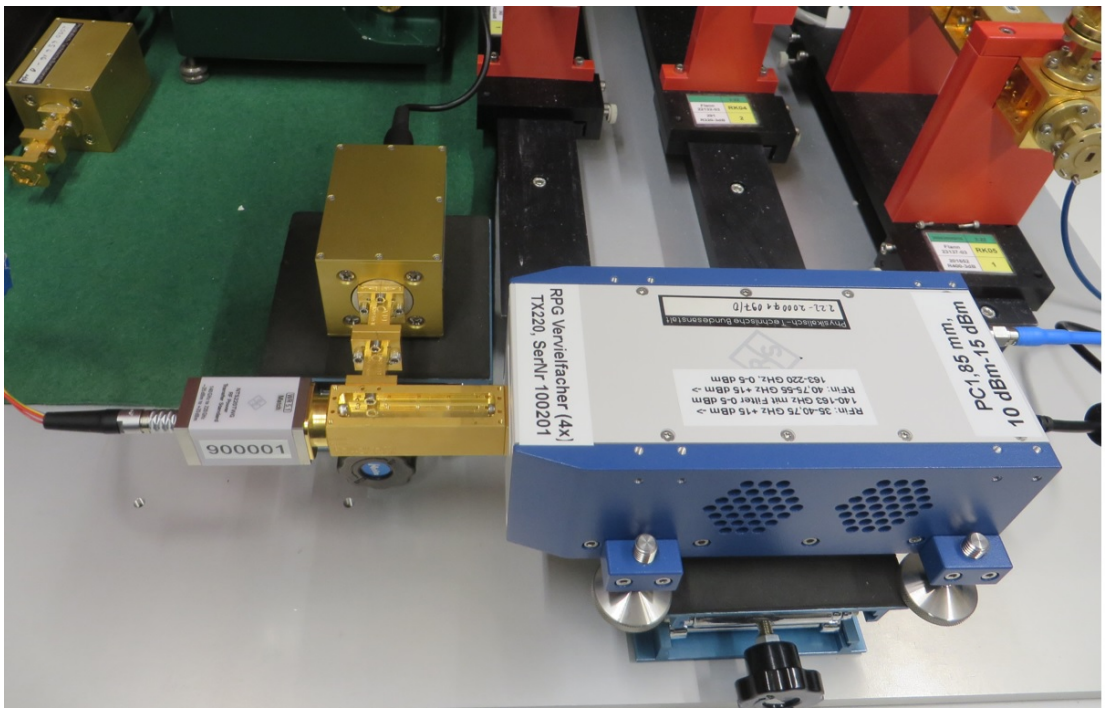

Figure 6.3: Measurement setup for the direct comparison transfer method.

The measurement uncertainty in determining the calibration factor K_{D} using the direct comparison transfer method arises from several key input quantities, as outlined in the model Equation 6.1. These inputs include: the calibration factor of the standard power sensor, mismatch correction factors for both the standard power sensor and the DUT power sensor, the resolution limits of the standard and DUT power measurements, and the measurement repeatability of the DUT sensor calibration.

The calibration factor of the standard sensor is derived from microcalorimeter measurements and is considered a Type B uncertainty. It is evaluated based on prior calibration data and, due to its systematic origin and established traceability, is assumed to follow a normal distribution.

Mismatch correction factors are determined from VNA reflection coefficient measurements. Their uncertainties are attributed to typical VNA measurement noise and sensitivity analysis, and are also assumed to follow normal distributions due to the influence of various random error sources.

DOI: 10.7795/110.20250905

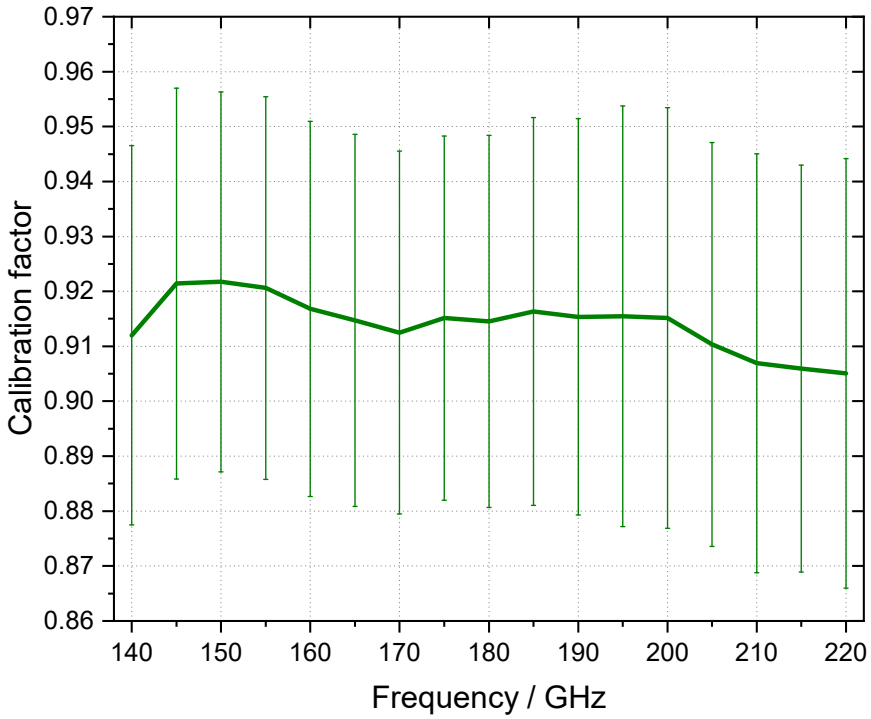

Figure 6.4: Calibration factor of the PM5B power meter with a WR-5 waveguide taper (serial number 785V).

Measurement repeatability of the DUT power sensor is evaluated from the variability in four repeated measurements under similar conditions. It is treated as a Type A uncertainty and follows a normal distribution.

The resolution limits of the power meters are not influenced by random variations but stem from the digitization characteristics of the instruments. Consequently, the associated uncertainties are modeled using a rectangular distribution.

All uncertainties are combined using the law of propagation of uncertainty in accordance with the Guide to the Expression of Uncertainty in Measurement. The combined standard uncertainty of K_{D} is expressed using a coverage factor $k = 2$, representing a 95 % confidence level [99]. This methodology ensures traceability of the calibration factor to the primary standard and compliance with international metrological standards. The measurement uncertainty of the calibration factor for the PM5B calorimetric power meter is approximately 4 % within

DOI: 10.7795/110.20250905

Table 6.1: Uncertainty budget for the calibration factor at 220 GHz using the direct comparison transfer method.

Quantity	**Probability distribution**	**Type**	**Standard uncertainty** $u(x_\mathbf{i})$	**Sensitivity coefficient** $c(x_\mathbf{i})$	**Uncertainty contribution** $\mathbf{\lvert}c(x_\mathbf{i})\mathbf{\rvert} \cdot u(x_\mathbf{i})$
Repeatability	Normal	A	0.01058	1	0.01058
Standard sensor	Normal	B	0.01415	1	0.01415
Mismatch of standard sensor	Normal	B	0.006	-1	0.006
Mismatch of DUT sensor	Normal	B	0.007	1	0.007
Resolution limit of standard sensor	Rectangular	B	0.00002886	-1	0.00002886
Resolution limit of DUT sensor	Rectangular	B	0.000002886	1	0.000002886
Combined standard uncertainty, u_c					0.01993
Expanded uncertainty (k = 2), U					0.040

the frequency range of 140 GHz to 220 GHz. Table 6.1 shows the uncertainty budget for the calibration factor at a frequency of 220 GHz using the direct comparison method.

6.3 Application of the Transfer Standard

Transfer standards allow calibration laboratories, research institutions, and commercial industries to maintain consistent measurement accuracy of RF power across various applications. Accredited calibration laboratories rely on transfer standards to provide traceable RF power calibrations for industries. Since calibration laboratories typically do not have access to primary standards, transfer standards serve as their main reference artifacts, ensuring long-term stability and reproducibility of measurements. Applications of transfer standards in calibration laboratories include:

- Calibration of commercial test equipment, such as vector network analyzers, spectrum analyzers, power sensors, and power meters.
- Verification of RF power levels in compliance with regulatory standards, such as those set by ISO/IEC 17025.
- Assuring consistency in power measurements across different calibration laboratories for interlaboratory comparisons.

Transfer standards are widely used in academic and research laboratories to advance the fields of millimeter-wave and terahertz metrology. Below are some applications of transfer standards in research institutes:

- Metrology for emerging technologies, such as THz imaging and spectroscopy [100].
- Material characterization [101].
- Research related to next generation wireless technologies, including 6G test equipment, satellite communications, and radar systems.

In industrial applications, transfer standards help maintain measurement consistency, ensure regulatory compliance, and support product quality control across sectors such as telecommunications, aerospace, semiconductor manufacturing, and medical technology. Transfer standards support companies in standardizing their RF measurement processes to confirm that their devices meet required performance specifications and industry regulations. Several industrial applications of transfer standards are:

- Calibration of power sensors in 5G base stations by telecommunication equipment manufacturers.
- Maintenance of consistency in millimeter-wave radar system calibration at aerospace companies.
- Accurate RF power testing of chips used in high frequency communication devices in semiconductor fabrication plants.
- Verification of RF power output in magnetic resonance imaging (MRI) scanners by medical device manufacturers [102].

DOI: 10.7795/110.20250905

7 Conclusion

This research has successfully developed a reliable dielectric waveguide microcalorimeter as a primary standard for millimeter-wave power measurements in the 140 GHz to 220 GHz frequency range. The development of this microcalorimeter addresses the growing need for accurate and traceable power measurement standards as technology advances into higher frequencies. By enabling traceable power calibrations, this primary power standard supports emerging applications such as 6G telecommunications, satellite communications, and advanced sensing technologies.

A comprehensive design and fabrication process was undertaken to confirm the effectiveness of the waveguide microcalorimeter. The study explored key elements such as the transmission line design, which utilized a dielectric waveguide as the feeding line, the application of tapering sections and a trumpet structure in the transition region, along with modifications to the thermopile. The dielectric waveguide structure was optimized to minimize losses and improve measurement accuracy. The thermal control of the system, including the use of the dielectric waveguide itself as thermal isolation and the utilization of thermal jackets, has contributed to the stability of the microcalorimetric measurements. In addition, by implementing a twin-line structure, the system has mitigated unwanted heat dissipation and environmental effects.

Extensive characterization was performed to validate the performance of the microcalorimeter. The correction factor for the microcalorimeter system was determined, with values ranging between 1.041 and 1.062. This factor compensates for signal losses and other small non-idealities in the system to ensure accurate measurement results. The developed primary standard was then used to calibrate transfer standards, which in turn facilitated the dissemination of millimeter-wave power measurements to working standards and industrial applications. This hierarchical approach has established measurement traceability for millimeter-wave power in that frequency range.

The generalized efficiency of a waveguide thermoelectric sensor as a transfer standard was measured in the microcalorimeter, with values ranging from 60 % to 74 % and an uncertainty of 3 %. This sensor was then employed to calibrate a commercial power meter using the direct comparison method, resulting in calibration factors ranging from 91 % to 93 %, with an uncertainty of 4 %. This method can further disseminate the calibration factor of the transfer standard to other RF devices.

This work contributes to the field of RF metrology by providing a primary standard for power measurements at frequencies beyond 170 GHz, exceeding those currently available. One of the main outcomes is the extension of the Calibration and Measurement Capability (CMC) entries for RF power measurements up to 220 GHz. These extended CMC entries serve as internationally recognized declarations of measurement competence, enabling traceable calibrations at millimeter-wave frequencies. The findings of this research provide a foundation for further improvements in RF power metrology. Future research could focus on enhancing sensor sensitivity and extending the frequency range beyond 220 GHz. As emerging technologies continue to push into the sub-terahertz and terahertz domain, the need for accurate power standards at even higher frequencies will grow. Developing the dielectric waveguide microcalorimeter to accommodate these higher frequencies would further strengthen its role as a primary standard in RF metrology.

DOI: 10.7795/110.20250905

List of Abbreviations

ABS .... acrylonitrile butadiene styrene

CAD .... computer-aided design

CMC ... Calibration and Measurement Capability

CNC .... computer numerical control

DC ..... direct current

DRW ... dielectric rod waveguide

EM .... electromagnetic

FEM .... finite element method

GUM ... Guide to the Expression of Uncertainty in Measurement

HDPE ... high-density polyethylene

IL ..... insertion loss

KRISS ... Korea Research Institute of Standards and Science

LNE .... Laboratoire national de métrologie et d'essais

NIST .... National Institute of Standards and Technology

NMIJ ... National Metrology Institute of Japan

NMIs ... National Metrology Institutes

NPL .... National Physical Laboratory

PEC .... perfect electric conductor

PEEK ... Polyetheretherketone

PTB .... Physikalisch-Technische Bundesanstalt

RF ..... radio frequency

RL ..... return loss

TE ..... transverse electric

TIS .... thermal isolation section

TM .... transverse magnetic

VNA .... vector network analyzer

WR . . . . rectangular waveguide

 DOI: 10.7795/110.20250905

List of Figures

 DOI: 10.7795/110.20250905

DOI: 10.7795/110.20250905

DOI: 10.7795/110.20250905

List of Tables

DOI: 10.7795/110.20250905

Bibliography

[1] R. J. Brown, "Measuring measurement-What is metrology and why does it matter?" *Measurement*, vol. 168, 2021.

[2] BIPM, "Report of the 33rd Meeting of Consultative Committee for Electricity and Magnetism (CCEM)," Bureau International des Poids et Mesures, Tech. Rep., 2023.

[3] LNE. "Report on the activities in Electricity and Magnetism." (2021), [Online]. Available: https://www.bipm.org/documents/20126/53254454/CCEM-21-Report-LNE.pdf/8361c8da-c333-bac0-5e46-a85c18854a89.

[4] A. Fantom, *Radio Frequency and Microwave Power Measurement*, IEE Electrical Measurement Series 7. Peter Peregrinus Ltd., 1990.

[5] ISO, "ISO/IEC 17025:2017 - General requirements for the competence of testing and calibration laboratories," International Organization for Standardization, Tech. Rep., 2017.

[6] J. W. Allen, F. Clague, N. T. Larsen, and M. P. Weidman, "NIST Microwave Power Standards in Waveguide," NIST, NIST Technical Note 1511, 1999.

[7] NPL. "Radio frequency and microwaves - Power standards." (2025), [Online]. Available: https://www.npl.co.uk/products-services/radiofrequency/power-standards.

[8] M. Kinoshita, Y. Tojima, M. J. Yamamoto, and M. Ishii, "Research progress of electromagnetic wave measurement using cesium atoms at NMIJ," in *2024 Conference on Precision Electromagnetic Measurements (CPEM)*, (Denver, CO, USA), IEEE, 2024.

[9] KRISS. "KRISS Establishes Electromagnetic Wave Measurement Standard." (2023), [Online]. Available: https://www.newswise.com/articles/kriss-establishes-electromagnetic-wave-measurement-standard-to-secure-6g-leadership.

[10] P. Howarth and F. Redgrave, *Metrology - in short*, 3rd ed. 2008. [Online]. Available: https://www.dfm.dk/wp-content/uploads/2020/12/Metrology_in_short_3rd_ed.pdf.

[11] BIPM. "Calibration and Measurement Capabilities." (Jul. 27, 2022), [Online]. Available: https://www.bipm.org/kcdb/.

[12] ITU-R, "Frequency bands and transmission directions for data relay satellite networks," International Telecommunication Union, Recommendation ITU-R SA.1019-1, 2017.

[13] T. S. Rappaport, Y. Xing, O. Kanhere, S. Ju, A. Madanayake, S. Mandal, A. Alkhateeb, and G. C. Trichopoulos, "Wireless Communications andApplications Above 100 GHz: Opportunities and Challenges for 6G and Beyond," *IEEE Access*, vol. 7, pp. 78 729–78 757, 2019.

[14] W. K. Perangin-Angin, K. Kuhlmann, and J. Ruehaak, "Development of the R 1.8k Dielectric Waveguide Microcalorimeter," IEEE Transactions on Instrumentation and Measurement, to be published, 2025.

[15] I. F. Akyildiz, C. Han, and S. Nie, "Combating the Distance Problem in the Millimeter Wave and Terahertz Frequency Bands," *IEEE Communications Magazine*, vol. 56, pp. 102–108, 6 2018.

[16] R. H. Judaschke, K. Kuhlmann, T. M. Reichel, and W. Perndl, "Millimeter-Wave Thermoelectric Power Transfer Standard," *IEEE Transactions on Instrumentation and Measurement*, vol. 64, no. 12, pp. 3444–3450, 2015.

[17] T. R. Kuphaldt, *Lesson in Electric Circuits*, 6th ed., 2 vols. 2007. [Online]. Available: `https://www.circuitbread.com/textbooks/lessons-in-electric-circuits-volume-ii-ac/v2c14-transmission-lines/waveguides`.

[18] A. Generalov, "Dielectric Rod Waveguide Components at Sub-THz Frequencies," Ph.D. dissertation, Aalto University, 2015.

[19] M. Celep and D. Stokes, "Characterization of a Thermal Isolation Section of a Waveguide Microcalorimeter," *IEEE Transactions on Instrumentation and Measurement*, vol. 70, 2021.

[20] N. S. Chung, J. Shin, H. Bayer, and R. Honigbaum, "Coaxial and Waveguide Microcalorimeters for RF and Microwave Power Standards," *IEEE Transactions on Instrumentation and Measurement*, vol. 38, pp. 460–464, 2 1989.

[21] R. Judaschke and J. Ruehaak, "Determination of the Correction Factor of Waveguide Microcalorimeters in the Millimeter Wave Range," *IEEE Transactions on Instrumentation and Measurement*, vol. 58, pp. 1104–1108, 4 2009.

 DOI: 10.7795/110.20250905

[22] R. Brink, M. Borfitz, A. Hegemann, P. Buedel, C. Greenberg, S. Henze, and P. DiTomas, "Microwave Calorimeters For Traceable Power Measurements," National Institute of Standards and Technology, Tech. Rep., 2019, ch. Supplementary Materials Related to NIST Policy on Metrological Traceability.

[23] BIPM. "JCGM 100:2008, Evaluation of measurement data - Guide to the expression of uncertainty in measurement (2008)." (2008), [Online]. Available: https://www.bipm.org/en/committees/jc/jcgm/publications.

[24] X. Cui, Y. S. Meng, Y. Shan, and Y. Li, "Microwave Power Measurements: Standards and Transfer Techniques," in *New Trends and Developments in Metrology*. InTech, 2016.

[25] D. Gu, X. Lu, B. F. Jamroz, D. F. Williams, X. Cui, and A. W. Sanders, "NIST-Traceable Microwave Power Measurement in a Waveguide Calorimeter With Correlated Uncertainties," *IEEE Transactions on Instrumentation and Measurement*, vol. 68, no. 6, pp. 2280–2287, 2019.

[26] W. K. Perangin-Angin, K. Kuhlmann, and J. Ruehaak, "Dielectric Waveguide as Transmission Line for R 1.8k Microcalorimeter," in *2024 Conference on Precision Electromagnetic Measurements (CPEM)*, IEEE, Denver, CO, USA, 2024, pp. 1–2.

[27] ITU-R, "Nomenclature of the frequency and wavelength bands used in telecommunications," International Telecommunication Union Radiocommunication Sector, Recommendation ITU-R V.431-8, 2015.

[28] Keysight, "Fundamental of RF and microwave power, Application NoteAN1449-1/2/3/-4," Keysight Technologies, Tech. Rep., 2017.

[29] M. P. Weidman, "Direct Comparison Transfer of Microwave Power Sensor Calibrations," NIST, NIST Technical Note 1379, 1996. [Online]. Available: https://www.nist.gov/system/files/documents/calibrations/tn1379.pdf.

[30] RWTH, *Microwave measurements an advanced physics lab experiment*. The Faculty of Mathematics, Computer Science and Natural Sciences at RWTH Aachen University, 2017. [Online]. Available: https://institut2a.physik.rwth-aachen.de/de/teaching/praktikum/Anleitungen/M6_HF_methods.pdf.

[31] C. E. Saavedra, "Analog Frequency Multiplier Design Techniques and Applications," in *CMOS Nanoelectronics: Analog and RF VLSI Circuits*. McGraw-Hill, 2011.

[32] Rohde and Schwarz. “Voltage and Power Measurements.” (1999), [Online]. Available: https://scdn.rohde-schwarz.com/ur/pws/dl_downloads/dl_common_library/dl_brochures_and_datasheets/pdf_1/SLMESS_E.PDF.

[33] Boonton, *Principles of Power Measurement, A Reference Guide on RF and Microwave Power Measurement*, 2014. [Online]. Available: https://electrometric.com/wp-content/uploads/2016/10/Boonton-Principles-of-Power-Measurement.pdf.

[34] TEGAM. “Application Note 220: Measuring RF Power Sensor Nonlinearity.” (2015), [Online]. Available: https://www.tegam.com/wp-content/uploads/2015/10/AN220.pdf.

[35] T. Reichel, “Power sensor with 1 mm coaxial connector covers the frequency range from DC to 110 GHz without interruption,” Rohde and Schwarz, News, 2013, pp. 23–25.

[36] J. A. Lane, *Microwave Power Measurement*, IEE Monograph Series. Peter Peregrinus Ltd, 1972, vol. 12.

[37] E. Vollmer, J. Ruhaak, D. Janik, W. Peinelt, W. Butz, and U. Stumper, “Microcalorimetric Measurement of The Effective Efficiency of Microwave Power Sensors Comprising Thermocouples,” in *Conference on Precision Electromagnetic Measurements Digest*, IEEE, Boulder, CO, USA, 1994, pp. 147–148.

[38] F. R. Clague, “A Method to Determine the Calorimetric Equivalence Correction for a Coaxial Microwave Microcalorimeter,” *IEEE Transactions on Instrumentation and Measurement*, vol. 43, no. 3, pp. 421–425, 1994.

[39] X. Cui and T. P. Crowley, “Comparison of Experimental Techniques for Evaluating the Correction Factor of a Rectangular Waveguide Microcalorimeter,” *IEEE Transactions on Instrumentation and Measurement*, vol. 60, no. 7, pp. 2690–2695, 2011.

[40] F. R. Clague and P. G. Voris, “Coaxial Reference Standard for Microwave Power,” NIST, NIST Technical Note 1357, 1993.

[41] L. Brunetti, L. Oberto, M. Sellone, and E. T. Vremera, “Comparison Between Thermoelectric and Bolometric Microwave Power Standards,” *IEEE Transactions on Instrumentation and Measurement*, vol. 62, no. 6, pp. 1710–1715, 2013.

 DOI: 10.7795/110.20250905

[42] V. Muthukrishnan. “Thermopile: A Device that Converts Heat into Electricity.” (Nov. 2, 2024), [Online]. Available: https://www.electrical4u.com/thermopile/.

[43] Y. Li, X. Cui, X. Gao, and W. Sun, “Analyzing and improvement of the thermopile output signal noise ratio of a calorimeter,” in *83rd ARFTG Microwave Measurement Conference*, IEEE, Tampa, FL, USA, 2014.

[44] Zhang, “Dielectric Waveguides and Resonators,” in *Electromagnetic Theory for Microwaves and Optoelectronics*. Springer Berlin Heidelberg, 2008, pp. 317–400.

[45] D. M. Pozar, *Microwave Engineering*, 4th ed. John Wiley and Sons, Inc., 2012, ch. Transmission Lines and Waveguides, 756 pp.

[46] EIT. “Technical References: Waveguides.” (2022), [Online]. Available: https://www.idc-online.com/technical_references/pdfs/electronic_engineering/ece3323waveguides.pdf.

[47] S. Dudorov, “Rectangular Dielectric Waveguide and Its Optimal Transition to a Metal Waveguide,” Ph.D. dissertation, Helsinki University of Technology, 2002.

[48] H. Engan, *Waveguide propagation*, in Norwegian University of Science and Technology, 2006. [Online]. Available: https://www.ntnu.no/wiki/download/attachments/81790668/Waveguide_propagation_06.pdf.

[49] X. Cui, Y. S. Meng, Y. Li, Y. Zhang, and Y. Shan, “An Improved Design and Simplified EvaluationTechnique for Waveguide Microcalorimeter,” *IEEE Transactions on Instrumentation and Measurement*, vol. 65, no. 6, pp. 1450–1455, 2016.

[50] L. Brunetti, L. Oberto, M. Sellone, N. Shoaib, and E. Vremera, “Improvements on INRIM Coaxial Microcalorimeter and Outcome of a Model Comparison,” *IEEE Transactions on Instrumentation and Measurement*, vol. 64, no. 6, pp. 1472–1476, 2015.

[51] P. Pousi, “Active and Passive Dielectric Rod Waveguide Components for Millimetre Wavelengths,” Ph.D. dissertation, Aalto University, 2010.

[52] D. Lioubtchenko, S. Tretyakov, and S. Dudorov, *Millimeter-Wave Waveguides*. Kluwer Academic Publishers, 2003.

[53] N. Dolatsha, C. Chen, and A. Arbabian, “Loss and Dispersion Limitations in mm-Wave Dielectric Waveguides for High-Speed Links,” *IEEE Transactions on Terahertz Science and Technology*, vol. 6, no. 4, pp. 637–640, 2016.

[54] S. J. Orfanidis, “Waveguides,” in *Electromagnetic Waves and Antennas*. 2016, pp. 361–410.

[55] C. Julie and G. R. Ramkumaar, "Qualitative Analysis of High Density Polyethylene Using FTIR Spectroscopy," *Asian Journal of Chemistry*, vol. 2, pp. 4477–4484, 2009.

[56] L. Kong, "Design and Analysis of Dielectric Waveguide Antennas," Ph.D. dissertation, KU Leuven, 2019.

[57] E. A. J. Marcatili, "Dielectric rectangular waveguide and directional coupler for integrated optics," *Bell System Technical Journal*, vol. 48, pp. 2071–2102, 7 1969.

[58] C. G. Wells, "Analysis of Shielded Rectangular Dielectric RodWaveguide Using Mode Matching," Ph.D. dissertation, University of Southern Queensland, 2005.

[59] K. H. Yeap, K. H. Teh, K. C. Yeong, K. C. Lai, and M. C. Loh, "Propagation in dielectric rectangular waveguides," *Optica Applicata*, vol. XLVI, no. 2, pp. 317–330, 2016.

[60] S. Kobayashi, R. Mittra, and R. Lampe, "Dielectric Tapered Rod Antennas for Millimeter-Wave Applications," *IEEE Transactions on Antennas and Propagation*, vol. 30, no. 1, pp. 45–48, 1982.

[61] G. Ponchak, N. Dib, and L. Katehi, "Design and Analysis of Transitions from Rectangular Waveguide to Layered Ridge Dielectric Waveguide," *IEEE Transactions on Microwave Theory and Techniques*, vol. 44, no. 7, pp. 1032–1040, 1996.

[62] D. Puhan and J. S. S. Wong, "Properties of Polyetheretherketone (PEEK) transferred materials in a PEEK-steel contact," *Tribology International*, vol. 185, pp. 189–199, 2019.

[63] Microwaves101. "Waveguide Construction." (Aug. 7, 2023), [Online]. Available: `www.microwaves101.com/encyclopedias/waveguide-construction`.

[64] Bieglo. "Why is PEEK considered as an alternative material to metal." (2023), [Online]. Available: `https://www.bieglo.com/peek-as-metal-alternative/`.

[65] A. R. Lavado, L. G. Munoz, A. Generalov, D. Lioubtchenko, K. Abdalmalak, S. L. Romano, A. G. Lamperez, D. S. Vargas, and A. Raisanen, "Design of a Dielectric Rod Waveguide Antenna Array for Millimeter Waves," *Journal of Infrared, Millimeter, and Terahertz Waves*, vol. 38, pp. 33–46, 2017.

[66] J. Weinzierl, J. Richter, G. Rehm, and H. Brand, "Simulation and Measurement of Dielectric Antennas at 150 GHz," in *29th European Microwave Conference*, IEEE, Munich, Germany, 1999, pp. 185–188.

 DOI: 10.7795/110.20250905

[67] W. K. Perangin-Angin, K. Kuhlmann, and J. Ruehaak. “Development of aWaveguide Microcalorimeteras RF Power Standard for Frequencies above 170 GHz.” (2024), [Online]. Available: https://doi.org/10.7795/810.20240709.

[68] W. K. Perangin-Angin, J. Ruehaak, and K. Kuhlmann, “Thermal Isolation in Microcalorimeter Measurement,” in *2024 15th German Microwave Conference (GeMiC)*, IEEE, Duisburg, Germany, 2024, pp. 159–162.

[69] IEEE, “IEEE Standard for Rectangular Metallic Waveguides and Their Interfaces for Frequencies of 110 GHz and Above. Part 1: Frequency Bands and Waveguide Dimensions,” IEEE Microwave Theory and Techniques Society, Tech. Rep.

[70] Flann. “Waveguide Parameters.” (2025), [Online]. Available: https://flann.com/wp-content/uploads/2024/12/Waveguide-Parameters-.pdf.

[71] Richconn. “Micro CNC Machining: Techniques, Application and Advantages.” (2024), [Online]. Available: https://richconn.com/micro-cnc-machining.

[72] V. Callcut and P. Webster, “The Brasses: properties and applications,” Copper Development Association, 2005.

[73] I. Rajagopal, K. S. Rajam, and S. R. Rajagopalan, “Gold plating of critical components for space applications: Challenges and solutions,” in *Gold Bulletin*. Springer Nature, 1992, vol. 25, pp. 55–66.

[74] A. Hofmann, E. Horster, J. Weinzierl, L.-P. Schmidt, and H. Brand, “Flexible Low-Loss Dielectric Waveguides for THz Frequencies with Transitions to Metal Waveguides,” in *33rd European Microwave Conference*, IEEE, Munich, Germany, 2003, pp. 955–958.

[75] S. Liu, G. Xie, G. Li, S. Yu, X. Lu, S. Liu, F. Yue, C. Jing, and J. Chu, “A robust PEEK-silver coated hollow waveguide for terahertz bendable transmission in hot and cold environments,” *Results in Physics*, 2022.

[76] Thermtest. “Thermal Conductivity of PEEK.” (2025), [Online]. Available: https://thermtest.com/application/thermal-conductivity-of-peek.

[77] J. Thakur, W. G. Kim, and Y. H. Kim, “Large Aperture Low Aberration Aspheric Dielectric Lens Antenna for W-Band Quasi-Optics,” *Progress In Electromagnetics Research*, vol. 103, pp. 57–65, 2010.

[78] K. Zhou, W. Miao, B. Fan, Y. Delorme, S. Caroopen, M. Batrung, and S. Shi, “Transmittance of high-density polyethylene from 0.1 THz to 15 THz,” in *Infrared, Millimeter-Wave, and Terahertz Technologies VI*, vol. 11196, SPIE, Hangzhou, China, 2019.

[79] IEC, "Hollow metallic waveguides-Part 2: Relevant specifications for ordinary rectangular waveguides (IEC 60153-2)," International Electrotechnical Commission, Tech. Rep., 2016.

[80] Rohde and Schwarz. "Calibration of power sensor." (2020), [Online]. Available: https://allice.de/wp-content/uploads/2018/12/Rohde-Schwarz-NRPC-Calibration-Kit-fuer-Powersensoren-Bro-Web.pdf.

[81] Isabellenhuette. "Features and Application Notes: E-Copper and ISOTAN." (2022), [Online]. Available: https://www.abcpol.pl/download/druty-oporowe/21-e-copper.pdf.

[82] Allectra. "Kapton." (2023), [Online]. Available: https://www.allectra.com/news/outlining-kapton-insulation-thermocouple/.

[83] P. Staerke, C. Carta, and F. Ellinger, "Direct Chip-to-Waveguide Transition Realized With Wire Bonding for 140-220 GHz G-Band," *IEEE Transactions on Terahertz Science and Technology*, vol. 10, no. 3, pp. 302–308, 2020.

[84] R. Payapulli, L. Zhu, S. H. Shin, M. Stanley, N. M. Ridler, and S. Lucyszyn, "Polymer-Based 3-D Printed 140 to 220 GHz Metal Waveguide Thru Lines, Twist and Filters," *IEEE Access*, vol. 11, pp. 32 272–32 295, 2023.

[85] Mi-Wave. "Full Band - Compact Isolators: Available in K-J Bands, WR-42 to WR-3," Millimeter Wave Products Inc. (2025), [Online]. Available: https://www.miwv.com/full-band-compact-faraday-isolators/.

[86] MiWave. "140 - 220 GHz, Electronic Attenuator." (2025), [Online]. Available: https://www.miwv.com/515g-387-wr-5-g-band-attenuator-frequency-range-140-ghz-220-ghz-insertion-loss-0-4-db-vswr-1-21/#.

[87] M. T. Sebastian, "Measurement of Microwave Dielectric Properties and Factors Affecting Them," in *Dielectric Materials for Wireless Communication*. Elsevier, 2008, pp. 11–47.

[88] W. K. Perangin-Angin, K. Kuhlmann, and J. Ruehaak, "Comparison of measurement methods for the correction factor of microcalorimeters," *Measurement: Sensors*, vol. 38, no. 101413, 2025.

[89] W. Yuan, S. Ma, S. Ding, J. Ding, and X. Cui, "A New Calculation Method of Correction Factor for Microcalorimeters," in *2021 IEEE MTT-S International Wireless Symposium (IWS)*, IEEE, 2021.

 DOI: 10.7795/110.20250905

[90] W. K. Perangin-Angin, J. Ruehaak, and K. Kuhlmann, "Characterization and Optimization of Correction Factor Determi-nation in Waveguide Microcalorimeters," *Measurement*, no. 118865, 2025.

[91] BIPM. "International Vocabulary of Metrology." (2021), [Online]. Available: https://www.bipm.org/documents/20126/54295284/VIM4_CD_210111c.pdf.

[92] W. K. Perangin-Angin, K. Kuhlmann, A. Steiger, and R. H. Judaschke. "Bridging the gap betweenWaveguide-based and Free-space Electromagnetic Power Traceability." (2025), [Online]. Available: https://thebipm150.org/posters-online/.

[93] W. K. Perangin-Angin, K. Kuhlmann, J. Ruehaak, and G. N. Phung, "Generalized Efficiency of Waveguide Thermoelectric Power Sensor," in *2022 Kleinheubach Conference*, IEEE, Miltenberg, Germany, 2022, pp. 1–4. [Online]. Available: https://ieeexplore.ieee.org/document/9954503.

[94] G. F. Engen, "Amplitude Stabilization of Microwave Signal Source," *IRE Transactions on Microwave Theory and Techniques*, vol. 6, no. 2, pp. 202–206, 1958.

[95] J. R. Juroshek, "A Direct Calibration Method for Measuring Equivalent Source Mismatch," *Microwave Journal*, pp. 106–118, 1997.

[96] K. Technologies. "Network analyzer architectures." (2024), [Online]. Available: https://www.keysight.com/us/en/assets/3119-1082/applicationnotes/5965-7708.pdf.

[97] W. K. Perangin-Angin, K. Kuhlmann, and J. Ruehaak, "Generalized Efficiency and the Uncertainty of Millimeter Wave Power Standard," *Advances in Radio Science*, vol. 21, pp. 7–13, 2023.

[98] VDI. "PM5B Operational Manual." (2025), [Online]. Available: https://www.vadiodes.com/images/Products/PowerMeter/PM5manual/VDI-724.1_PM5B_Manual.pdf.

[99] E. A. L. Committee. "Evaluation of the Uncertainty of Measurement in calibration." (2022), [Online]. Available: https://european-accreditation.org/wp-content/uploads/2018/10/EA-4-02.pdf.

[100] T. Kleine-Ostmann, T. Schrader, M. Bieler, U. Siegner, C. Monte, B. Gutschwager, J. Hollandt, A. Steiger, L. Werner, R. Mueller, G. Ulm, I. Pupeza, and M. Koch, "THz Metrology," *Frequenz*, vol. 62, no. 5-6, pp. 137–148, 2008.

[101] C. Sklarczyk, "Microwave, millimeter wave and terahertz (MMT) techniques for materials characterization," in *Materials Characterization Using Nondestructive Evaluation (NDE) Methods*. Woodhead Publishing, 2016, ch. 5, pp. 125–159.

[102] B. Zhang, K. Wang, and T. Jiang, "RF power design optimization in MRI system," *Magnetic Resonance Letters*, vol. 1, pp. 89–98, 1 2021.

 DOI: 10.7795/110.20250905

List of Publications

1. W. K. Perangin-Angin, K. Kuhlmann, J. Ruehaak, and G. N. Phung, "Generalized Efficiency of Waveguide Thermoelectric Power Sensor," in 2022 Kleinheubach Conference, IEEE, Miltenberg, Germany, 2022, pp. 1–4.
   https://ieeexplore.ieee.org/document/9954503.

2. W. K. Perangin-Angin, K. Kuhlmann, and J. Ruehaak, "Generalized Efficiency and the Uncertainty of Millimeter Wave Power Standard," Advances in Radio Science, vol. 21, pp. 7–13, 2023.
   DOI: https://doi.org/10.5194/ars-21-7-2023.

3. W. K. Perangin-Angin, K. Kuhlmann, and J. Ruehaak, "Thermal Isolation in Microcalorimeter Measurement," in 2024 15th German Microwave Conference (GeMiC), IEEE, Duisburg, Germany, 2024, pp. 159–162.
   DOI: https://doi.org/10.23919/GeMiC59120.2024.10485242.

4. W. K. Perangin-Angin, K. Kuhlmann, and J. Ruehaak, "Dielectric Waveguide as Transmission Line for R 1.8k Microcalorimeter," in 2024 Conference on Precision Electromagnetic Measurements (CPEM), IEEE, Denver, CO, USA, 2024, pp. 1–2.
   DOI: https://doi.org/10.1109/CPEM61406.2024.10646069.

5. W. K. Perangin-Angin, K. Kuhlmann, and J. Ruehaak, "Development of a Waveguide Microcalorimeter as RF Power Standard for Frequencies above 170 GHz," in PTB-Seminar, Aktuelle Fortschritte von Kalibrierverfahren im Nieder- und Hochfrequenzbereich 2024, Braunschweig, Germany, 2024.
   DOI: https://doi.org/10.7795/810.20240709.

6. W. K. Perangin-Angin, K. Kuhlmann, A. Steiger, R. H. Judaschke, "Bridging the gap between Waveguide-based and Free-space Electromagnetic Power Traceability," in BIPM 150 Years of the Metre Convention, Paris, France, 2025.
   https://thebipm150.org/posters-online.

7. W. K. Perangin-Angin, K. Kuhlmann, and J. Ruehaak, "Comparison of measurement methods for the correction factor of microcalorimeters," Measurement: Sensors, vol. 38, no. 101413, 2025.
   DOI: https://doi.org/10.1016/j.measen.2024.101413.

8. W. K. Perangin-Angin, J. Ruehaak and K. Kuhlmann, “Characterization and Optimization of Correction Factor Determination in Waveguide Microcalorimeters,” Measurement, 118865. 2025.
   DOI: https://doi.org/10.1016/j.measurement.2025.118865.

9. W. K. Perangin-Angin, K. Kuhlmann, and J. Ruehaak, “Development of the R 1.8k Dielectric Waveguide Microcalorimeter,” IEEE Transactions on Instrumentation and Measurement, to be published, 2025.

DOI: 10.7795/110.20250905

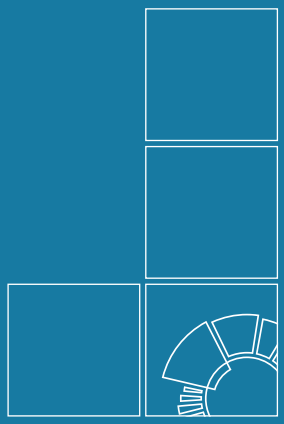

Herausgeber:
Physikalisch-Technische Bundesanstalt
ISNI: 0000 0001 2186 1887
Presse und Öffentlichkeitsarbeit
Bundesallee 100
38116 Braunschweig
Telefon: (05 31) 592-93 21
Telefax: (05 31) 592-92 92
www.ptb.de